A New Probabilistic Model to Evaluate the Age and Erosion Rate of Young Sedimentary Rock on Mars

By
An Li

Submitted in partial fulfillment of the requirements for
BACHELOR OF SCIENCE DEGREES WITH HONORS in both
ASTROPHYSICS AND GEOPHYSICAL SCIENCES
at the UNIVERSITY OF CHICAGO

May 21, 2021

Presented to
Advisor: Edwin Kite
Readers: Daniel Fabrycky and Michael Foote

ACKNOWLEDGMENTS

I am very grateful to my advisor Edwin Kite for the detailed email exchanges, Skype discussions, and feedback on my thesis. This project would not have been possible without Edwin, and I learned so much about both Mars and the research process from him over this past year.

My thesis readers Daniel Fabrycky and Michael Foote provided invaluable insights that have strengthened my thesis. I am astounded by Dan's mental agility in tackling a field so different from his own. I deeply appreciate both readers' time and energy spent in providing feedback.

Amy Tian and Dahlia Walters have been so thoughtful and patient with me in times of stress, and I couldn't have asked for better quarantine roommates. I am also very thankful for my conversations on statistical concepts with Nathan Lee and Bobby Shi. Finally, I would like to thank my family Dan, Jan, and Zhong Li for their extraordinary love and support.

ABSTRACT

The Medusae Fossae Formation (MFF) is an enigmatic sedimentary unit in the equatorial region of Mars with an uncertain formation process and age. Previously believed to be entirely Amazonian in age, recent stratigraphic studies have suggested that the Medusae Fossae Formation initially formed in the Hesperian but was later reworked throughout the Amazonian (Kerber and Head, 2010; Kerber et al., 2011). The MFF's low dielectric constant suggests either subsurface porous rock or ice (Watters et al., 2007), related to potential implications for volcanism or in-situ resource utilization in the equatorial region of Mars. For ice, based on Hudson et al. (2007), we estimate the minimum erosion rate needed for metastable water ice at depths shallow enough to be detected by Gamma Ray Spectroscopy (GRS) or Neutron Spectroscopy (NS) to be 1000 nm/a. Due to the heavily wind-eroded surface, it is difficult to determine the age of the MFF using existing crater count data and an one-parameter model based on the crater size-frequency distribution function to estimate age (Tanaka, 2000; Kerber and Head, 2010). One-parameter models typically estimate an overabundance of small craters (Kite and Mayer, 2017). A recent two-parameter model (Palucis et al., 2020) uses a Monte Carlo approach for determining best age and erosion rate estimates. However, we created a new two-parameter probabilistic model that estimates both age and erosion rate (β) by treating cratering as a random Poisson process. Our study uses new crater count data of 14 sites of the Medusae Fossae Formation and other young equatorial units found from Context Camera (CTX) imagery. Adapting an instantaneous global sedimentation rate based on (Lewis and Aharonson, 2014) and a single period of erosion, we also estimate each site's volume over time. Based on our new model's best fit predictions, the Central Medusae Fossae Formation and the top of Aeolis Mons (otherwise known as Upper Mount Sharp) formed earlier in the Hesperian and had low erosion rates (<650 nm/a), whereas East Medusae Fossae, Far East Medusae Fossae, Aeolis Planum, and Eastern Candor most likely formed in the Amazonian and had higher erosion rates (>740 nm/a). Based on estimated erosion rates, we also identify Aeolis Planum, Far East Medusae Fossae A and C, and East Medusae Fossae B out of the sites we studied as the most likely locations of a shallow subsurface ice table that is detectable by GRS/NS. In addition to estimating ages consistent with previous studies, our new model also provides a better picture of how locations with higher rates of erosion rate seem to have younger ages and MFF locations with lower rates of erosion rate have older best fit ages.

TABLE OF CONTENTS

INTRODUCTION

1.1 Description of the geology of the Medusae Fossae Formation

The Medusae Fossae Formation (MFF) is a large sedimentary unit located near the equator of Mars (130°-240°E and 15°S to 15°N) between the Tharsis and Elysium volcanic centers (Scott and Tanaka, 1986; Bradley et al., 2002, Kerber and Head, 2010). The formation process of the MFF is unknown. As one of the largest sedimentary deposits on the surface of Mars, MFF spans an area of 2.1 $\times 10^6$ km^2 and a volume of over 1.4 $\times 10^6$ km^3 (Bradley et al., 2002). The Medusae Fossae Formation is estimated to have a density of 1,765 $\pm$ 105 kg m^{-3} and a mass of 2.3-2.6$\times 10^{18}$ kg (Ojha and Lewis, 2018). Almost all of the MFF deposits are within dust-blanketed regions with low thermal inertia (Kieffer et al., 1977; Palluconi and Kieffer, 1981; Christensen, 1986; Zimbelman and Griffin, 2010), which make the MFF difficult to study using spectral data (Kerber et al., 2012). In addition, images show that the deposits are fine-grained, friable, and easily eroded by the wind, thus making age estimation by crater counting difficult (Schultz and Lutz, 1988; Tanaka, 2000; Kerber and Head, 2010).

The MFF has extremely wind-eroded surfaces (Bradley et al., 2002; Head and Kreslavsky, 2001, Head and Kreslavsky, 2004; Hynek et al., 2003; Malin et al., 1998; Zimbelman et al., 1997; Greeley and Guest, 1987; Scott and Tanaka, 1986; Frey et al., 1998; Takagi and Zimbelman, 2001; Schultz and Lutz, 1988; Williams et al., 2013). Common landforms throughout the MFF include yardangs (tens of kilometers long according to Ward, 1979), layering, and collapse features (Mandt et al., 2008). Additional features include bedding implying intermittent accumulation (Malin and Edgett, 2000), draping (Watters et al., 2007), and an apparent thickening toward Tharsis based on Mars Orbiter Laser Altimeter (MOLA) data (Hynek et al., 2002, Hynek et al., 2003) (additional features summarized in Mandt et al., 2008). Yardangs are long, wind-eroded ridges that typically form from a unidirectional, prevailing wind carrying sediment (El-Baz et al., 1979). Smooth yardangs are more commonly found in the middle and upper MFF members while rough yardangs are more common in the middle and lower members (Mandt et al., 2008). MOLA measured the surface roughness of the MFF to be 2-3 times greater than that of the average Martian surface, likely due to the presence of yardangs (Sakimoto et al., 1999).

Due to the Medusae Fossae Formation's highly eroded nature, it has been hypothesized that the MFF once covered a larger area (Kerber and Head, 2010; Wasilewski and Gregg, 2021). From examining the height of the reliefs of yardangs, Zimbelman and Griffin (2010) estimate that a minimum of 19,000 km^3 of lower member MFF deposits were eroded away by the wind and overall volume loss estimates are on the magnitude of 10^6 km^3 (Tanaka, 2000; Bradley et al., 2002). Similarly, pedestal crater heights that average 115 m (Kadish et al., 2009) and reach up to 2 km (Schultz et al., 2007) indicate that the thickness of what was eroded was (locally) at least equal to these heights (Kerber and Head, 2010).

Yardangs are also used for relative age-dating of the MFF. For example, in Gunjur Crater in Aeolis Planum, MFF yardangs are in delta deposits and on the delta surface, indicating active fluvial activity when the MFF formed or reformed (Wang et al., 2018). Similarly, Zimbelman et al. (2000) noted a topographic channel that appears to be diverted by MFF material. In addition, yardangs have altered layered ejecta craters on Mars (Liu et al., 2021). By dating the layered ejecta to be 0.11-2.0 billion years old (Ga), Liu et al. (2021) determined that yardangs were recently formed in the geologic record.

The MFF is relatively young when compared to other surfaces of Mars (Tanaka et al., 2014), which may be due to regular reworking and re-induration of the MFF (Kerber et al., 2011). Because liquid water is required for aqueous cementation of loose sediment, it is likely that water was somehow involved in forming the MFF, which constitutes relatively recent evidence for liquid water on the surface of Mars. The MFF is divided into three main geologic units based on tone and erosion states: an upper member (Amu) with smooth and light-colored plains, a middle member (Amm) with more erosion, and a darker colored lower member (Aml) with the most erosion (Scott and Tanaka, 1986; Greeley and Guest, 1987). Initially, these units were predicted to have formed in the Middle to Late Amazonian (1.4-0.3 Ga and 0.3 Ga to present-day) based on crater counts (Scott and Tanaka, 1986; Greeley and Guest, 1987), and later work estimated a formation age of 1.6 Ga (Werner, 2005). Stratigraphic relations also show that the MFF overlies Hesperian (3.7-2.9 Ga) outflow channels and is superposed on Amazonian-aged lowland terrain (Bradley and

Sakimoto, 2001; Bradley et al., 2002). Recent work on polygonal ridge networks show cross-cutting relationships with Medusae Fossae Formation, in which the lava intruded in the MFF, though age was not evaluated (Kerber et al., 2017). However, stratigraphic relationships with Hesperian-aged lava flows suggest that the MFF is as old as the Hesperian (Kerber and Head, 2010). As a result, the leading hypothesis is that the MFF was initially deposited in the Hesperian and later reworked throughout the Amazonian. Nevertheless, we do not know the exact age of the Medusae Fossae Formation and existing crater counting methods are typically not capable of solving simultaneously for erosion and finite age, with the partial exception of Palucis et al. (2020). As a result, a new pipeline is needed that takes into account both age and erosion rate parameters in order to estimate the age of the MFF.

1.2 Formation hypotheses for the MFF

Despite the importance of the unit, the formation mechanisms for the Medusae Fossae Formation remain enigmatic. Varied hypotheses for the formation of MFF include: ignimbrites (Scott and Tanaka, 1982; Scott and Tanaka, 1986), ashfall tuff (Tanaka, 2000; Bradley et al., 2002; Hynek et al., 2003), aeolian deposits (Greeley and Guest, 1987; Scott and Tanaka, 1986; Tanaka, 2000; Head and Kreslavsky, 2004), paleo-polar deposits (Schultz and Lutz, 1988; Schultz, 2002), exhumed fault rocks (Forsythe and Zimbelman, 1988), carbonate platform (Parker, 1991), shoreline terraces (Rice, 1997), rafted pumice (Mouginis-Mark, 1993; Mouginis-Mark and Zimbelman, 2020), lacustrine deposits (Malin and Edgett, 2000), and deposits from meteorite impact into a subsurface aquifer (Nussbaumer, 2005). Mandt et al. (2008) ruled out the paleo-polar deposit, and lacustrine deposit hypotheses on the basis of a requirement for Noachian (4.1 - 3.7 billion years ago) or Early Hesperian (3.7 - 2.9 billion years ago) formation age since the MFF was previously thought to be only Amazonian (Scott and Tanaka, 1986; Greeley and Guest, 1987; Tanaka, 2000; Head and Kreslavsky, 2001; Head and Kreslavsky, 2004; Bradley et al., 2002). While later work indicated an earlier emplacement age during the Hesperian (Kerber and Head, 2010; Zimbelman and Scheidt, 2012b), the carbonate platform hypothesis was rejected as image resolution improved

(Mandt et al., 2008; Kerber and Head, 2010). Paleopolar deposits were also rejected due to a lack of tectonic signatures of polar wander (Grimm and Solomon, 1986) and because no significant polar wandering occurred since the early Hesperian (Tanaka, 2000; Kite et al., 2009). While rafted pumice deposits are deemed unlikely due to a lack of observed shorelines (Malin and Carr, 1999; Bradley et al., 2002; Mandt et al., 2008), they are not eliminated as a possibility (Mouginis-Mark and Zimbelman, 2020).

While researchers have hypothesized the possibility of subsurface ice at the MFF, there have also been arguments disfavoring this hypothesis. Analysis of the dielectric properties of the MFF help us better understand its subsurface content. Typically, dielectric properties are ascertained by using sounding radar data and averaging over the depth to a basal interface, or from radar reflectivity (Mouginot et al., 2010). The dielectric properties of the MFF are consistent with both clean water ice and sand-sized particles (Watters et al., 2007; Campbell et al., 2021). Some studies argue that the bulk density and sounding radar data (Carter et al., 2009) rule out ice (Ojha and Lewis, 2018; Mouginis-Mark and Zimbelman, 2020). However, Campbell et al. (2021) reasons that we would expect to see widespread sand or dune fields at the margins of the MFF if the subsurface consisted of coarse-grained sand with low compressibility rather than water ice. In addition, using neutron data from the Mars Odyssey Neutron Spectrometer, Wilson et al. (2018) determines that a water equivalent hydrogen (WEH) abundance >40 wt.% at Aeolis Planum must be buried water ice or hydrated salts since it is much too great for hydrous silicates (typically at 10-20 wt.% according to Feldman et al., 2004). However, Pathare et al. (2018) questioned this WEH abundance >40 wt.% inference and argued that (if real) it would have to come from a single layer of ice extending to the surface of Mars that would be unlikely due to the instability of equatorial water ice (Mellon and Jakosky, 1993; Schorghofer, 2007).

Campbell et al. (2021) instead proposes a two-layer deposit. The top layer consists of 300-600 m of fine-grained, self-compacting material, whereas the bottom layer is a minimally compacting material (Campbell et al., 2021). The authors suggest that the bottom layer is predominantly ice-rich capped by a dry component, possibly produced through pyroclastic volcanism, in order

to explain the bulk density values from gravity analysis from Ojha and Lewis (2018) (Campbell et al., 2021). Further data from Shallow Radar (SHARAD) on the Mars Reconnaissance Orbiter is necessary to further test this hypothesis (Campbell et al., 2021). Since neutron spectroscopy is sensitive to 1 meter depth, if Campbell et al. (2021)'s 300-600 m dry layer hypothesis is correct, then Wilson et al. (2018)'s inferred WEH content close to the surface cannot be explained by ice.

Therefore, ignimbrites (from pyroclastic flow), volcanic ash (from pyroclastic fall), and loess (aeolian dust) are the three leading hypotheses for the formation of the Medusae Fossae Formation (Zimbelman et al., 1997; Mandt et al., 2008; Kerber and Head, 2010; Ojha et al., 2019). Recently, however, Ojha and Lewis (2018) deemed aeolian materials unlikely due to a lack of possible geological processes to deposit and lithify the huge volume of dust that constitutes the MFF's volume of 1.4×10^6 km^3 in the Martian equatorial latitudes, which is equal to a global equivalent layer of 9.7 m (Ojha and Lewis, 2018).

Many authors favor the volcanic origin hypothesis as either pyroclastic flow or ash fall (Scott and Tanaka, 1986; Head and Wilson, 1998; Bradley et al., 2002; Hynek et al., 2003; Mandt et al., 2007; Kerber et al., 2011; Kerber et al., 2012; Ojha and Lewis, 2018). Mandt et al. (2008) favored pyroclastic fall since the top down induration process required to form the type of observed loess deposits are rarely pervasive at a large scale. After analyzing the volcano Apollinaris Patera as a plausible source for the MFF, Kerber et al. (2011) suggested that if Apollinaris Patera and MFF deposits are both composed of pyroclastic deposits, then the Apollinaris Patera could have been emplaced by pyroclastic flows and the MFF by pyroclastic airfall (Kerber et al., 2011). Both pyroclastic ashfall and ignimbrites are consistent with the measured low dielectric constant (Watters et al., 2007; Ojha and Lewis, 2018) and the enrichment of major volcanic gases such as sulfur and chlorine (Ojha et al., 2018) suggested that the deposits were derived from a deposition source of explosive volcanic eruptions.

1.3 Significance in understanding Martian climate history and dust budget

Understanding the MFF has global implications. Determining the sediment source locations for the Medusae Fossae Formation might better define the possible explosive volcanic history of Mars (Horvath et al., 2021) and provide a better idea of the past climate and the global dust distribution on Mars. Recently, Ojha et al. (2019) estimated that during the deposition of the MFF, over 10^{17} kg of sulfur, could have been delivered to the atmosphere. While the effect of the outgassing of S on the climate of Mars would depend on the eruption timescale for MFF, it is possible that S may have implications for both liquid water (Halevy et al., 2007; Halevy and Head, 2014) and lower the pH of surface waters, which would prevent carbonate saturation and explain the lack of widespread carbonates on Mars (Halevy and Schrag, 2009; Ojha et al., 2019). However, S-induced warming may be offset by cooling due to sulfate and sulfur aerosols (Tian et al., 2010; Ojha et al., 2019). In terms of the global dust cycle, (Ojha et al., 2018) predicted that based on the enrichment of both S and Cl, the S:Cl ratio, and matching characteristics of the dust between where both the Mars Exploration Rovers and Mars Science Laboratory rover landed in comparison with the MFF, the MFF was the single largest global dust source on Mars. In addition to similar chemical signatures with dust at other locations on Mars, the MFF also has similar material and geological features as the upper part of Mt. Sharp in Gale Crater (Thomson et al., 2008; Thomson et al., 2011; Zimbelman and Scheidt, 2012a; Wang et al., 2018), which we discuss further in §4.5.

1.4 Description of new two-parameter model approach

In this study, to better quantify the age and erosion rate of the Medusae Fossae Formation and similar sedimentary regions such as Eastern Candor and Upper Mount Sharp, we examined 14 regions and applied a probabilistic model that accounts for both erosion and age. Fitting for both erosion and age simultaneously has been attempted previously by Palucis et al. (2020). Palucis et al. (2020) applied their model in Monte Carlo mode to subsample parent surfaces generated over a range of ages and β values and to find a corresponding crater size-frequency distribution. The study site was then assigned the most likely surface ages and β values when the model generated a count of

craters that matched within 25 percent of the observed crater count in all size bins (Palucis et al., 2020). Our approach is different in that we treat cratering as a random Poisson process in order to apply a probabilistic model to find the best fit age and β. This model considers each region's surface area, crater size-frequency distribution, and crater erosion rate β in nanometers per year (nm/a) to predict the most probable age and erosion rate. Taking the model's predicted best fit ages and erosion rates, we then plotted thickness and volume over time. To do this, we used the global sedimentation rate compilation of Lewis and Aharonson (2014), who infer sedimentation rates of 10–100 μm/a for young sedimentary rocks. This is >10 times faster than our model-fit erosion rates, so we approximate sedimentation rate as instantaneous and that deposition occurs in one continuous interval before erosion occurs in a following continuous interval without interruption for each site. We also estimated the present thickness of each unit based on previous literature and our own basal-surface interpolation in ArcGIS.

1.5 Inadequacy of an one-parameter model

Since there are repeated periods of burial and shielding interrupted by exhumation (Schultz and Lutz, 1988; Schultz, 2002), it is expected that crater counts would underestimate the formation age of the MFF, leading to an estimation of the modification age instead (Greeley et al., 2001; Kerber and Head, 2010). However, our model finds a simultaneous fit for both erosion and age. This dual approach is more nuanced than fitting only an age, which ignores the underabundance of small craters, as shown in Figures 1.1 and 1.2.

Our model also includes consideration of β, whereas age alone does not provide an accurate best fit estimation corresponding to crater count data. In Figure 1.3, we compare different best fit age estimates with negligible (β = 1 nm/a) rates of erosion. We see that none of the three best fits without erosion fall along the real data, in contrast with what we will see in Figure 3.3c. In fact, as shown in Figure 1.1, the erosion-less best fit predictions overestimate the number of craters in smaller crater size bins. As described in Figure 1.2, this is due to the preferential erosion of smaller craters over time. In §4.5, we also provide a statistical justification of the two-parameter model by

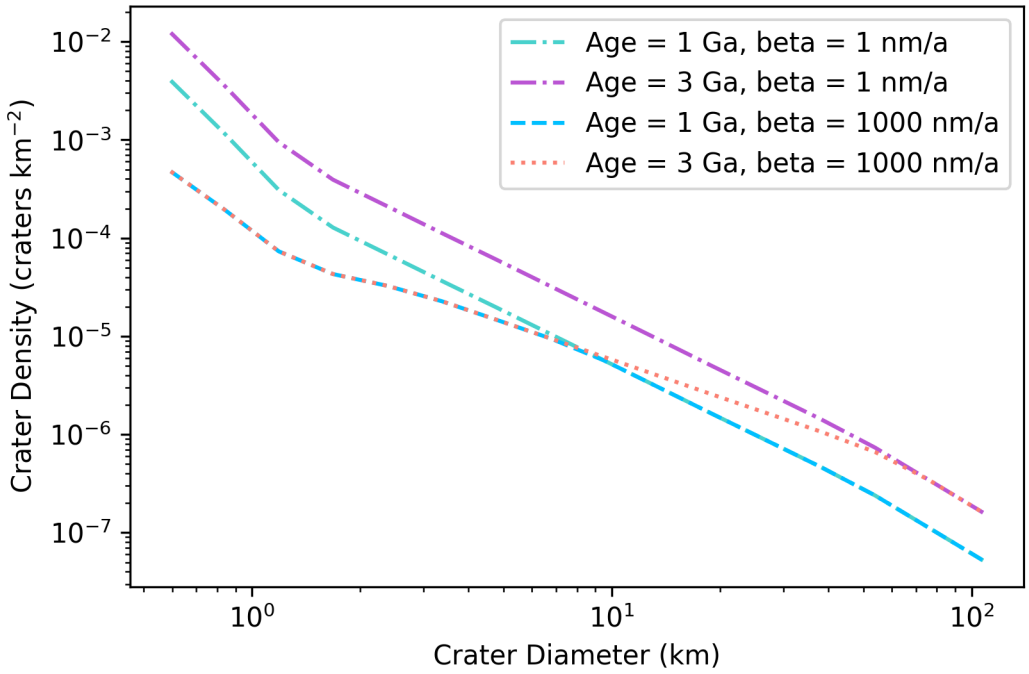

Figure 1.1: When erosion is included in the model while the age remains the same, smaller craters are preferentially eroded away. This explains the dip in the curves with β equal to 1000 nm/a for smaller crater bin sizes. See Figure 1.2 for a visualization of why smaller craters are eroded more quickly.

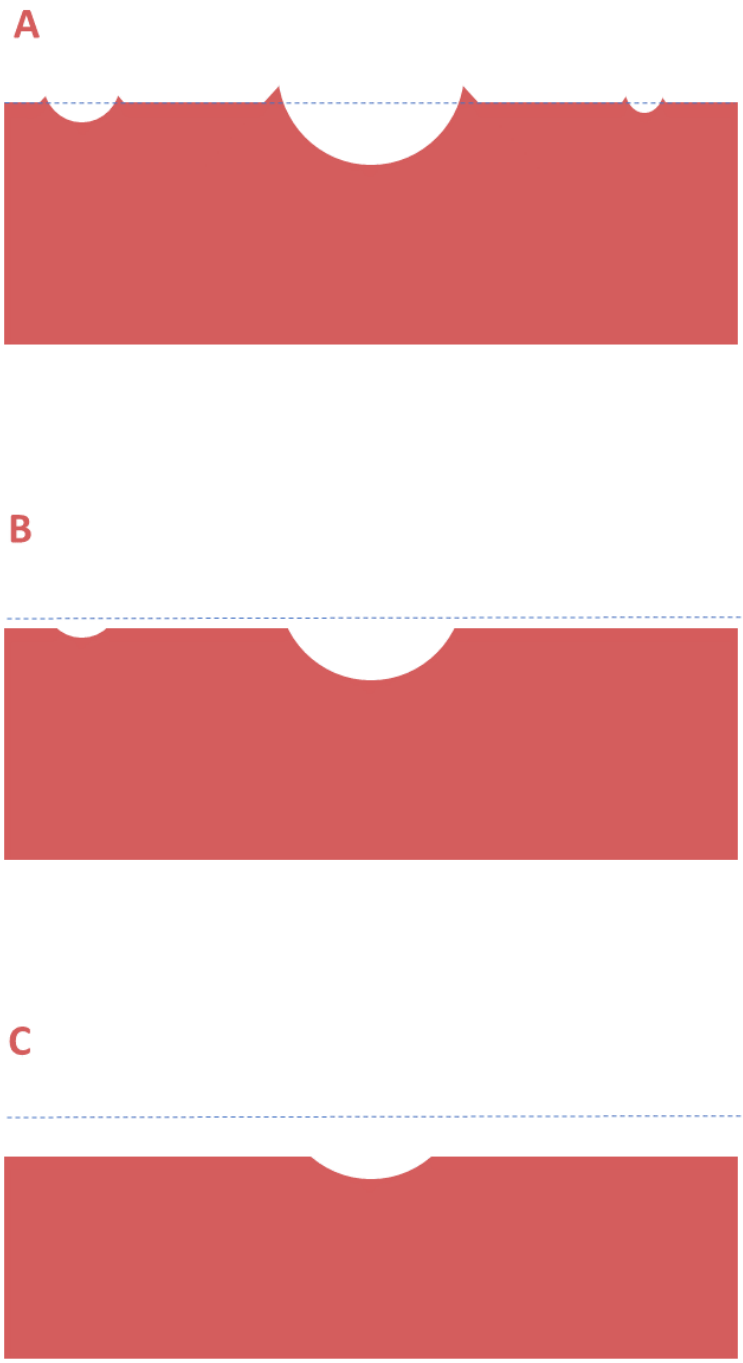

Figure 1.2: A simple diagram of the effect of erosion on crater removal. (a) We see big and small craters on the surface. (b) Small craters are eroded away faster, leaving only the larger two craters. The blue dotted line represents the eroded surface that was present in (a). (c) After a period of erosion, only the largest crater remains but much of it has also been eroded. The blue dashed line minus the red surface corresponds to sediment lost.

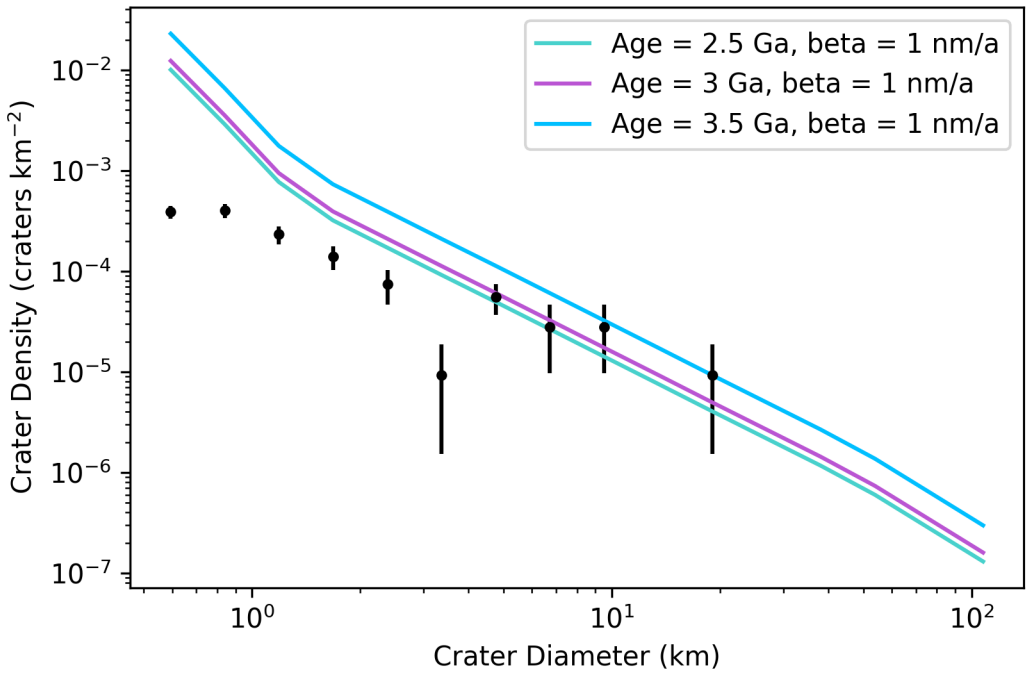

Figure 1.3: A simpler model only considering age with negligible erosion for Central Medusae Fossae 1 C, which is site 1C.

performing chi-square goodness-of-fit tests for the two-parameter model of both age and β and for each one-parameter model.

We also study new crater count data covering all young sedimentary rock within the Medusae Fossae Formation and nearby locations of Eastern Candor and Upper Mount Sharp. Our model assumes that there is one pulse of sedimentation, with no hiatuses, and then erosion occurs at a constant rate. Since there is evidence of multiple cycles of erosion and deposition, along with varying rates of erosion, the model proposed in this study is a simple next step as appropriate given the small number of craters available in our database (see Table 1). Our goal was to not only create a new model that takes into account both age and erosion for the sedimentary regions of interest, but also to evaluate the model's range of parameters that were consistent with the model.

1.6 Overview of this study

In the next section (§2), we explain our new modeling technique that uses crater count data to estimate a best fit erosion and age for each site. In §2.4, we outline how we used our best fit estimates for age and erosion rate along with a global average deposition rate to examine the history of the volume at each site. We then present our results (§3) from the two-parameter model including both age and erosion rate (§3.1), the one-parameter results marginalizing only on age or erosion rate (§3.2), the best fit predictions for each site plotted against the real data (§3.3), and a simple mound thickness history by site (§3.4). In §4, we discuss the overall trends for the 14 study sites (§4.1, §4.2), potential model uncertainties (§4.3, §4.4), a χ^2 test comparing the two-parameter and one-parameter models (§4.5), implications for a subsurface ice table at the Medusae Fossae Formation (§4.6), and implications for the global sedimentary cycle on Mars (§4.7). Finally, we provide our conclusions in §5.

METHODS

2.1 Crater count data

We focused on 14 regions within the Medusae Fossae Formation and other nearby regions believed to be young sedimentary rock. For the purposes of this study, the terms regions, areas, and zones will be used interchangeably to describe the 14 sedimentary sites. All 14 locations are shown individually in Figure 2.1. Two regions within Central Medusae Fossae were subset into six zones (Figures 2.1b, 2.1g). East Medusae Fossae was subset into two zones (Figure 2.1h, Far East Medusae Fossae was subset into three zones (Figure 2.1e), and Aeolis Planum (Figure 2.1c), Eastern Candor (Figure 2.1d), and Gale's Mound (Figure 2.1f) were kept as one area each. Crater count data uncertainties will be discussed more in §3 and §4.

The craters for each region were counted by former University of Chicago undergraduate student Katarina Keating using Mars Reconnaissance Orbiter Context Camera (CTX) imagery. Craters were distributed into two categories: "standard" and "marked", see Figure 2.2. Standard craters were recognized clearly as craters, whereas marked craters were not definitively craters. As a result, the model used all of the standard craters and did not consider the marked craters.

We defined the boundaries of one subset within the first Central Medusae Fossae region based on "C", a large lobe northeast of Memnonia Sulci, in Figure 4 of Orosei et al. (2017). Similarly, we based another zone within the second Central Medusae Fossae on the terrain north of Tartarus Scopulus, labeled "B" in Figure 4 of Orosei et al. (2017). By taking radargrams of Lucus Planum, Orosei et al. (2017) found "B" and "C" as areas with concentrated reflectors, unlike the central section of Lucus Planum. As a result, both "B" and "C" indicate changes within the subsurface material at Lucus Planum in comparison with areas of no radar signal (Orosei et al., 2017). Both areas also had a rougher surface morphology than adjacent areas and were considered to be most likely pyroclastic in origin (Orosei et al., 2017). In addition, for Central Medusae Fossae 2 and the Far East Medusae Fossae, we used a global geologic map (Tanaka et al., 2014) to separate distinct geologic units.

In Figure 2.3, we plotted the logarithm of the number of counted craters in the data set for each given minimum diameter. From this plot, we found the diameter roll-off to be 0.510 km.

Site	Area (km^2)	Geographic location (°E,°N)	Number of craters	Basal elevation (m)	Present mound thickness (m)
1A	27700	-174.0, -0.753	112	-2600[a]	599
1B	87800	-177.3, -7.941	138	-2400[a]	2200
1C	108000	-172.7, -4.49	147	-2400[a]	1970
2	77800	153.0, 0.121	36	–	300[c]
3	6690	-66.8, -7.832	5	–	1000[d]
4A	63800	179.0, -8.629	141	-2400[a]	1900[f]
4B	52600	178.0, -1.131	94	-2530[a]	477[f]
4C	97800	176.5, -5.294	944	-2530[a]	1230[g]
5A	54500	-146.6, -1.997	12	1000[b]	801[g]
5B	132000	-144.2, 3.102	151	1000[b]	388[g]
5C	196000	-133.8, 3.391	101	-1000[b]	475[g]
6A	118000	-159.8, 8.296	153	-3200[a]	1230[f]
6B	234000	-158.2, -0.613	80	-3200[a]	3810[f]
7	1000	138, -4.99	5	–	1000[e]

Table 2.1: Area, location, number of craters, basal elevation, and present mound thickness for each site. [a]: From Bradley et al. (2002) Table 2. [b]: Detrended Digital Elevation Model (DEM) values from Bradley et al. 2002 that were not used to calculate present thickness. [c]: Kite et al., 2015. [d]: Scott and Tanaka, 1986. [e]: Kite et al., 2016. [f]: Found by subtracting basal elevation from maximum elevation found in ArcGIS. [g]: Calculated in ArcGIS using inverse distance weighting (IDW) interpolation.

This rollover at approximately 0.5 km represents where the crater counts are affected by survey incompleteness. As a result, we set 0.5 km as the minimum bin diameter for the smallest crater bin. We used manually counted craters within each of the 14 sites and divided the craters into bins based on crater diameters 0.5-128 km, which are bin indices -2 to 13 in Table 1 of Michael (2013), for a total of 16 bins that are spaced by a factor of about 0.71 between each consecutive minimum diameter. The Hartmann isochrons in Table 1 of Michael (2013) are defined as the size distribution of craters with a specified age and without erosion processes based on a widely-used Mars crater chronology model (Hartmann, 2005).

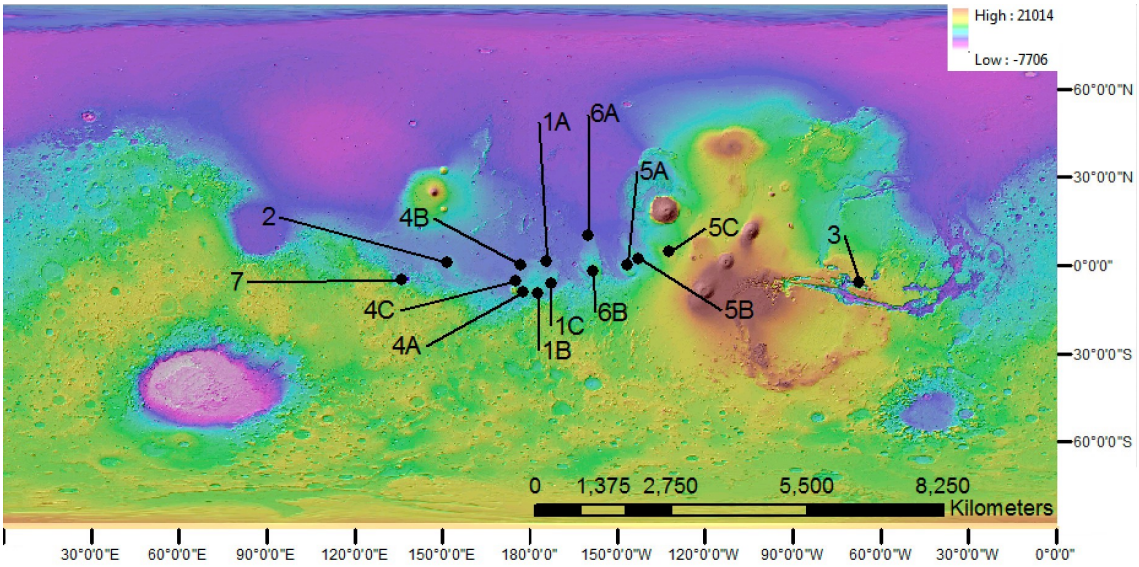

(a) Location of all 14 sites including Medusae Fossae Formation, Upper Mount Sharp, and Eastern Candor.

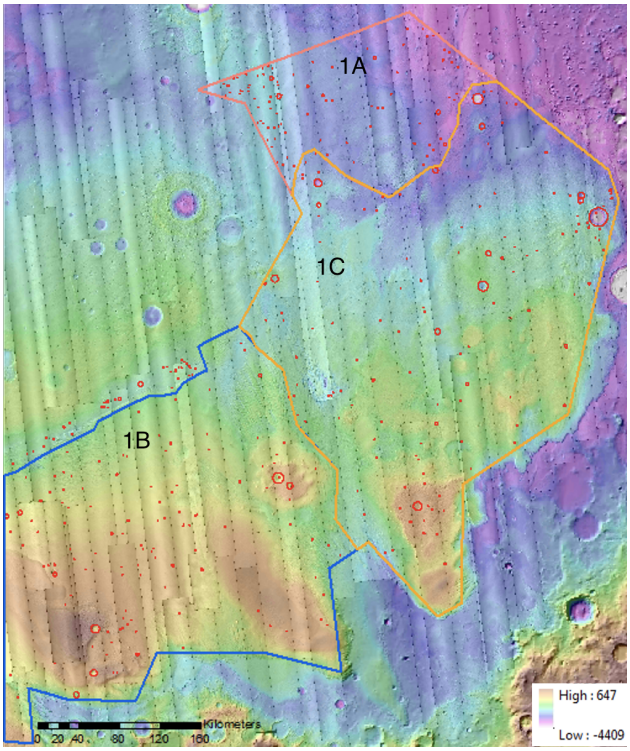

(b) Central Medusae Fossae 1 A (outlined in pink) at -173.95°E, -0.753°N; 1 B (blue) at -177.298°E, -7.941°N; 1 C (orange) at -172.663°E, -4.49°N.

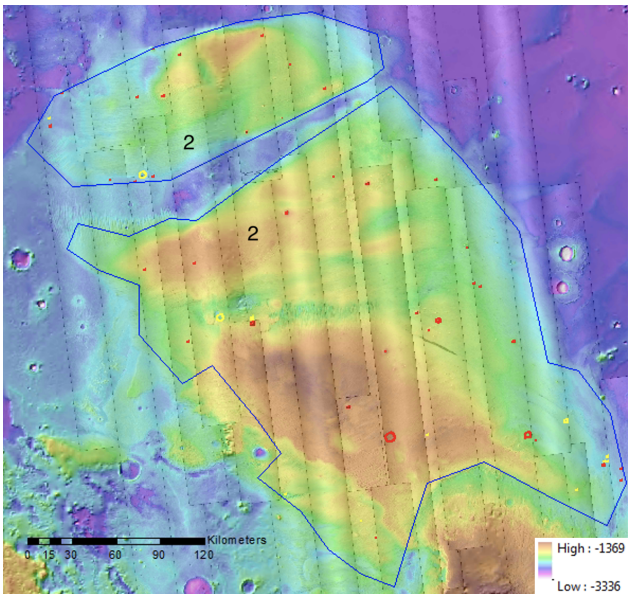

(c) Aeolis Planum (West Medusae Fossae) outlined in blue and centered at 153.028°E, 0.121°N.

2.2 Model description

Previous models typically only consider crater count data in order to estimate the age of the sedimentary areas. The next step–and the route that we explore in this study–is to create a two-parameter model that addresses both erosion rate and age. The simplest method for incorporating

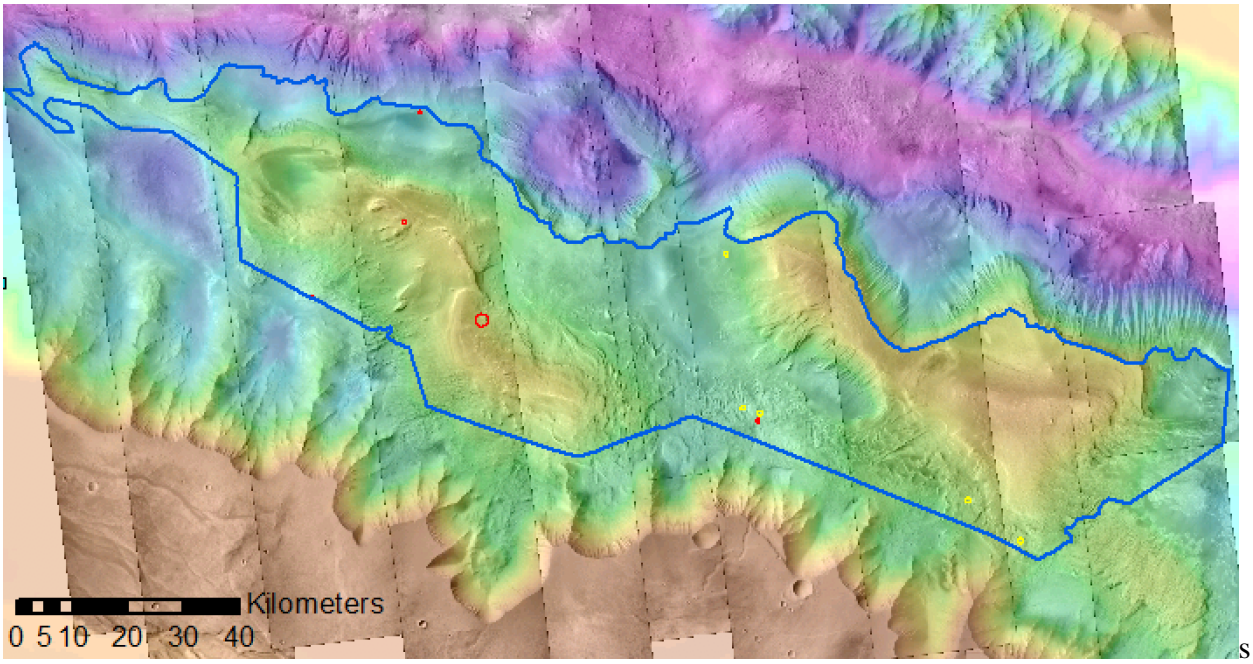

(d) Eastern Candor outlined in blue and centered at -66.813°E, -7.832°N.

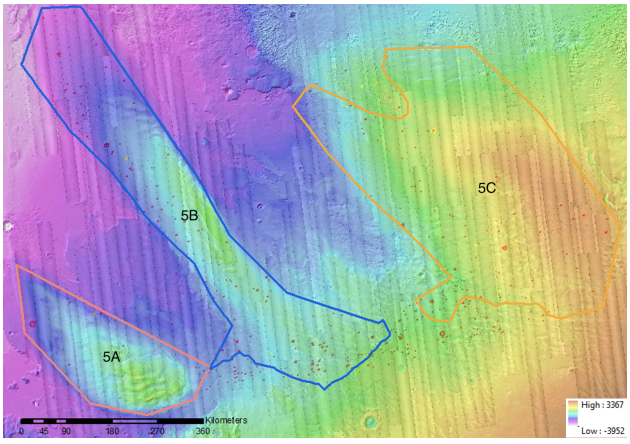

(e) Far East Medusae Fossae Formation: A (pink) at -146.575°E, -1.997°N; B (blue) at -144.242°E, 3.102°N; and C (orange) at -133.779°E, 3.391°N.

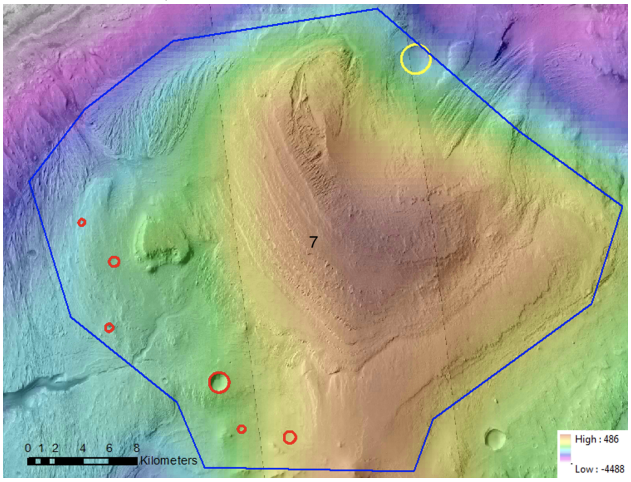

(f) Aeolis Mons/Upper Mt. Sharp outlined in blue and centered at 137.729°E, -4.99°N. The Curiosity Rover is approaching the mound from outside the upper left of the blue boundaries.

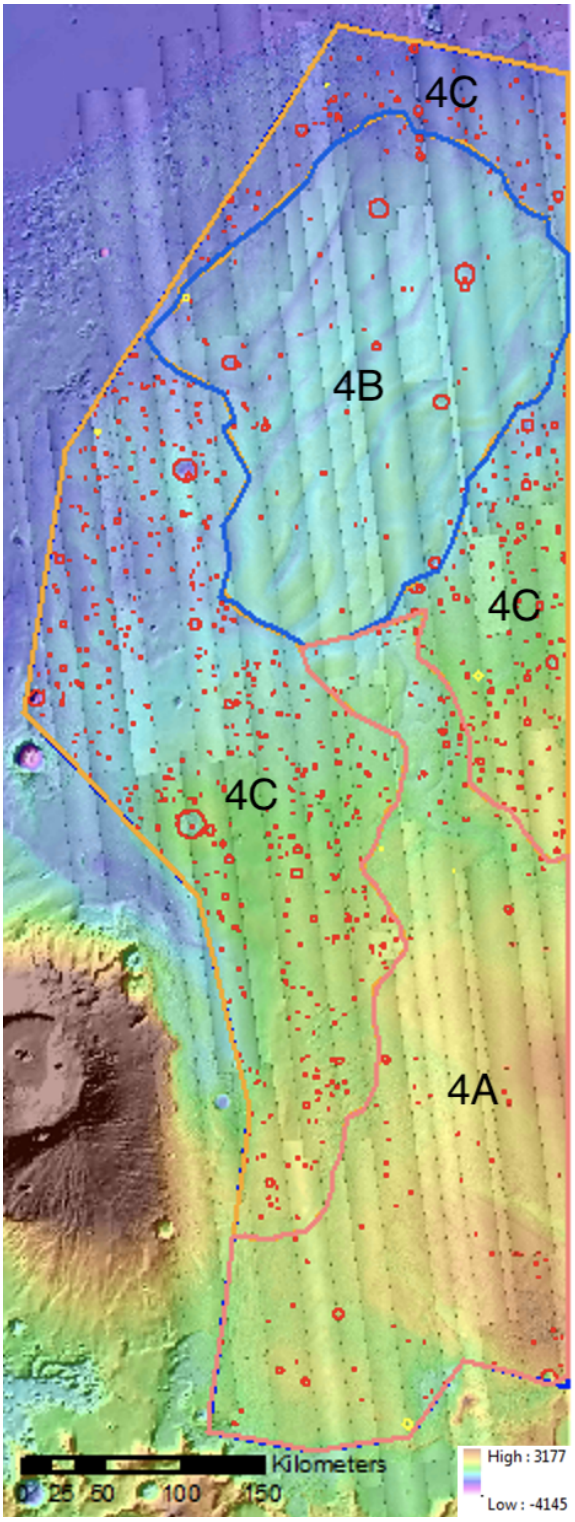

(g) Central Medusae Fossae Formation 2: A (pink) at 178.984°E, -8.620°N; B (blue) at 178.028°E, -1.131°N; and C (orange) at 176.528°E, -5.294°N.

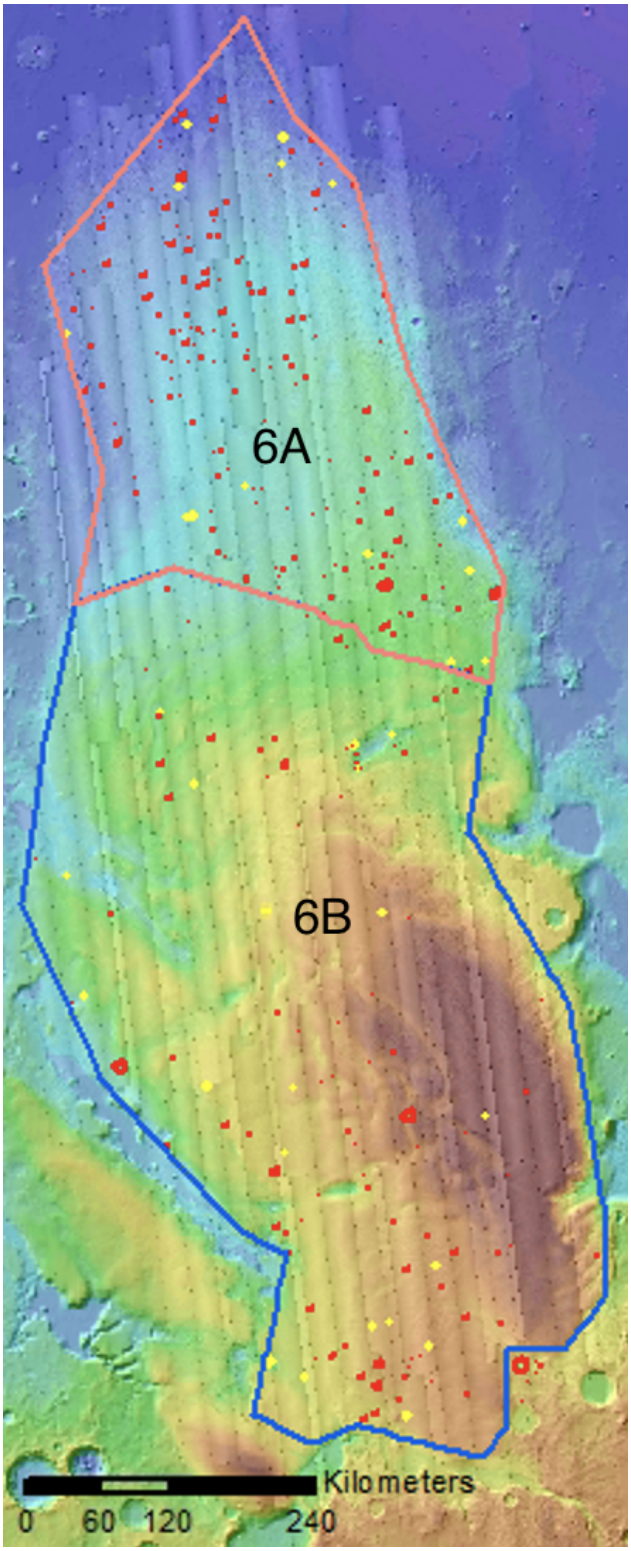

(h) East Medusae Fossae Formation: A (pink) at -159.76°E, 8.296°N; and B (blue) at -158.246°E, -0.613°N.

Figure 2.1: All 14 studied regions shown with Context Camera (CTX) images (Malin et al., 2007). Colored topography map is from the Mars Orbiter Laser Altimeter (MOLA) (Smith et al., 2001). Red circles indicate standard craters while yellow circles indicate marked craters.

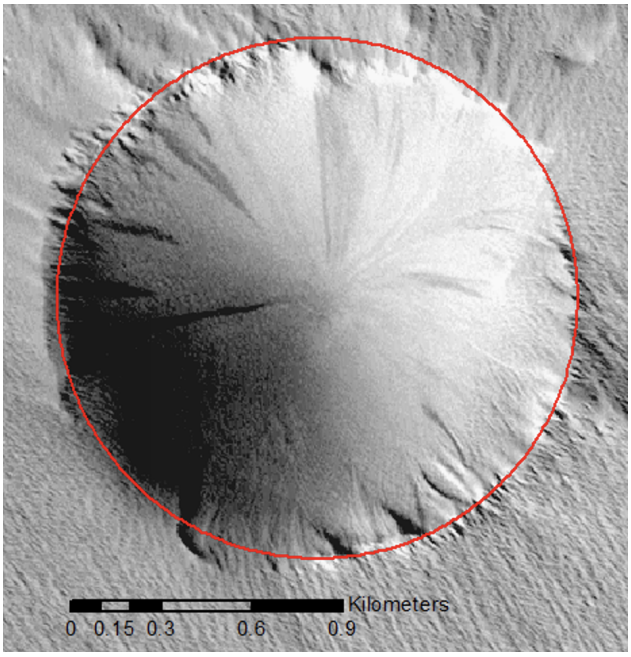

(a) Standard crater from region 5, Far East Medusae Fossae A. The diameter of the red circle was used as the diameter of the crater.

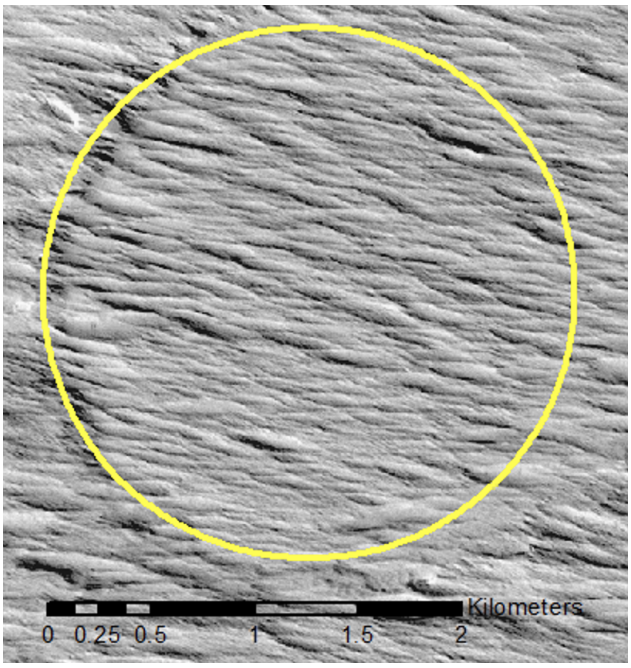

(b) Marked crater from region 5, Far East Medusae Fossae A. The diameter of the yellow circle was used as the diameter of the crater.

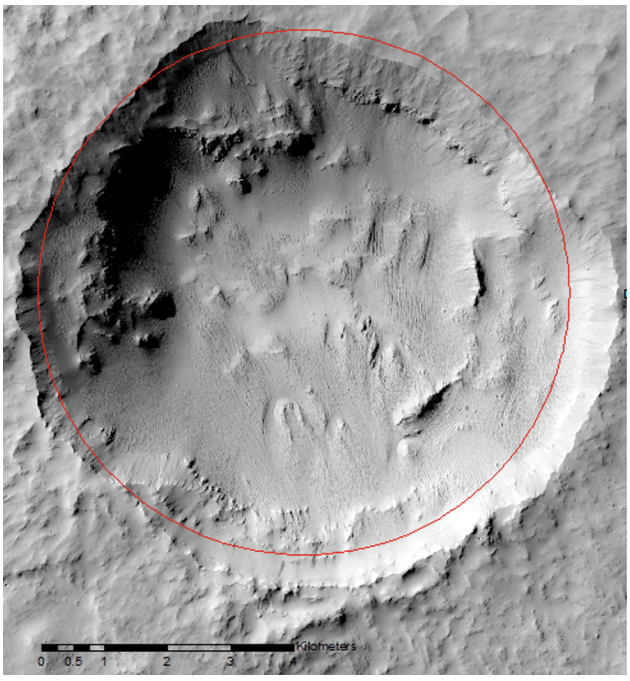

(c) Standard crater from region 1, Central Medusae Fossae 1A. The diameter of the red circle was used as the diameter of the crater.

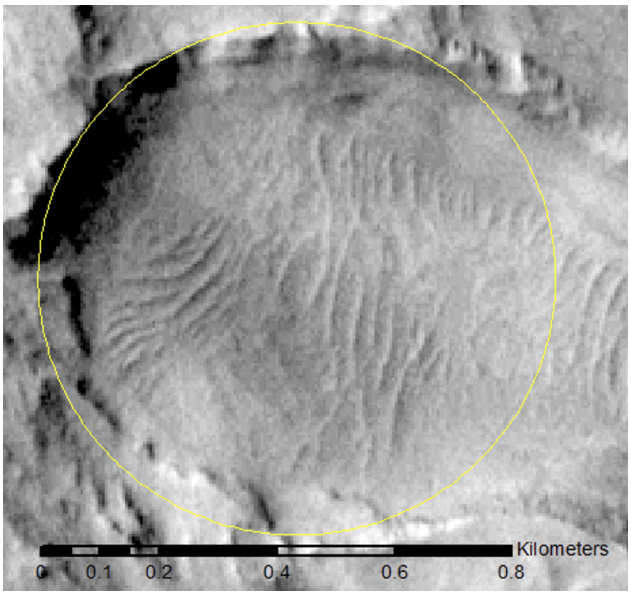

(d) Marked crater from region 3, Eastern Candor. The diameter of the yellow circle was used as the diameter of the crater.

Figure 2.2: Red circles represent standard craters. Yellow circles represent marked craters. Crater images are from Context Camera (CTX) data (Malin et al., 2007)).

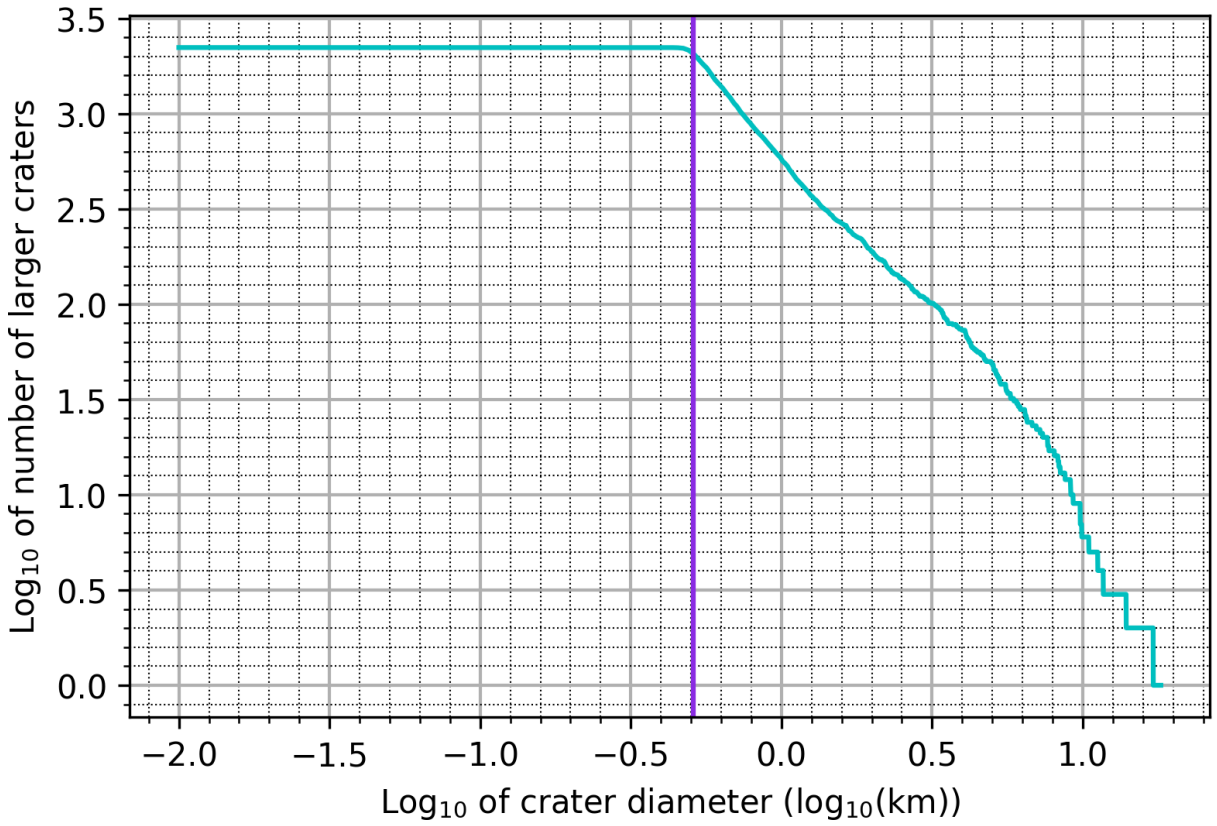

Figure 2.3: Log_{10} of number of craters with diameters larger than the crater bin diameter versus the $\log_{10}$ of crater bin diameter. The rollover diameter is marked with the vertical purple line at -0.29266, which corresponds to a measure of survey completeness down to a diameter of 0.50973 km.

erosion rate is to set it as a fixed rate that occurred continuously in Martian history without interruption or periods of deposition. While in §1 we recognize that the Medusae Fossae Formation is likely created by cycles of deposition and erosion, here we apply this simpler model to see how including erosion rate may allow us to better quantify the age of the Medusae Fossae Formation. In our model, we assume that craters are generated randomly as a Poisson process, given by the equation:

$$P(n) = \frac{e^{-\mu}\mu^{n}}{n!} \tag{2.1}$$

where $P(n)$ is the Poisson probability of observing n craters. n is the observed number of craters based on crater counts. Our model fits an expected number of craters, μ and estimates μ with

erosion and without erosion. The model then chooses the smaller value between the erosion and no erosion case. The equation for the expected number of craters assuming no erosion is as follows:

$$\mu = Hat \tag{2.2}$$

H is the expected number of craters for each crater diameter bin (craters km^{-2} Ga^{-1}) taken from Michael (2013) Table 1, which is based on the Hartmann production function (Hartmann, 2005). a is the area of the crater count region (km^2) and t is the age (Ga).

The equation for the expected number of craters with erosion is as follows:

$$\mu = Had/\beta \tag{2.3}$$

H is still the expected number of craters for each crater diameter bin (craters km^{-2} Ga^{-1}) and a is the area of the crater count region (km^2) as mentioned above for the no erosion case. β is the inputted erosion rate (nm/a). d is the logarithmic mid-depth based on the minimum and maximum diameter for each specific crater bin. The depth is related to diameter as follows:

$$d = \begin{cases} 0.2D, & \text{if } D < 2.82\text{km} \\ 0.323D^{0.538} & \text{if } D \geq 2.82\text{km} \end{cases} \tag{2.4}$$

D is the diameter of the crater in meters. For less than 1.0 km, this depth-to-diameter relationship was first determined by Pike (1980) and later used by both Palucis et al. (2020) and Smith et al. (2008). However, Palucis et al. (2020) and Smith et al. (2008) used the $0.2D$ case with a transition at $D = 5.8$ km. The component $0.323D^{0.538}$ in Equation 2.4 is from Tornabene et al. (2018). Tornabene et al. (2018) uses this depth-diameter scaling relationship for diameters larger than 12 km. We adapted the equation to better fit observed depth-to-diameter relationships (such as the idealized cases mentioned in Gabasova and Kite, 2018 and Watters et al., 2015). We chose 2.82 km as the transition diameter because it is the intersection between the two equations $0.2D$ and $0.323D^{0.538}$. The depth-to-diameter relationship for smaller craters is different from the depth-

to-diameter relationship for larger craters since smaller craters are more likely to be eroded away, as seen in Figure 1.2. In addition, Watters et al. (2015) found a similar ratio as $0.2D$ from Pike (1980) for their dataset of primarily craters <1 km. As a result, we adjusted the cutoff to 2.82 km to make sure the depth estimates were continuous between the two equations and monotonically increasing. To find the logarithmic mid-depth, we set D as the logarithmic mid-diameter, found as follows:

$$D = \sqrt{D_{min} D_{max}} \tag{2.5}$$

The μ for both the erosion and no erosion case are also multiplied by a correction factor to account for the increased impact flux for early in Mars history. Based on Table 1 from Michael, 2013, N is the expected number of craters in the last column (craters km^{-2} Ga^{-1}). Taking the cumulative density N at 1 km from Table 1, we have $N_{wrong} = 5.84 \times 10^{-4} t$ which incorrectly assumes that the modern impact flux over the past 10 million years has always held. Empirical estimates of modern impact flux are based on satellite observations of newly-appeared craters (Daubar et al., 2013) and vary from model predictions by about a factor of four (Daubar et al., 2014). This observed present-day crater flux is uncertain due to spatial nonrandomness in the observations (Daubar et al., 2013), even though the true flux is expected to be almost spatially random (Le Feuvre and Wieczorek, 2008; Kite and Mayer, 2017). In addition, satellite observations may not reflect the changes in flux throughout the different orbital cycles of Mars over the recent past 10 million years (Kite and Mayer, 2017). As a result, we focus on the Michael (2013) flux instead of a flux derived from empirical observations.

Equation 3 from Michael (2013) states that $N = 3.79 \times 10^{-14}(e^{6.93t} - 1) + 5.84 \times 10^{-4} t$. This gives us:

$$correction factor = \frac{N}{N_{wrong}} = \frac{3.79 \times 10^{-14}(e^{6.93t} - 1) + 5.84 \times 10^{-4} t}{5.84 \times 10^{-4} t} \tag{2.6}$$

for the case without erosion. For the case with erosion, t is replaced by d/β where d is again the logarithmic mid-depth (m) for a given crater bin and β is again the erosion rate (nm/a). Uncertain-

ties in this correction factor are discussed in §4.4.

For our model, the range of ages considered were one second to 4.5 Ga with 1000 ages linearly spaced in-between. Similarly, β initially ranged from 1 nm/a to 2000 nm/a with 1000 βs linearly spaced in-between. We then adjusted β so that the plot contained the 1σ, 2σ, and 3σ regions surrounding highest probability. Taking each array of *P(n)* values from each individual crater bin, we found the total probability as the product of all 16 bins:

$$P_{total} = \prod_{n=1}^{16} P(n) \tag{2.7}$$

In addition to evaluating the two-parameter probability distribution, we also collapsed the two-parameter probability array by summing along one dimension (either β or time) to find the normalized one-parameter probability array for time and β. Then for the one-parameter cumulative probability array, we found the cumulative sum of the probability array and then normalized it to a maximum cumulative probability of one.

We calculated the crater density predicted by the best-fit model using the time and β corresponding to the highest predicted probability from our model. We found the expected crater density per km^2 using equations 2.2 and 2.3. The error bars for the crater densities came from the 1σ standard deviation from the center of the cumulative probability distribution in which n, observed number of craters, is equal to μ, expected number of craters for the crater count data.

2.3 Model tests

The purpose of the model tests (Fig. 2.4) is to generate crater distributions based on Michael (2013)'s Table 1 for a given age and erosion rate. We then apply our model to estimate the best fit for age and erosion rate and compare our model's result with the known input. In doing so, we assess whether our model is accurate and examine the uncertainty in our model's predictions.

For test 1, we first found the expected number of craters per bin using Michael (2013) Table 1 (based on Hartmann, 2005) and Equations 2.3 and 2.2. The input parameters for test 1 were Age = 4 Ga, β = 1 nm/a, and Area = 100,000 km^2. The expected craters per bin (corresponding to

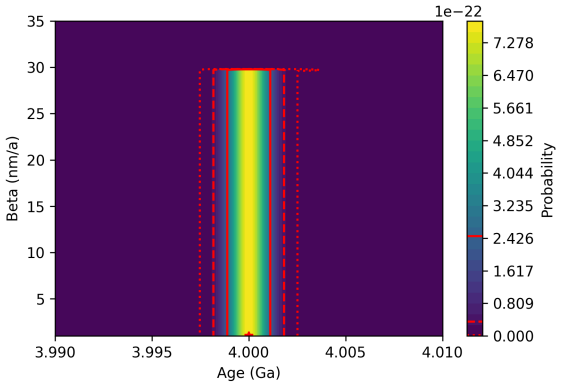

(a) Test 1: Age = 4 Ga. β = 1 nm/a. Area = 100,000 km^2

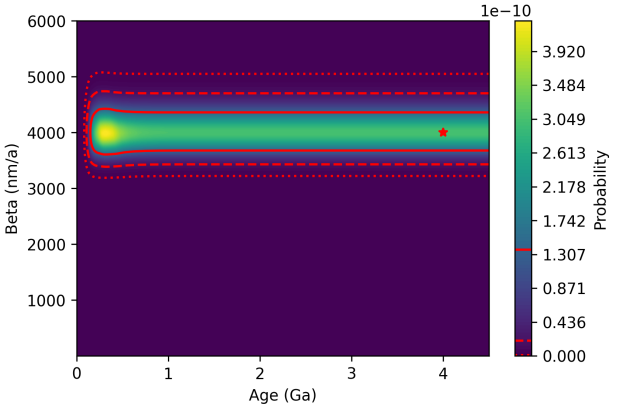

(b) Test 2: Age = 4 Ga. β = 4000 nm/a. Area = 1,000,000 km^2

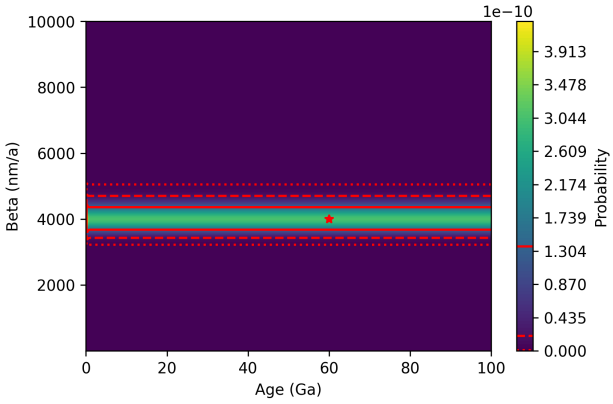

(c) Test 3: Age = 60 Ga. β = 4000 nm/a. Area = 1,000,000 km^2

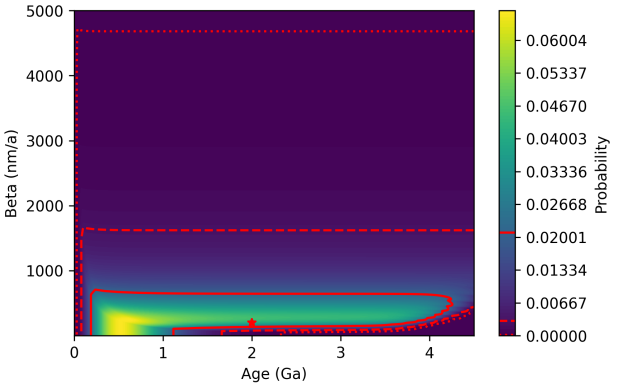

(d) Test 4: Age = 2 Ga. β = 200 nm/a. Area = 1000 km^2.

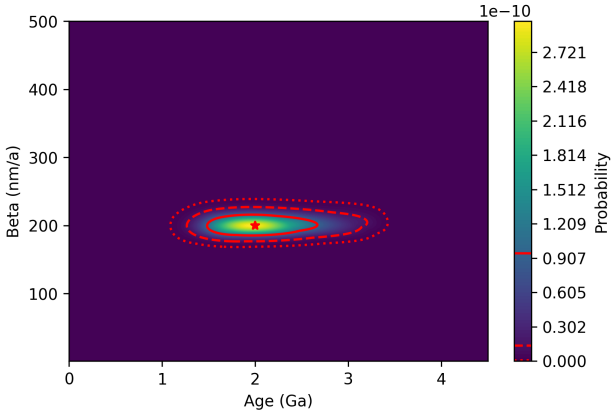

(e) Test 5: Age = 2 Ga. β = 2000 nm/a. Area = 100,000 km^2.

Figure 2.4: Four tests for the model with different age, β, and area inputs. The red star corresponds to the input age and β. Solid line is 1σ, dashed line is 2σ, and dotted line is 3σ.

Michael, 2013 Table 1 bin indices -2 to 13) rounded to the nearest whole number were [30124, 8618, 2308, 959, 513, 275, 148, 79, 43, 23, 12, 7, 3, 2, 1, 0]. From Figure 2.4a, the 1σ range of ages was narrow between 3.99 and 4.01 Ga, however, the 1σ, 2σ, and 3σ uncertainty region for β

almost reached 29.8 nm/a, larger by almost a factor of 30 than the input β = 1 nm/a. The yellow region of highest probability contained the red star, which signified the input parameters.

The input parameters for test 2 were Age = 4 Ga, β = 4000 nm/a, and Area = 1,000,000 km^2. The expected craters per bin were [120, 48, 18, 11, 8, 6, 4, 2, 2, 1, 1, 0, 0, 0, 0, 0]. From Figure 2.4b, we see that age was not well constrained. 3σ for β was better constrained than age, ranging from 3180 to 5080 nm/a. The yellow region of highest probability did not contain the red star representing the input parameters. However, the 1σ region which enclosed 68 percent of the total probability, did contain the red star.

The input parameters for test 3 were Age = 60 Ga, β = 4000 nm/a, and Area = 1,000,000 km^2, corresponding to an unrealistically old surface and assuming the same relationship for impact flux as described in §2.2. The expected craters per bin were [120, 48, 18, 11, 8, 6, 4, 2, 2, 1, 1, 0, 0, 0, 0, 0]. From Figure 2.4c, we see that age was not constrained at all. However, 3σ for β was better constrained to near 4000 nm/a (3180-5080 nm/a for 3σ uncertainty region). In addition, the 1σ uncertainty region contained the red star, indicating the input parameters.

The input parameters for test 4 were Age = 2 Ga, β = 200 nm/a, and Area = 1000 km^2, corresponding to a small area, which is the approximate area of region 7, Upper Mount Sharp. The expected craters per bin (corresponding to Michael, 2013 Table 1 bin indices -2 to 13) were [2, 1, 0, 0, 0, 0, 0, 0, 0, 0, 0, 0, 0, 0, 0, 0]. From Figure 2.4d, we see that age was not well constrained, ranging from 0 to 4.5 Ga for the 3σ region. This is likely due to the minimal number of craters. Maximum β for 1σ versus 3σ varied greatly, from 710 nm/a to 4730 nm/a. The yellow region of highest probability did not include the input parameters, but the 1σ region did.

The input parameters for test 5 were age = 2 Ga, β = 200 nm/a, and area = 100,000 km^2, corresponding to the approximate area of Central Medusae Fossae 1 and the age and β predicted for the region. The expected craters per bin (corresponding to Michael, 2013 Table 1 bin indices -2 to 13) were [239, 97, 37, 21, 14, 7, 4, 2, 1, 1, 0, 0, 0, 0, 0, 0]. The 1σ region had an age above 1.48 Ga and below 2.67 Ga with β between 185 and 216 nm/a. The 3σ region estimated an age between 1.08 and 3.43 Ga with a similar β to the 1σ region between 168 and 239 nm/a. The region

of highest probability contained the red star.

Thus, we see that for older ages and smaller number of craters, it is more difficult for the model to sharply constrain age. However, for all cases, the 1σ error envelope included the input parameters for age and erosion rate.

2.4 Finding sedimentation and erosion for each region

Using the best fit time and β, we also created plots to demonstrate the periods of sedimentation and erosion for each of the 14 areas. Mound thickness lost for each region was the best fit time multiplied by the best fit β:

$$T_{lost} = \beta t \tag{2.8}$$

Present-day thickness for each sedimentary mound was found with a range of techniques (Table 2.1), depending on available values in literature. Present-day thickness for Aeolis Planum was assumed to be 0.3 km (Kite et al., 2015), 1 km for Eastern Candor (Scott and Tanaka, 1986), and 1 km for Upper Mt. Sharp (Kite et al., 2016).

For the two Central Medusae Fossae regions and the East Medusae Fossae region, we calculated present-day thickness as follows:

$$T_{present} = E_{maximum} - E_{basal} \tag{2.9}$$

where $T_{present}$ is present-day thickness in meters (m). $E_{maximum}$ is the region's maximum elevation obtained from Mars Orbiter Laser Altimeter (MOLA) data (Smith et al., 2001). E_{basal} in meters (m) is from values of matching regions within Bradley et al. (2002)'s Table 2. Both Central Medusae Fossae regions corresponded to "Section 2" in Table 2 of Bradley et al. (2002). East Medusae Fossae corresponded to Section 3 in Bradley et al. (2002). Since our regions did not align perfectly with the subsections in Bradley et al., 2002, if a region overlapped several sections from Table 2, we took the average basal elevation of the overlapped sections. Since the Far East

Medusae Fossae had a negative detrended Digital Elevation Model (DEM) basal elevation estimate in Bradley et al. (2002), we determined the region's present-day thickness using inverse distance weighting (IDW) interpolation in ArcGIS to calculate the basal surface elevation.

Figure 16 from Lewis and Aharonson (2014) reveals common stratigraphic periodicity across multiple rhythmic geologic units, which may indicate a common origin from regional-scale deposition. We calculated the global average deposition rate $R_{sedimentation}$ by taking the average bedding scale in meters from the eleven sites in Figure 16 of Lewis and Aharonson (2014) divided by the 120 kyr obliquity of Mars. Adopting the idea of a common deposition origin, we consider the simple case in which the sedimentation occurs in a single episode and as mentioned in §1.4, based on sedimentation rates over ten times greater than our erosion rates, we can approximate the sedimentation rate as instantaneous. While hiatuses in deposition may have occurred along with unconformities in the stratigraphy, our approach focuses only on a single episode of sedimentation.

The thickness for each mound in meters was estimated as follows:

$$T_{mound} = \begin{cases} T_{present} + \beta t & T \leq T_{maxthickness} \\ T_{max} - R_{sedimentation} t & T_{maxthickness} < T \end{cases} \tag{2.10}$$

where $T_{maxthickness}$ is the maximum mound thickness. We approximate maximum thickness as the best fit time multiplied by the best fit β predicted by our two-parameter model.

Mound volume is the mound thickness multiplied by the area:

$$V_{mound} = T_{mound} a \tag{2.11}$$

The error envelope was constrained by the 2σ uncertainty of the two-parameter probability distribution. The minimum and maximum t and β corresponded to the maximum and minimum values of these parameters lying within the 2σ region. Both the minimum and maximum β were then used in the first part of equation 2.10 to find minimum and maximum thickness, as well as minimum and maximum volume using equation 2.11. Up to the age of maximum thickness, the

error envelope was between the minimum and maximum thickness (or volume). After the age of maximum thickness, the upper bound of the error envelope remained at maximum thickness (or volume), but the lower bound dropped to zero.

Model Python scripts to generate the figures are available in the Appendix, §A.1.

RESULTS

3.1 Two-parameter model output

All two-parameter contour plots are in Figure 3.1 and model predictions are summarized in Table 3.1. Region specific results are below.

3.1.1 Central Medusae Fossae 1

From Figure 3.1a, while the estimated age ranges are similar between all three areas of Central Medusae Fossae 1, areas B and C have a higher β between 420 to 879 nm/a, whereas area A has a smaller erosion rate closer to 200 nm/a.

3.1.2 Aeolis Planum

For the 3σ region, at very young ages, the β also drops to 0.00 nm/a, suggesting that such low β values would only be possible with very young ages.

3.1.3 Eastern Candor

Within the entire Eastern Candor region studied, there were only five craters, with four craters in the smallest crater bin diameter size.

3.1.4 Central Medusae Fossae 2

Region C of Central Medusae Fossae 1 had the most tightly constrained age between 2.98 to 3.51 Ga and β between 77.7-99.2 nm/a.

3.1.5 Far East Medusae Fossae

While best fit age is low, we see that the 3σ uncertainty range is very wide, spanning a range of about 4 billion years. Region C of Far East Medusae Fossae is similar to region B with a younger age estimated within the 1σ region but a right tail permitting higher ages for larger σ uncertainty regions.

Site	Best Fit		1σ		2σ		3σ	
	t (Ga)	β (nm/a)	t (Ga)	β (nm/a)	t (Ga)	β (nm/a)	t (Ga)	β (nm/a)
1A	1.43	205	1.00-2.88	176-239	0.814-3.51	161-266	0.662-3.66	147-293
1B	1.89	562	0.952-3.683	493-639	0.570-3.94	455-698	0.419-4.09	422-762
1C	1.67	646	1.13-3.82	570-734	0.883-4.03	528-799	0.635-4.18	491-869
2	0.473	1910	0.123-4.50	0.00-2470	0.088-4.50	0.00-2970	0.060-4.50	0.00-3580
3	0.420	1140	0.065-4.50	0.00-2470	0.036-4.50	0.00-4490	0.017-4.50	0.00-8970
4A	1.81	394	1.02-3.42	348-452	0.709-3.72	321-492	0.548-3.90	298-537
4B	2.59	496	1.47-3.76	352-580	1.039-3.97	385-646	0.687-4.13	423-720
4C	3.41	87.6	3.26-3.44	83.1-92.5	3.15-3.48	80.3-95.8	2.98-3.51	77.7-99.2
5A	0.272	4010	0.022-4.50	0.00-6410	0.037-4.50	0.00-9040	0.063-4.50	0.00-13200
5B	0.675	747	0.457-1.20	662-853	0.375-3.93	614-929	0.305-4.24	570-1020
5C	0.373	1690	0.235-4.50	1450-1980	0.146-4.50	1330-2200	0.111-4.50	1220-2440
6A	0.730	657	0.486-1.41	582-747	0.398-3.83	539-812	0.320-4.12	500-885
6B	0.420	2590	0.092-4.50	2180-3010	0.123-4.50	1970-3450	0.202-4.50	1790-3890
7	2.04	165	0.553-3.95	0.00-360	0.272-4.40	0.00-655	0.146-4.50	0.00-1308
All	1.37	516	1.03-1.611	500-536	0.926-1.90	488-548	0.828-2.34	478-560

Table 3.1: Summary of two-parameter model predictions for age and β including best fit estimates, and 1σ, 2σ, and 3σ uncertainty ranges.

3.1.6 East Medusae Fossae

We see that both the Far East Medusae Fossae and East Medusae Fossae regions have younger ages with older age tails for larger σ regions. Despite being next to each other, region A and region B have very different predicted erosion rates (500-885 nm/a vs. 1790-3890 nm/a).

3.1.7 Gale's Mound/Upper Mount Sharp

Besides having a broad range for the erosion rate estimate, we also see that on the left-hand side of the plot, the 3σ uncertainty region drops to 0.00 nm/a for erosion rate, indicating that the lowest erosion rate values only occur with younger ages. Within the entire Upper Mount Sharp region studied, there were only five craters, with two craters in the two smallest crater bin diameter sizes.

3.1.8 All 14 areas

When combining the crater count data for all 14 areas, we see that the age and especially β are tightly constrained within the framework of the model assumptions. The 3σ certainty for age is from over 0.7 Ga to 2 Ga. The 3σ certainty for β is between 478 nm/a to 560 nm/a.

3.2 One-parameter posterior probability distribution functions

After collapsing the two-parameter probability contour plot along β to form a one-parameter probability distribution function (PDF) of age in Figure 3.2a, we compared the age probability distributions for each region. Central Medusae Fossae 2 region C (4c), has a much higher and more defined probability by over a factor of seven in comparison with the other regions.

After removing area 4c in Figure 3.2b, we see that Eastern Candor (3), has a well-defined PDF for young age at less than 0.2 Ga, though at a relatively smaller probability and with a long right tail for older ages up to 4.5 Ga. Areas Far East Medusae Fossae B (5b) and East Medusae Fossae A (6a) also have similar behavior to Eastern Candor and very similar behavior to each other. Central Medusae Fossae 1 (1a-1c), Central Medusae Fossae 2 (4a, 4b), Far East Medusae Fossae (5a), East Medusae Fossae (6b) and Upper Mount Sharp (7) are much less well-defined.

Figure 3.2c reveals that β values are better constrained than age values. Again, here we see that area Central Medusae Fossae 2 region C (4c) stands out with the sharpest peak at a relatively small β around 100 nm/a with a peak probability by over a factor of two times the other probability maxima. Sites Central Medusae Fossae 1 (1a-1c), Central Medusae Fossae 2 (4a-4c), Far East Medusae Fossae B (5b), and East Medusae Fossae A (6a) have well-constrained β probability densities between 100 to 1000 nm/a. Aeolis Planum (2), Far East Medusae Fossae region C (5c), and East Medusae Fossae region B (6b) have higher well-constrained β values between 1000 nm/a to 10000 nm/a. Eastern Candor (3), Gale's Mound, and Far East Medusae Fossae A (5a) are the least well-defined with the flattest and widest probability peaks.

As expected, Figure 3.2d is consistent with Figure 3.2a and we see that area 4c, Central Medusae Fossae 2 region C, has the most well-defined age constrained within 0.1 Ga or 100 million years in the 1σ error region in contrast with the cumulative probability distribution function (CDF) curves for the other locations. The least well-defined age is for Far East Medusae A (5a), which has the widest 1σ error region that spans over 2 billion years. Aeolis Planum, Far East Medusae Fossae C, East Medusae Fossae B, and Gale's Mound all have similiar CDFs as well. On the other hand, Far East Medusae B (5b) has a narrower 1σ error regions that span about a length of time

corresponding to 0.5 Ga. Eastern Candor (3) and East Medusae Fossae A (6a) also both have 1σ error regions constrained within 1 Ga. Eastern Candor (3) has an upper 1σ error bound below 1 Ga in age. All six Central Medusae Fossae regions (1a-1c, 4a-4c) have lower 1σ error bounds older than 1 Ga and upper 1σ error bounds between 2.0 and 3.2 Ga, which makes the Central Medusae Fossae regions the oldest among the sedimentary mounds examined in this study.

In Figure 3.2e, well-constrained cumulative probability curves (with tight 1σ error bounds) include all regions except Eastern Candor (3) and Gale's Mound (7). All but Aeolis Planum, Eastern Candor, Far East Medusae Fossae A and C (5a, 5c), and Upper Mt. Sharp have 1σ uncertainty β values below 1000 nm/a. Eastern Candor is the least well-defined.

3.3 Best fit assessment

Since there are fewer impacts on Mars with larger crater diameters, crater density decreases with increasing crater diameter (Figure 3.3). Table 3.1 provides a summary of best fit and uncertainty region values for all 14 areas. From Figures 3.3a through 3.3n, the regions with best fit model predictions that were the most consistent with the crater data included Central Medusae Fossae 1a 3.3a and 1b 3.3b, Central Medusae Fossae 2 A and 2 C 3.3h, Far East Medusae Fossae B 3.3j and C 3.3k, East Medusae Fossae A 3.3l), and all 14 regions. It is unclear whether the model was a good fit for regions such as Eastern Candor in Figure 3.3e, where there were relatively few filled crater bins to compare with the model. We also see that for Central Medusae Fossae 1 C, the lower crater density in the sixth bin decreases the model's predictions for other bins.

3.4 Mound thickness history by region

Figures 3.4a through 3.4n demonstrate erosion and sedimentation periods for each of the 14 regions. As described in §2.4, the center black line was calculated from the best fit β and time from our model and present-day thickness values. The lighter cyan envelope represents the 2σ error region and the darker cyan envelope represents the 1σ region.

The sedimentation history that is best constrained (within the framework of our model assumptions) is Central Medusae Fossae 2 C (4c) in Figure 3.4h, signifying that the region was most likely

formed between 3.1 to 3.5 Ga. The least well constrained areas for age are Aeolis Planum in Figure 3.4d, Eastern Candor in Figure 3.4e, Far East Medusae Fossae A in Figure 3.4i, Far East Medusae Fossae C in Figure 3.4k, East Medusae Fossae B in Figure 3.4m, and Upper Mt. Sharp in Figure 3.4n.

As seen from Figure 3.5 (a), according to the best fit, the sedimentation mounds that are predicted to contribute the most volume are Central Medusae Fossae 1B and 1C (volume 1b and 1c) Central Medusae Fossae 2B and 2C (volume 4b and 4c) and East Medusae Fossae B (volume 6b). Based on best fit age estimates, for ages older than 1 billion year, Central Medusae Fossae 1 B and C (volumes 1b and 1c) and Central Medusae Fossae 2 B and C (volumes 4b and 4c) contribute the most to the total volume. For ages younger than 0.5 Ga, East Medusae Fossae (volume 6b) contributes the highest proportion of the total volume. Aeolis Planum (volume 2), Eastern Candor (volume 3), Far East Medusae Fossae A and B (volumes 5a, 5b) and East Medusae Fossae A and B (volumes 6a and 6b) are all volume additions younger than 0.75 Gyr. As a result, there is evidence for young sedimentary rocks for all regions other than Central Medusae Fossae based on the model's best fit predictions, however, these results require further validation because of the model's untested assumptions and large parameter uncertainties in the model output.

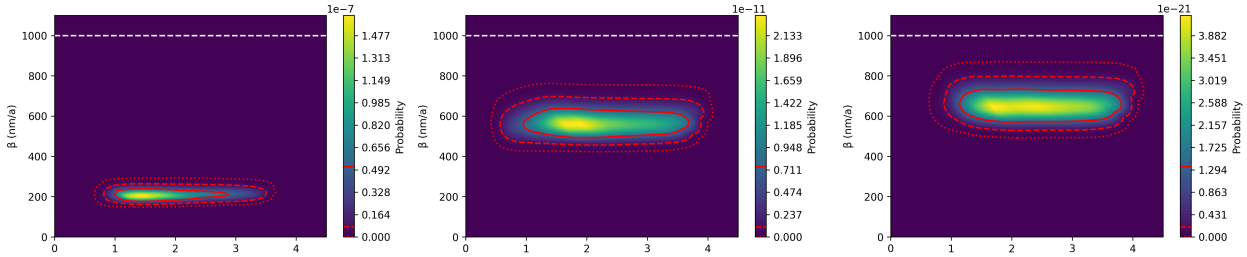

(a) Central Medusae Fossae 1: A (b) Central Medusae Fossae 1: B (c) Central Medusae Fossae 1: C

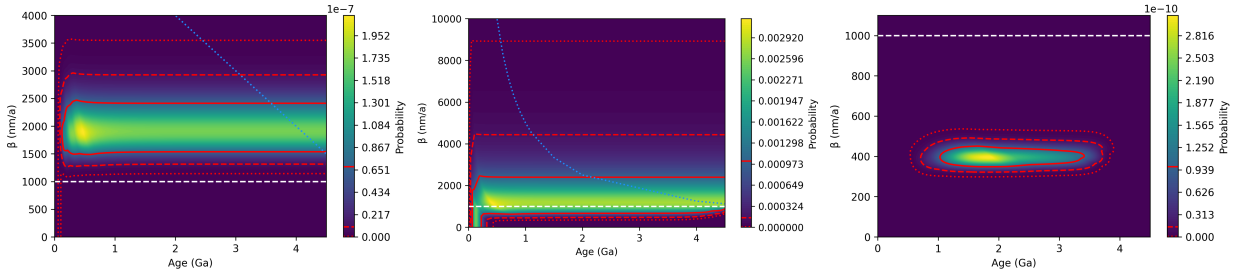

(d) Aeolis Planum (e) Eastern Candor (f) Central Medusae Fossae 2: A

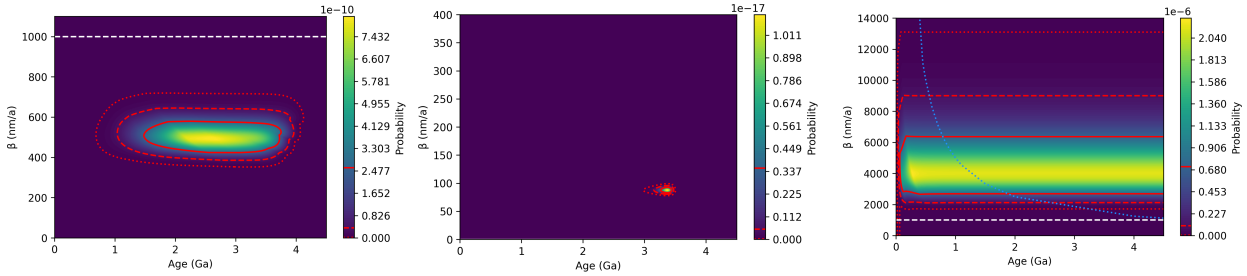

(g) Central Medusae Fossae 2: B (h) Central Medusae Fossae 2: C (i) Far East Medusae Fossae: A

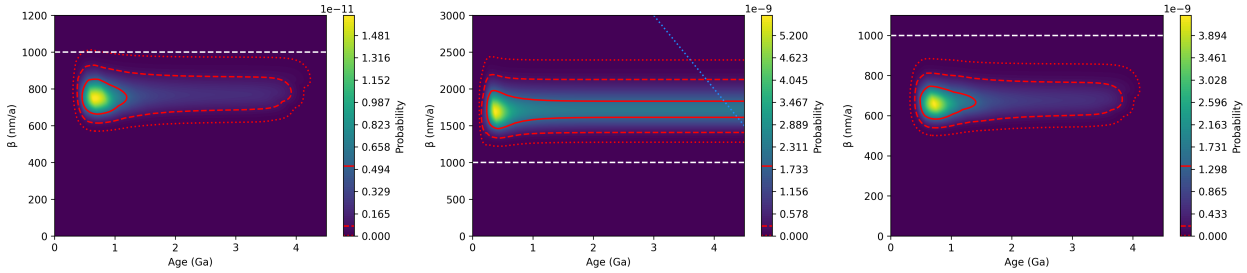

(j) Far East Medusae Fossae: B (k) Far East Medusae Fossae: C (l) East Medusae Fossae: A

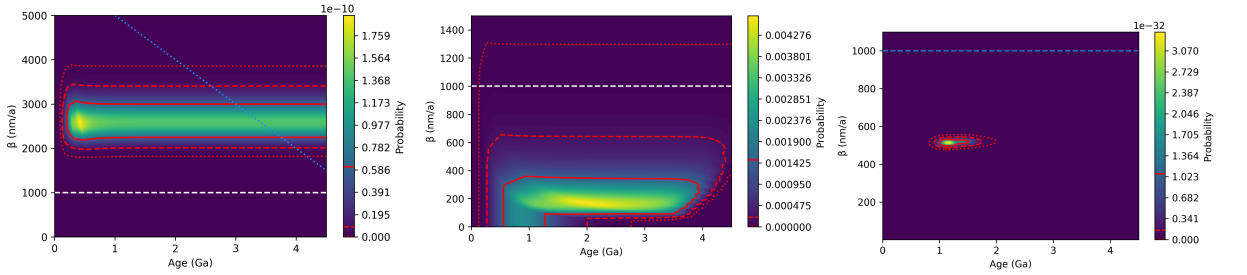

(m) East Medusae Fossae: B (n) Upper Mount Sharp (o) All 14 Regions

Figure 3.1: For the plot of each region, the red solid line represents the 1σ uncertainty region, the dashed red line represents the 2σ uncertainty region, and the dotted red line represents the 3σ uncertainty region. Yellow regions highlight the area of most probable age and β while the darkest purple is for least likely age and β. The y-axis scale for β varies between each area to best showcase the probability region. The dashed white line at 1000 nm/a indicates the minimum erosion rate needed for metastable water ice at depths shallow enough to be detected by Gamma Ray Spectroscopy (GRS) or Neutron Spectroscopy (NS). The value of 1000 nm/a is based on the right dashed line of Figure 12 from Hudson et al. (2007). The right dashed line demonstrates retreat depth versus time for a higher value of the diffusion coefficient in the lag-forming case with an initial barrier of 1 mm. The lag forming case occurs when ice fills a low-porosity regolith so that the removal of ice leaves behind a lag that increases in thickness (Hudson et al., 2007). From Figure 12, the right dashed line shows a retreat depth to 1 m in 10^6 years, which is equivalent to 1000 nm/a. This means that if β is greater than 1000 nm/a, the depth to the buried ice will be less than 1 m. The dotted blue line is a reference value for 5 km of erosion at each given age and β value.

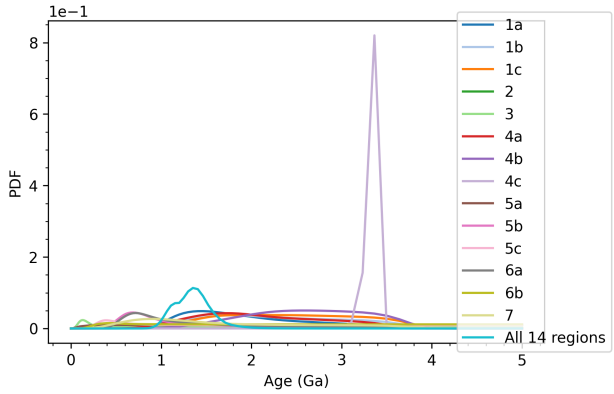

(a) Age probabilities for all regions.

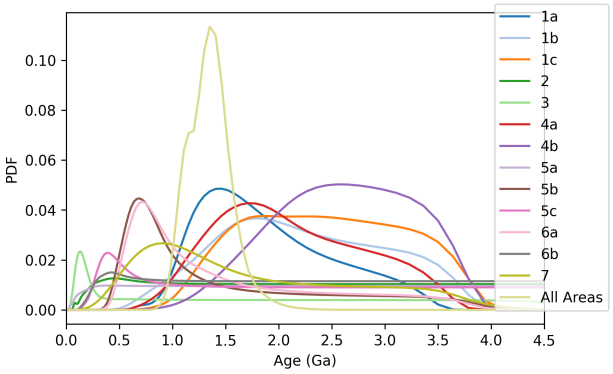

(b) Age probabilities for 13 regions, not including Central Medusae Fossae 2 C.

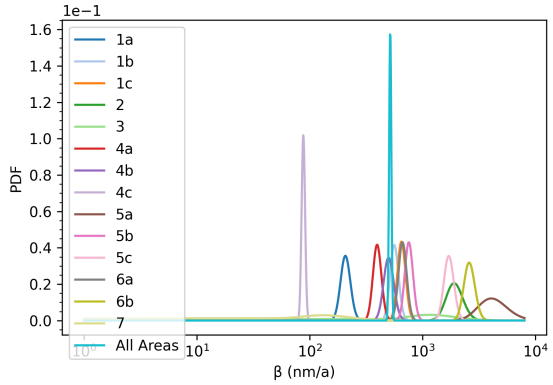

(c) β probabilities for all 14 regions.

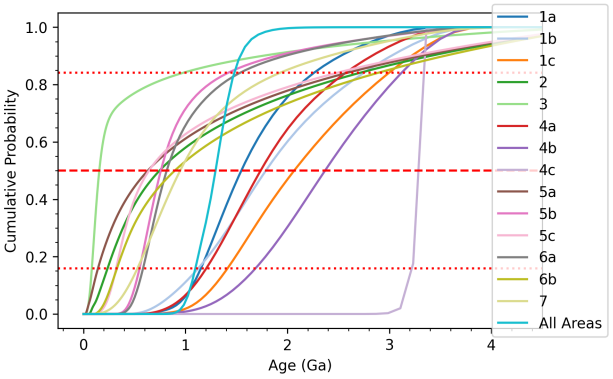

(d) Age cumulative probabilities for all 14 regions.

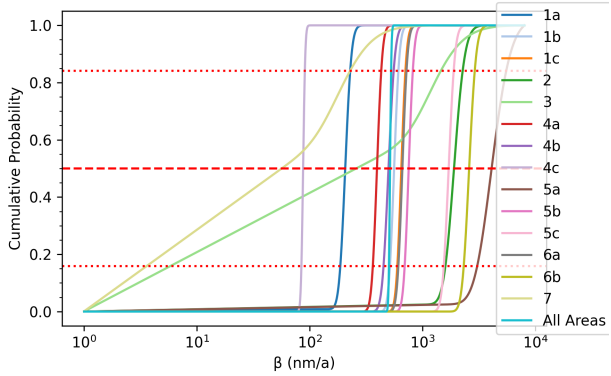

(e) β cumulative probabilities for all 14 regions.

Figure 3.2: Legend: 1a, 1b and 1c corresponds to Central Medussae Fossae 1 A, B, and C. 2 represents Aeolis Planum. 3 represents Eastern Candor. 4a, 4b, and 4c corresponds to Central Medusae Fossae 2 A, B, and C. 5a, 5b, and 5c corresponds to Far East Medusae Fossae A, B, and C. 6a and 6b correspond to East Medusae Fossae A and B. 7 is Upper Mt. Sharp. (a), (b), and (c) corresponds to probability distributions for the regions, including both age (a, b) and β (c). (d) and (e) present the cumulative probability distributions (CDFs) for both age (d) and β (e) in all 14 regions. The dashed red line corresponds to the median of the cumulative distribution and the red dotted lines correspond to the 1σ error range.

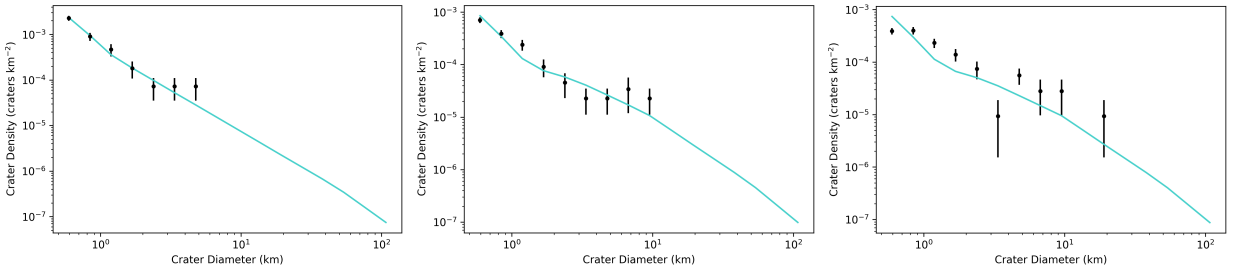

(a) Central Medusae Fossae 1: A (b) Central Medusae Fossae 1: B (c) Central Medusae Fossae 1: C

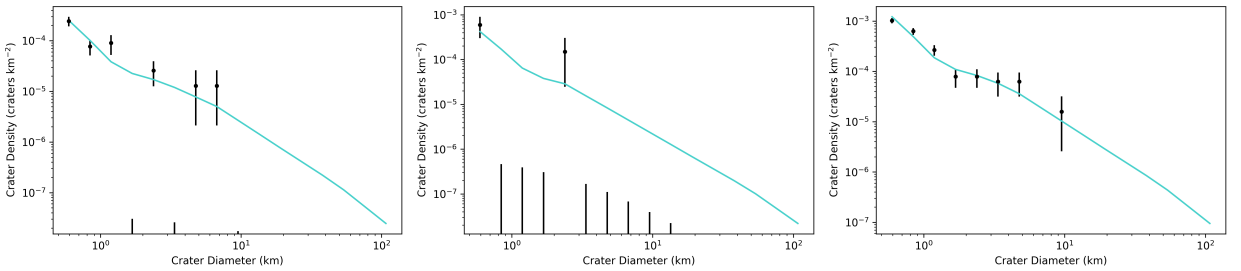

(d) Aeolis Planum (e) Eastern Candor (f) Central Medusae Fossae 2: A

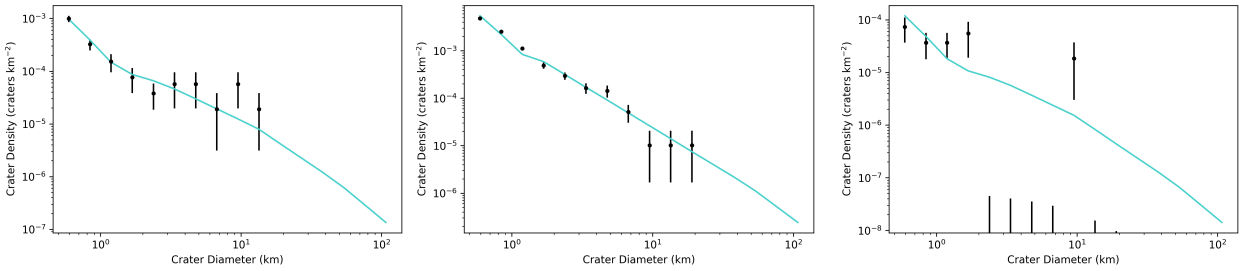

(g) Central Medusae Fossae 2: B (h) Central Medusae Fossae 2: C (i) Far East Medusae Fossae: A

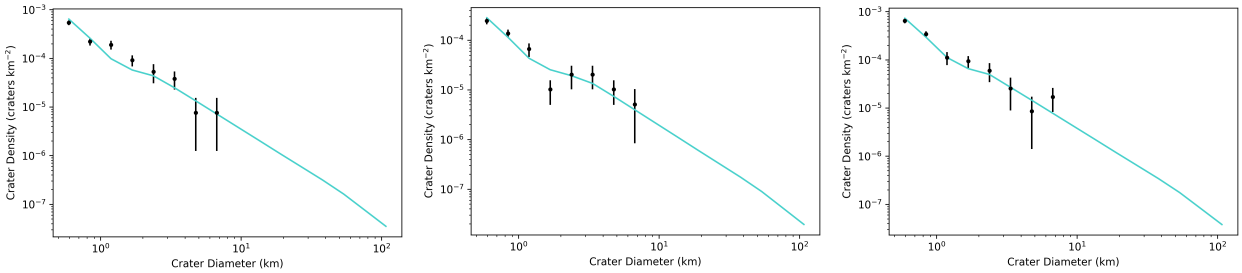

(j) Far East Medusae Fossae: B (k) Far East Medusae Fossae: C (l) East Medusae Fossae: A

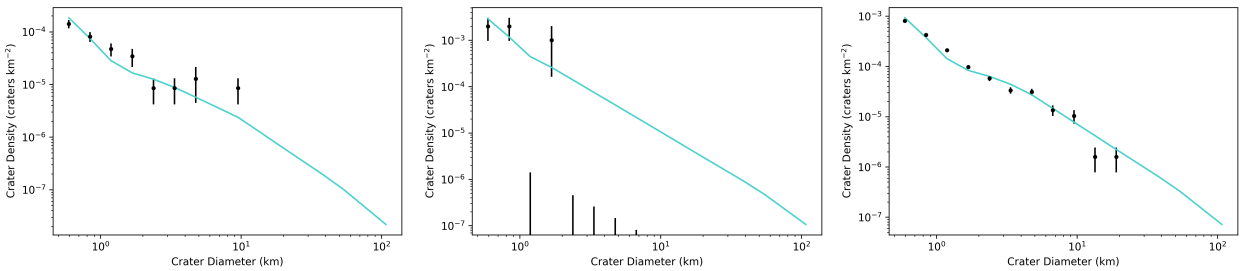

(m) East Medusae Fossae: B (n) Upper Mount Sharp (o) All 14 Regions

Figure 3.3: The cyan line in each plot represents the crater density calculation using the model's best fit age and β for each region. The black data points signify the crater density (craters/km^2) per bin. Bins without craters do not have black points. Black vertical bars represent the 1σ error range by extrapolating from a cumulative distribution of each crater bin. The error bars of the larger bins are not visible because they are on the magnitude of 10^{-10}.

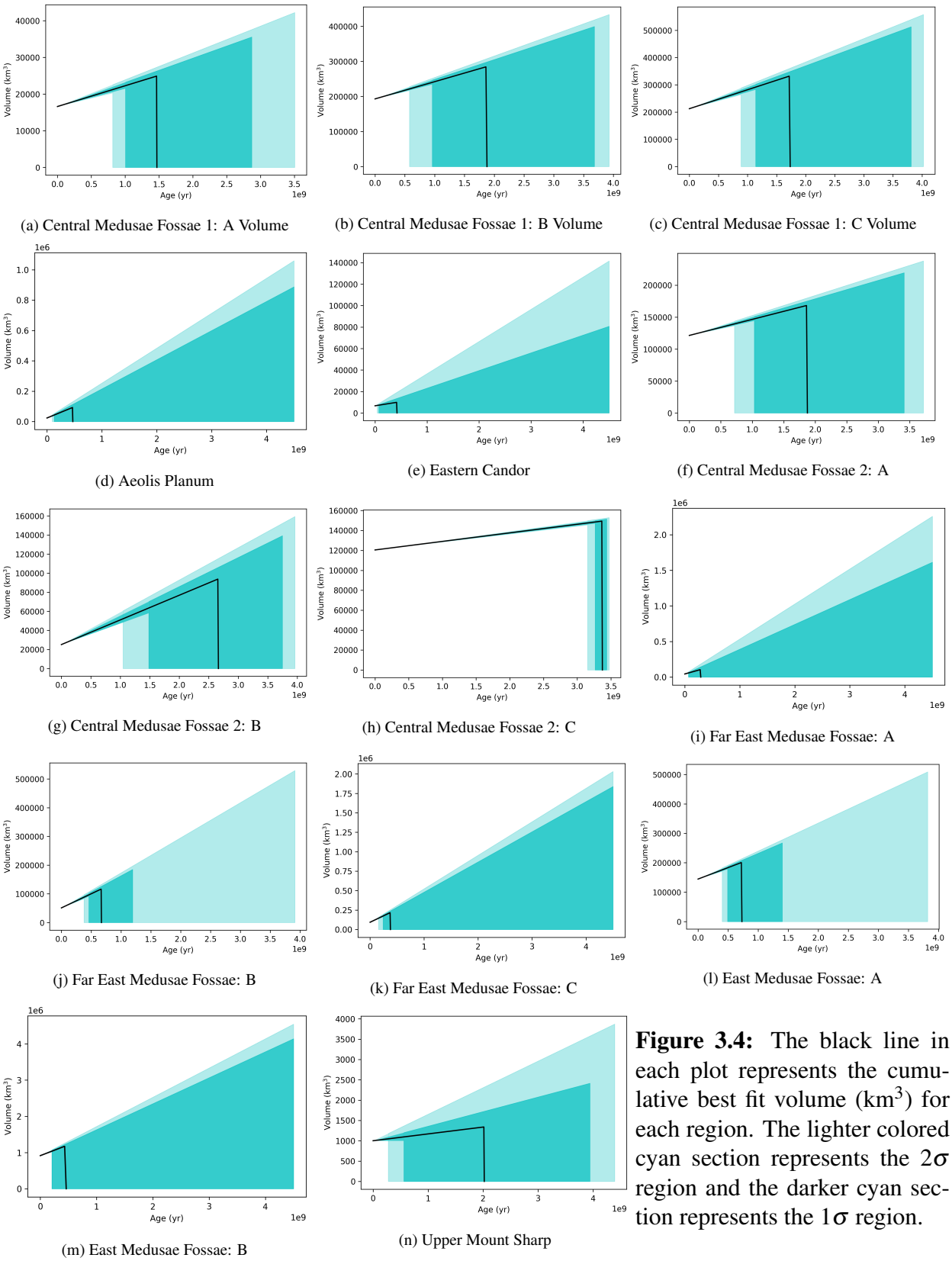

(a) Central Medusae Fossae 1: A Volume

(b) Central Medusae Fossae 1: B Volume

(c) Central Medusae Fossae 1: C Volume

(d) Aeolis Planum

(e) Eastern Candor

(f) Central Medusae Fossae 2: A

(g) Central Medusae Fossae 2: B

(h) Central Medusae Fossae 2: C

(i) Far East Medusae Fossae: A

(j) Far East Medusae Fossae: B

(k) Far East Medusae Fossae: C

(l) East Medusae Fossae: A

(m) East Medusae Fossae: B

(n) Upper Mount Sharp

Figure 3.4: The black line in each plot represents the cumulative best fit volume (km^3) for each region. The lighter colored cyan section represents the 2σ region and the darker cyan section represents the 1σ region.

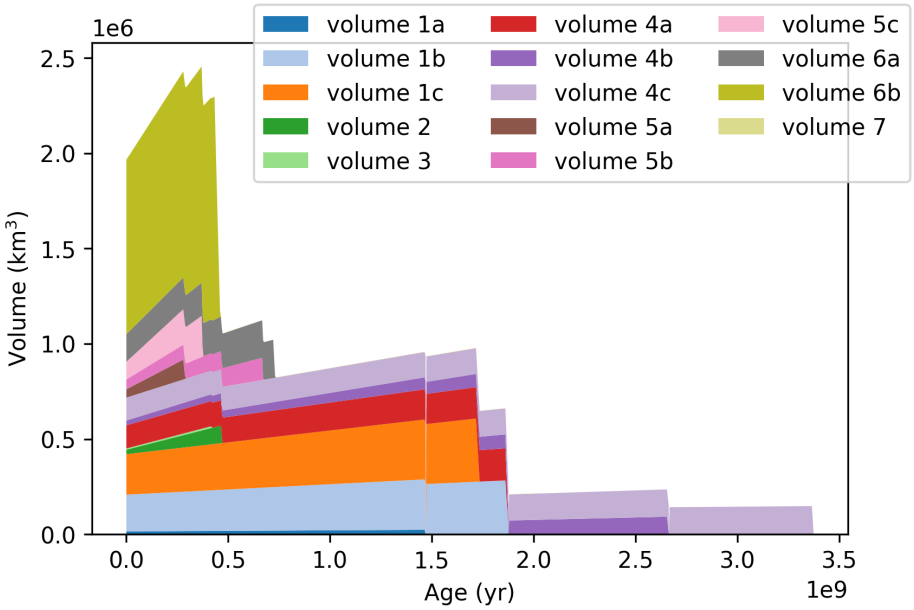

(a) Cumulative volume labeled by color for each of the 14 regions. Volume 1a, 1b and 1c correspond to Central Medusae Fossae 1 A, B, and C. Volume 2 represents Aeolis Planum. Volume 3 represents Eastern Candor. Volume 4a, 4b, and 4c correspond to Central Medusae Fossae 2 A, B, and C. Volume 5a, 5b, and 5c correspond to Far East Medusae Fossae A, B, and C. Volume 6a and 6b correspond to East Medusae Fossae A and B. Volume 7 represents Upper Mt. Sharp.

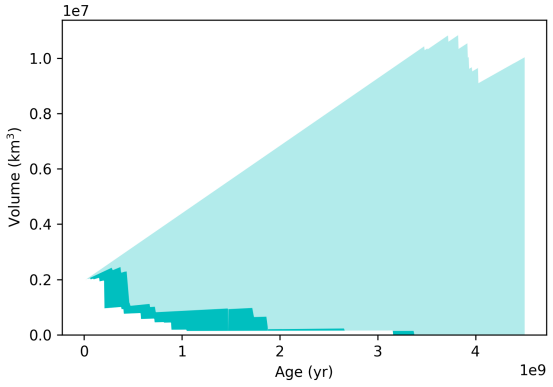

(b) The darker cyan section represents the cumulative best fit volume for all 14 regions. The lighter colored cyan section represents the upper 2σ limit. The edge between the darker cyan section and the white section represents the lower 2σ limit.

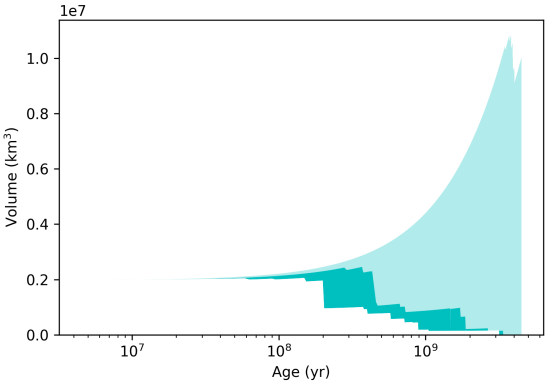

(c) The same as (b) but with a log scale on time.

Figure 3.5

DISCUSSION

4.1 Synthesis and overall trends from figures

4.1.1 Central Medusae Fossae

A common trend throughout the two-parameter probability figures, one-parameter probability figures, best fit figures, and sedimentation figures is the tight precision on Central Medusae Fossae 2 C (4c) in contrast with the other regions. Central Medusae Fossae 2 C in Figure 3.1a has the most tightly constrained age and β out of all the regions, with all three σ error regions falling between 2.98-3.51 Ga for age, and a best fit prediction for β between 77.7-99.2 nm/a. All six Central Medusae Fossae regions have well-defined β values that are also all below 1000 nm/a. However, besides Central Medusae Fossae 2 C (4c), the five remaining regions have poorly constrained ages that have 3σ error regions that span around 3 Ga. Out of the six Central Medusae Fossae regions, the model had the most difficulty predicting Central Medusae Fossae 1 C, Figure 3.3c. In terms of total volume deposited, Figure 3.5 reveals that out of all the regions, the model predicts that Central Medusae Fossae 1 and 2 were the main source of volume for ages over 0.75 Ga, with Central Medusae Fossae 1 B and C (1b, 1c) contributing the most volume for ages older than 0.75 Ga.

4.1.2 Far East Medusae Fossae

For all three regions of Far East Medusae Fossae, the best fit of the model predicted young ages below 1 Ga, however, the 2σ and 3σ regions extend to older ages, such as up to 4.50 Ga for 5a and 5c. The β estimate for Far East Medusae Fossae A (5a) had the greatest uncertainty and the highest beta estimate at over 4000 nm/a. Similarly, the age estimate for Far East Medusae Fossae A (5a) also had the greatest uncertainty predicting a non-zero probability over a period of 4.5 billion years. According to Figures 3.3, the model's prediction aligned well with the craters for Far East Medusae Fossae B and C, the model did not predict Far East Medusae Fossae A as accurately. According to the best fit volume prediction in Figure 3.5, all of the material for Far East Medusae Fossae was deposited within the last 0.75 Ga.

4.1.3 East Medusae Fossae

The best fit predictions for East Medusae Fossae A and B both have a young age below 1 Ga. However, the 3σ upper bounds go up to older ages of 4.12 Ga and 4.50 Ga for the 2 σ and 3 σ error regions of East Medusae Fossae A and B. While East Medusae Fossae A has a more well-defined β prediction at 657 nm/a, East Medusae Fossae B has a maximum probability prediction of β at 3890 nm/a. While age is not very well-defined for both regions, East Medusae Fossae A has a more pronounced peak at 0.730 Ga (Figure 3.2a, whereas East Medusae Fossae B has a less well-defined peak at 0.420 Ga with a non-zero probability extending up to 4.5 Ga. According to Figure 3.3l and 3.3m, the model fit the data of East Medusae Fossae A better than East Medusae Fossae B. Like Far East Medusae Fossae, according to the best fit prediction, all of the material was deposited within the last 0.75 Ga.

4.1.4 Aeolis Planum and Eastern Candor

While both Aeolis Planum and Eastern Candor have young best fit age predictions below 1 Ga (Figures 3.1d, 3.1e). In comparison with other regions for the one-parameter probabilities in Figure 3.2, both Aeolis Planum and Eastern Candor have the least well-defined age and β predictions. While the best fit model predicts that both Aeolis Planum and Eastern Candor have younger ages around 0.5 Ga, the upper 3σ bound on error extends up to 4.50 Ga. However, both 3.3d and 3.3e show the best fit lines falling slightly below the data. Eastern Candor in particular has very few craters, making it difficult for the model to predict an accurate best fit (Figure 3.3e. According to Figures 3.4d and 3.4e, while the best fit volume predicts that the material was deposited within the last 0.5 Ga, the upper 2σ error bound extends up to around 4.5- Ga.

4.1.5 Upper Mount Sharp/Gale's Mound

Similar to Eastern Candor, the two-parameter contour plot for Upper Mount Sharp (Figure 3.1n) demonstrates that β only drops to 0.00 nm/a for the youngest ages within the error regions. While the best fit age estimate is 2.04 Ga for Upper Mount Sharp, the 3σ error envelope extends to 4.5 Ga (3.2a). Other than two bins, Figure 3.3n demonstrates that the best fit from the model aligned

with the crater count data. According to Figure 3.4n, Upper Mount Sharp's volume accumulated 2 billion years ago, however, the upper 2 σ error extends to over 4 billion years.

4.2 Variations with longitude

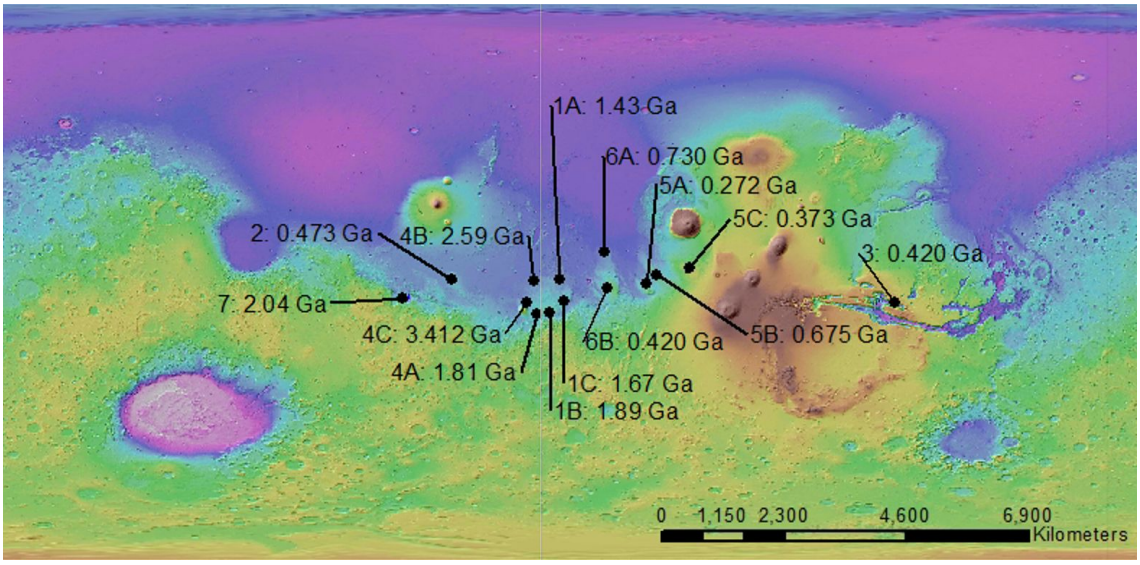

(a) Global map of Mars with 14 study sites labeled with the model's best fit ages.

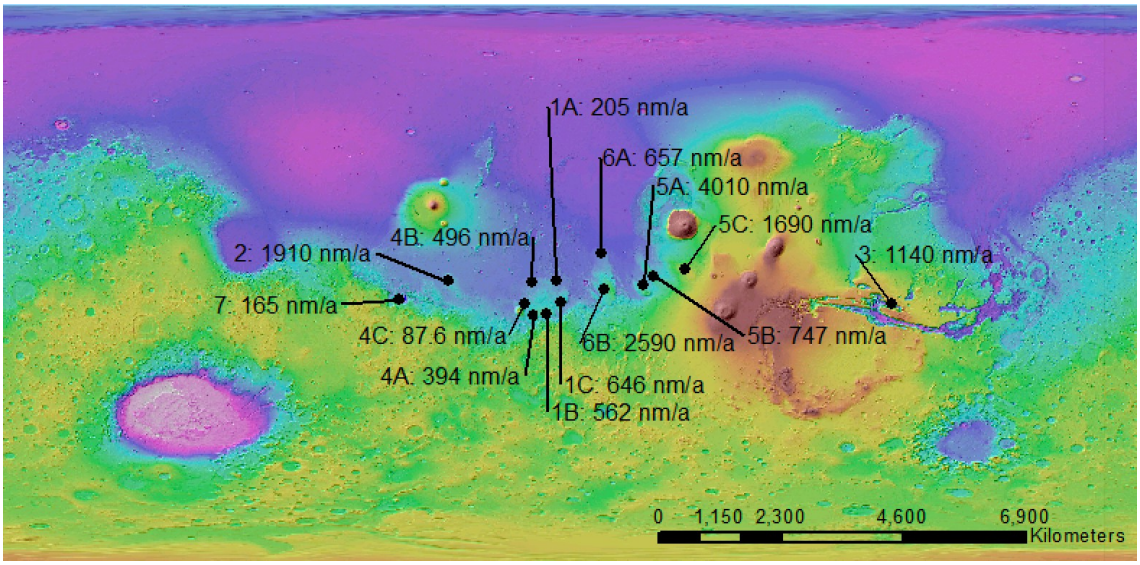

(b) Global map of Mars with 14 study sites labeled with the model's best fit β values.

Figure 4.1: Global map of best fit age and β values.

The global map of best fit age and β values in Figure 4.1 demonstrates trends in age and β by location. Older ages greater than 1 Ga dominate Central Medusae Fossae (sites 1 and 4). Upper Mt. Sharp, which is hypothesized to have similar material to the Medusae Fossae Formation

(Zimbelman and Scheidt, 2012a; Lewis and Aharonson, 2014; Edgett et al., 2020), also has an older age of 2.04 Ga. East Medusae Fossae (6), Far East Medusae Fossae (5), Aeolis Planum (2), and Eastern Candor (3) all had young best fit ages below 0.750 Ga.

For β, the model fitted the lowest erosion rates below 650 nm/a for Central Medusae Fossae (sites 1 and 4) and for Upper Mt. Sharp. On the other hand, for all of the other regions, the model's best fit β predictions were above 740 nm/a. As a result, the results suggest a trend in older ages and lower erosion rates for Central Medusae Fossae and Upper Mt. Sharp, while East Medusae Fossae, Far East Medusae Fossae, Aeolis Planum, and Eastern Candor have younger ages and larger erosion rates.

4.3 Sensitivity test and exclusion of "marked" craters

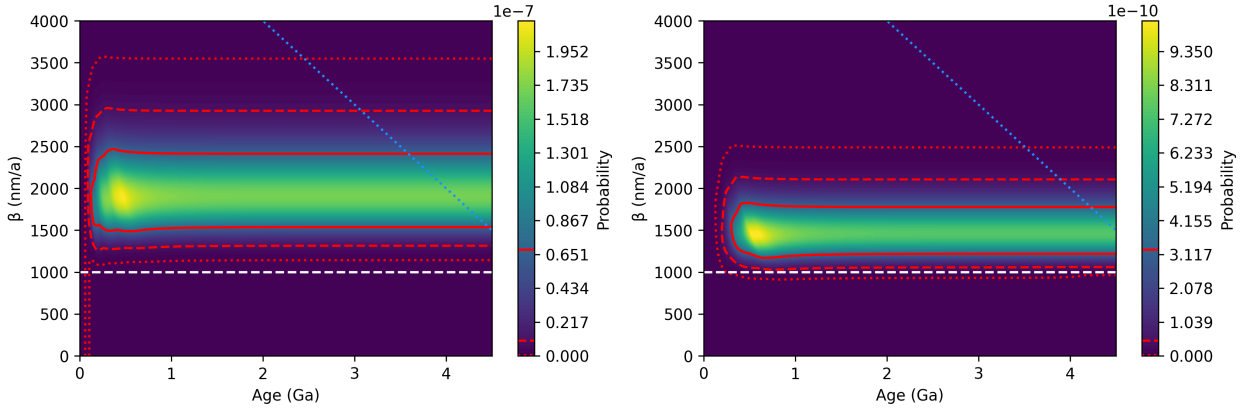

(a) Area 2 Aeolis Planum two-parameter contour plot including only "standard" craters.

(b) Area 2 Aeolis Planum two-parameter contour plot including "marked" and "standard" craters.

Figure 4.2: Comparison of best fit between standard crater and standard with marked crater data.

Site	Best fit		1σ		2σ		3σ	
	t (Ga)	β (nm/a)	t (Ga)	β (nm/a)	t (Ga)	β (nm/a)	t (Ga)	β
Standard craters: 2, Aeolis Planum	0.473	1910	0.123-4.50	0.00-2470	0.088-4.50	0.00-2970	0.060-4.50	0.00-3580
Standard and marked craters: 2, Aeolis Planum	0.576	1450	0.301-4.50	1170-1830	0.198-4.50	1020-2140	0.128-4.50	911-2520

Table 4.1: Comparison of best fit values and 1σ, 2σ, 3σ uncertainty ranges for Site 2 Aeolis Planum with only standard craters versus standard and marked craters.

As described in §2.1, within the crater count data, counts that were not definitively craters were labeled as "marked" and excluded from our study. In this section, we return to the marked craters and compare the model results for Site 2 Aeolis Planum for the dataset without marked craters

and the dataset with marked craters. There were nine craters that were marked in Site 2 Aeolis Planum. As a result, by including these nine craters, Site 2 has 47 counted craters total instead of 36. From the two-parameter plots and the corresponding table of best fit and σ ranges, we can see that the dataset including marked craters had a better constrained β and age, which is expected since typically the more craters that are available in the data, the more accurate the model. The best fit erosion rate decreases by 460 nm/a (a factor of about 0.759), while the best fit age increases from 0.473 Ga to 0.576 Ga (increases by a factor of about 1.22). While marked craters were disregarded in favor of the more confidently observed standard craters in our study, in the case of regions with fewer craters such as Aeolis Planum, we can see that including marked craters does allow a tighter error constraint. Thus, we permit larger uncertainty regions by using only standard craters.

4.4 Model uncertainties

Uncertainties in adapting the Hartmann isochrons (Michael, 2013; Hartmann, 2005) include crater identification, crater counting, homogeneous terrain selection, and secondary crater populations, as well as the application of a crater-flux model that was originally based on lunar crater counts (Hartmann, 2005). The known problem of the overestimation of small craters by crater production functions (Hartmann, 2005; Kite and Mayer, 2017) is addressed by the inclusion of erosion rate in our model (as illustrated in Figure 1.1). The probabilistic model does not take into account variable erosion rate, burial rate, and the obliteration of craters by impacts. In addition, for consideration of each sedimentary mound's sedimentation and erosion history, we assumed an instantaneous sedimentation rate that was the same across all units, based on common trends in periodicity across rhythmic sites in Lewis and Aharonson (2014). For sedimentation on Earth, the Sadler effect predicts that one would expect to see faster sedimentation rates corresponding to thinner stratigraphic sections which cover shorter amounts of time and slower sedimentation rates corresponding to thicker stratigraphic sections that cover longer amounts of time (Jerolmack and Sadler, 2007). While we assumed the same global sedimentation rate for all mound sites, we may be observing a Sadler effect based on the trend between age and erosion rates. We saw in §4.2 that sites with

older ages corresponded to lower erosion rates and sites with younger ages corresponded to higher erosion rates. However, the Sadler effect only becomes an issue when comparing processes that occurred during time periods of widely differing magnitudes (Quantin-Nataf et al., 2019), and the ages in our study were similar in terms of magnitude. Nevertheless, we recommend further work to better constrain the cases in which the Sadler effect has an important role in affecting age and erosion rate estimations on Mars.

4.5 Chi-square test comparison between two-parameter and one-parameter models

Model type	χ^2 test statistic	p-value	Degrees of freedom
Age (x-parameter)	10700	0.0	9
β (one-parameter)	5.10e8	0.0	9
Age and β (two-parameter)	82.1	1.82e-14	8

Table 4.2: Minimum chi-square test results for two-parameter and one-parameter models. Degrees of freedom were calculated as k - 1 - N where k is the number of bins and N is the number of parameters (Wall and Jenkins, 2012). To perform the chi-square test, we combined the five largest crater bins that had <5 craters so that k = 11 bins. This was necessary to ensure that the model-predicted number of craters is >5 craters for 80 percent of the bins.

To examine whether a simpler one-parameter model is preferable to our two-parameter model, we performed minimum chi-square tests–an extension of chi-square goodness-of-fit tests (Wall and Jenkins, 2012)–for the best fit based on the two-parameter model for age and β, best fit along the x-axis for age, and best fit along the y-axis for β for all 14 regions grouped together. All three tests were significant at the 99 percent confidence level since p-values < 0.01, so we can reject the null hypothesis that the crater distributions from the three models are the same as the crater count data. For our purposes of comparing the one-parameter tests with the two-parameter test, we only performed the test on the data from all 14 regions rather than each individual region. As a result, the χ^2 values for all three models were large, in particular for the one-parameter models.

The χ^2 of 82.1 for the two-parameter model was the smallest, however, the χ^2 exceeds the number of bins - 1 then multiplied by 2, since 82.1 > 20. As a result, we still reject the null hypothesis that the two-parameter model's distribution was the same as the crater count distribution. The crater distribution predicted by the two-parameter model ("observed") was the most similar to

the craters in the data ("expected") in comparison with both one-parameter models. On the other hand, the χ^2 values were especially large for both one-parameter models, which suggests that the one-parameter model-predicted values are quite different from the data. Thus, the two-parameter model performs better than the one-parameter models in fitting values that are more consistent with the crater distribution data.

4.6 Implications for the subsurface ice table and in-situ resource utilization

The subsurface ice table is the predicted location or depth of the boundary between icy ground and ice-free ground in the soil. The equatorial climate of Mars is extremely dry and relatively warm, which makes water ice unstable. As a result, the water ice at the equator can sublimate forming water vapor that is then lost by diffusion through empty soil pore space and escapes to the dry atmosphere (ultimately going to the North Polar ice cap). With erosion rates less than 1000 nm/a, the ice can retreat to hundreds of meters of depth, making it too deep to be detected by GRS/NS, which only probe around one meter down. By contrast, if the erosion rate is above 1000 nm/a, the ice table can persist at shallow depths for short durations. The source of the erosion rate 1000 nm/a was explained in the caption of Figure 3.1. The water ice would still be too deep for detection by cameras or infrared spectroscopy, but it would be shallow enough to be detected by GRS/NS. Aeolis Planum, Eastern Candor, Far East Medusae Fossae A, Far East Medusae Fossae C, and East Medusae Fossae B all have β values in the 1σ confidence region above 1000 nm/a. On the other hand, all six regions of Central Medusae Fossae, Far East Medusae Fossae B, East Medusae Fossae A, and Gale Mound have slower erosion rates. As a result, we expect Aeolis Planum, Eastern Candor, Far East Medusae Fossae A, Far East Medusae Fossae C, and East Medusae Fossae B to have the highest likelihood for water ice detection by GRS/NS.

The potential presence of subsurface water at the equator of Mars has implications for in-situ resource utilization (ISRU) as a source of liquid water and propellant. Liquid water is necessary for humans to survive and for life as we know it. While the poles of Mars have large amounts of water ice (Byrne, 2009; Smith et al., 2009), this is less relevant to ISRU because early human

missions are unlikely at those high latitudes (Starr and Muscatello, 2020). Readily accessible water ice at minimal depths (on the meter scale) at the equatorial region of Mars would be invaluable for ISRU (Starr and Muscatello, 2020). In addition to liquid water, through the reaction $CO_2 + 2H_2O$ to $CH_4 + 2O_2$, water would also be useful for producing methane propellant. Producing propellant on Mars is important in order to return a crew from Mars' surface since it is unlikely that the crew would be able to carry all of the propellant they need with them from Earth (Ash et al., 1978). As a result, further investigation of potential subsurface ice tables in the equatorial and mid-latitude regions of Mars are key for future human missions.

4.7 Implications for the sedimentary rock cycle on Mars

According to the best fit volume history for these 14 regions, as summarized in Figure 3.5, we may separate sedimentation into two main periods: ages older than 0.75 Ga and ages younger than 0.75 Ga. For ages older than 0.75 Ga, the volume from Central Medusae Fossae dominated the total volume of the 14 regions. However, for more recent ages younger than 0.75 Ga, East Medusae Fossae B dominates the volume as it contributes over a third of the volume for ages below 0.75 Ga, and around a half of the volume for ages below 0.5 Ga. While there is a large upper error for these regions, it is interesting to note that Eastern Candor, Aeolis Planum, Far East Medusae Fossae, and East Medusae Fossae are all predicted to to be very recent (younger than 0.75 Ga) volume additions. Due to the factor of two to four uncertainty in cratering rates and ages, the dating of lava units around 2 Ga is especialy unreliable (Hartmann, 2005), which is why the incorporation of erosion rate in this study is particularly useful for these older ages observed in Central Medusae Fossae. However, even with the uncertainty, younger ages are insightful as they may require modern volcanism (Hartmann, 2005), as shown through the new sediment added by volcanism in Figure 4.3b. As a result, the predicted young ages of Eastern Candor, Aeolis Planum, Far East Medusae Fossae and East Medusae Fossae may signify interesting requirements on the global martian climate. For example, these young ages are consistent with Fassett et al. (2014)'s predictions of the northern mid-latitude ice periods from the Middle (1.4-0.3 Ga) to Late

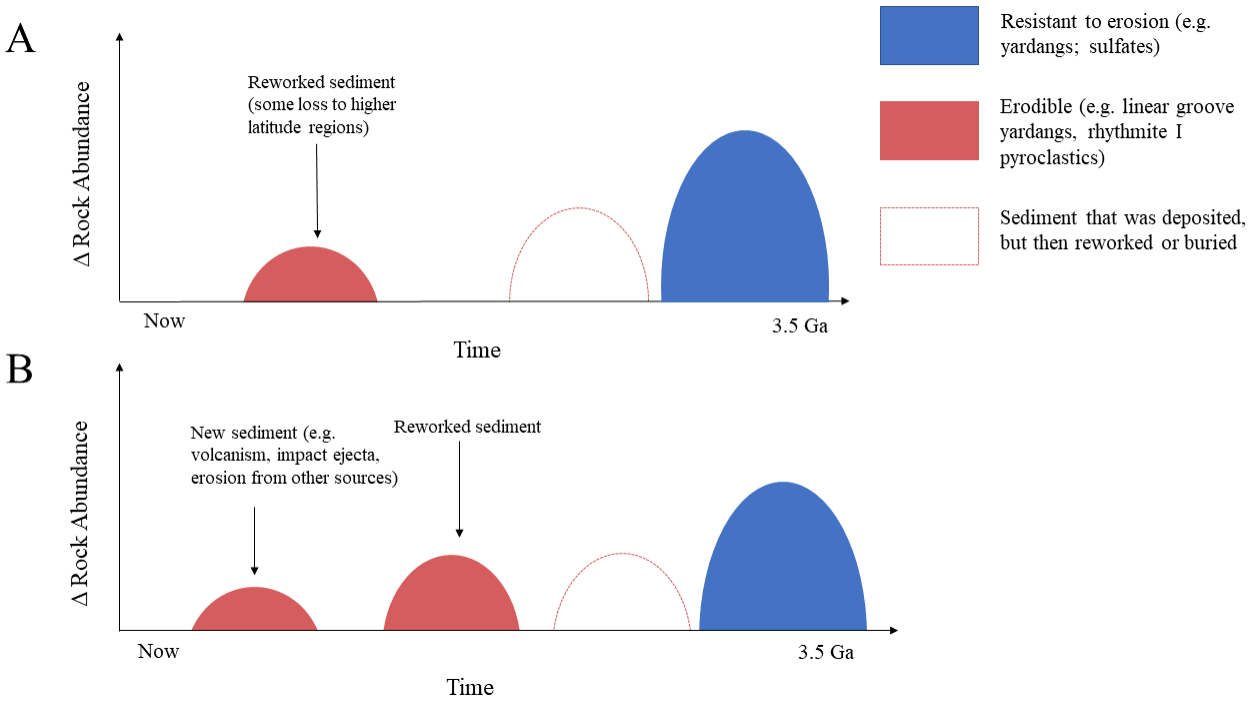

Figure 4.3: Two hypotheses for the Medusae Fossae Formation. Y-axis is change in rock abundance and x-axis is time. Change in rock abundance only includes indurated rock and does not take dust into account. Dashed lines represent rock that was added and then reworked (net zero rock contribution). (a) Decreasing total volume case in which sediment is being eroded and reworked, but also removed to a higher-latitude sink. (b) Increasing total volume case in which new sediment is being added from volcanic eruptions, erosion elsewhere on Mars, and/or impact ejecta. Sediment may also be reworked.

Amazonian (0.3 Ga up to present-day). Dating by Mars Sample Return of the Mafic Floor Unit at Jezero (Shahrzad et al., 2019) should reduce the uncertainties.

Both the β and volume estimations from our model were consistent with previous work. Similar to Dunning (2019), we also predict an overall loss of mass from the Medusae Fossae Formation, as seen in Figure 3.5. Dunning (2019) estimated a deflation rate of 400-600 nm/yr. While the deflation rate estimated in Dunning (2019) was derived from the estimated volumetric erosion rate, our calculated erosion rate only considers a top down erosion. Nevertheless, by comparing our erosion rate with Dunning (2019)'s deflation rate, we find that they appear to be consistent for a few of the subregions and for our crater count data when we combine all 14 regions. 12 of our 14 regions examined the Medusae Fossae Formation, and four of these regions were consistent

with Dunning (2019)'s estimation. These included Central Medusae Fossae 1 B and C and Central Medusae Fossae 2 A and B. In Figure 3.1o, which includes the crater count data from all 14 regions, our estimated erosion rate of 450-580 nm/a is consistent with the 400-600 nm/a deflation rate calculated by Dunning (2019). Similarly, Grindrod and Warner (2014) state that erosion rates are 300-800 nm/a after converting horizontal retreat rates to vertical erosion and Kite and Mayer (2017) found the crater-obliteration rate of light-toned layered sedimentary rock to be on the same order of magnitude, at 10^2 nm/a. For volume, similar to previous work (Tanaka, 2000; Bradley et al., 2002, we also estimated total volume lost on the order of $10^6 km^3$.

In addition to the predicted sediment recycling by Kerber and Head (2010), extraformational sediment recycling, the process of sedimentary rock being buried than exposed by erosion repeatedly, is known to occur at the top of Gale's Mound (Edgett et al., 2020). Zimbelman and Scheidt (2012a) described that the stratigraphically upper part of the lower member of MFF contains material of early Amazonian age (Aml2), which is similar to layers near the top of the Gale Mound. On the other hand, the other component of the lower member of the MFF analyzed by Zimbelman and Scheidt (2012a) has an age near the Amazonian-Hesperian boundary (AHml1), which is consistent with cratering ages of Gale Mound (Thomson et al., 2011). In addition, Lewis and Aharonson (2014) also notes that the dominant bedding scales are similar but not identical for the two sites (0.221 ± 0.017 m^{-1} at Gale versus 0.352 ± 0.042 m^{-1} and 0.290 ± 0.063 m^{-1} for the MFF) and suggests a possible analogous formation link. Due to the similarities between Gale's Mound and the MFF, it is possible that similar processes occur at MFF.

CONCLUSION

As outlined in §1, the Medusae Fossae Formation is a sedimentary deposit on Mars that has very limited existing information on formation age. We constructed a model of the crater size distribution function based on area size, craters counted, and erosion rate β based on infilling. We applied the model to both the Medusae Fossae Formation and other regions, such as Aeolis Planum, Eastern Candor, and Gale's Mound. Due to wide age uncertainties however, Central Medusae Fossae 1 C was the only region that was clearly constrained to an age of 2.98-3.51 Gyr by the model, which is consistent with Kerber and Head (2010)'s estimation of MFF forming during the Hesperian. On the other hand, β had much better constraints and regions Central Medusae Fossae 1 A-C, Central Medusae Fossae 2 A-C, Far East Medusae Fossae B, East Medusae Fossae A, and Upper Mount Sharp had β values constrained below 1000 nm/a (expect the 3σ error region for Upper Mount Sharp).

The regions with less well-defined β fits (due to wider error regions) were Aeolis Planum, Eastern Candor, Far East Medusae Fossae A and C, and East Medusae Fossae B. However, these five regions all had β error regions predominantly above 1000 nm/a (excluding Eastern Candor). From §4.6, we saw that Aeolis Planum, Eastern Candor, Far East Medusae Fossae A, Far East Medusae Fossae C, and East Medusae Fossae B (5 out of 14 regions) have the highest likelihood for water ice detection by GRS/NS since all five regions have erosion rates above 1000 nm/a. This means that these regions have the highest potential for preservation of subsurface ice at shallow depths. As a result, we recommend further investigation of these five sites due to their potential implications for ISRU.

According to Figure 3.5, the model's best fit determined these five regions were all formed within the past 0.74 billion years, consistent with Amazonian age estimates (Scott and Tanaka, 1986; Greeley and Guest, 1987). This would have interesting implications for deposition events that may have occurred within the last 1 billion year. However, taking into account the wide error regions, the upper 2σ and 3σ error bounds permit older ages as well. For all six Central Medusae Fossae regions, deposition occurred more than 1 billion years ago according to Figure 3.5. From the global map of the model's best fit values for age and β, we saw common trends depending on

the site. While Central Medusae Fossae and Upper Mt. Sharp had older ages (>1.40 Ga) and lower erosion rates (<650 nm/a), East Medusae Fossae, Far East Medusae Fossae, Aeolis Planum, and Eastern Candor all had younger ages (<0.740 Ga) and higher erosion rates (>740 nm/a).

In the future, this model may also be applied for additional sedimentary regions on Mars. In particular, the model can provide a more precise age and β estimation for regions that contain higher amounts of craters. For these 14 regions, the model was able to estimate a much more precise β than age. As a result, future work should also focus on methods for better constraining age.

Appendix

A.1 Code

```
 -*- coding: utf-8 -*-
'''
Originally a Google Colab notebook.
'''
!pip install geopandas
!pip install scipy
# !pip install mpld3 #this is for Jupyter notebook to zoom in on 2-D contour plots
!pip install matplotlib

from google.colab import drive
drive.mount('/content/drive')

import os
import matplotlib.pyplot as plt
import geopandas as gpd
import numpy as np
from scipy.special import factorial
import scipy.stats as stats # for calculating standard error
from decimal import Decimal
import scipy.stats as stats
from scipy.stats import poisson
from scipy.interpolate import interp1d
from scipy.stats import chisquare
import math
from IPython.display import display, Markdown
from matplotlib.ticker import AutoMinorLocator
import pandas as pd
import time #check runtime
from collections import OrderedDict
from scipy.integrate import simps
from numpy import trapz
from scipy.special import lambertw
from scipy.stats import chi2_contingency
# import mpld3
# from mpld3 import plugins

#read shapefiles
df1a = gpd.read_file('1a.shp')
df1b = gpd.read_file('1b.shp')
df1c = gpd.read_file('1c.shp')
df2 = gpd.read_file('2.shp')
df3a = gpd.read_file('3a.shp')
df3b = gpd.read_file('3b.shp')
df4a = gpd.read_file('4a.shp')
df4b = gpd.read_file('4b.shp')
df4c = gpd.read_file('4c.shp')
df5a = gpd.read_file('5a.shp')
df5b = gpd.read_file('5b.shp')
df5c = gpd.read_file('5c.shp')
df6a = gpd.read_file('6a.shp')
df6b = gpd.read_file('6b.shp')
```

```
df7a = gpd.read_file('7a.shp')
df7b = gpd.read_file('7b.shp')

#make data list
data_list = [df1a, df1b, df1c, df2, df3a, df3b, df4a, df4b, \
             df4c, df5a, df5b, df5c, df6a, df6b, df7a, df7b]

#Finding total area
def find_area(df_list):
  '''
  Finds total area of all dataframes.
  Input:
    df_list: List of dataframes
  Output: Total area
  '''
  total_area = 0
  for df in df_list:
    total_area += sum(df.Area)
  return total_area

area_counted = find_area(data_list)
area1 = find_area([df1a, df1b, df1c])
area1a = find_area([df1a])
area1b = find_area([df1b])
area1c = find_area([df1c])
area2 = find_area([df2])
area3 = find_area([df3a, df3b])
area3a = find_area([df3a])
area3b = find_area([df3b])
area4 = find_area([df4a, df4b, df4c])
area4a = find_area([df4a])
area4b = find_area([df4b])
area4c = find_area([df4c])
area5 = find_area([df5a, df5b, df5c])
area5a = find_area([df5a])
area5b = find_area([df5b])
area5c = find_area([df5c])
area6 = find_area([df6a, df6b])
area6a = find_area([df6a])
area6b = find_area([df6b])
area7 = find_area([df7a, df7b])
area7a = find_area([df7a])
area7b = find_area([df7b])


df1a_craters = gpd.read_file('1a_clipped_1.shp')
df1b_craters = gpd.read_file('1b_clipped_1.shp')
df1c_craters = gpd.read_file('1c_clipped_1.shp')
df2_craters = gpd.read_file('2_clipped.shp')
df3a_craters = gpd.read_file('3a_clipped_1.shp')
df3b_craters = gpd.read_file('3b_clipped.shp')
df4a_craters = gpd.read_file('4a_clipped.shp')
df4b_craters = gpd.read_file('4b_clipped_1.shp')
df4c_craters = gpd.read_file('4c_clipped_2.shp')
df5a_craters = gpd.read_file('5a_clipped.shp')
df5b_craters = gpd.read_file('5b_clipped_1.shp')
```

```
df5c_craters = gpd.read_file('5c_clipped.shp')
df6a_craters = gpd.read_file('6a_cliipped.shp')
df6b_craters = gpd.read_file('6b_clipped_1.shp')
df7a_craters = gpd.read_file('7a_clipped_1.shp')
df7b_craters = gpd.read_file('7b_clipped_1.shp')

# df1_craters = [df1a_craters, df1b_craters, df1c_craters]
df1a_craters['Region'] = '1a'
df1b_craters['Region'] = '1b'
df1c_craters['Region'] = '1c'
df1_craters = gpd.GeoDataFrame(pd.concat([df1a_craters, df1b_craters, df1c_craters], ignore_index=True), crs=df1a_craters.crs)
# df2_craters = [df2_craters]
df2_craters['Region'] = '2'

# df3_craters = [df3a_craters, df3b_craters]
df3a_craters['Region'] = '3a'
df3b_craters['Region'] = '3b'
df3_craters = gpd.GeoDataFrame(pd.concat([df3a_craters, df3b_craters], ignore_index=True), crs=df3a_craters.crs)

# df4_craters = [df4a_craters, df4b_craters, df4c_craters]
df4a_craters['Region'] = '4a'
df4b_craters['Region'] = '4b'
df4c_craters['Region'] = '4c'
df4_craters = gpd.GeoDataFrame(pd.concat([df4a_craters, df4b_craters, df4c_craters], ignore_index=True), crs=df4a_craters.crs)

# df5_craters = [df5a_craters, df5b_craters, df5c_craters]
df5a_craters['Region'] = '5a'
df5b_craters['Region'] = '5b'
df5c_craters['Region'] = '5c'
df5_craters = gpd.GeoDataFrame(pd.concat([df5a_craters, df5b_craters, df5c_craters], ignore_index=True), crs=df5a_craters.crs)

# df6_craters = [df6a_craters, df6b_craters]
df6a_craters['Region'] = '6a'
df6b_craters['Region'] = '6b'
df6_craters = gpd.GeoDataFrame(pd.concat([df6a_craters, df6b_craters], ignore_index=True), crs=df6a_craters.crs)

# df7_craters = [df7a_craters, df7b_craters]
df7a_craters['Region'] = '7a'
df7b_craters['Region'] = '7b'
df7_craters = gpd.GeoDataFrame(pd.concat([df7a_craters, df7b_craters], ignore_index=True), crs=df7a_craters.crs)

dfall_craters_dup = gpd.GeoDataFrame(pd.concat([df1_craters,df2_craters,df3_craters,df4_craters,\
                    df5_craters,df6_craters,df7_craters], ignore_index=True))
dfall_craters = dfall_craters_dup.drop_duplicates()

def count_craters(df, min_diam=0.5, max_diam=False):
  '''
  Finds total number of craters in list of dataframes.
  Input:
    df: List of dataframes
    min_diam: minimum diameter (km)
    max_diam: max diameter
  Output: Total number of craters
  '''
  crater_count = 0
  # for df in df_list:
```

```
  red_df = df[(df.Diam_km >= min_diam) & (df.tag == 'standard')]
    # print(red_df)
  if max_diam:
    red_df = red_df[red_df.Diam_km < max_diam]
  crater_count += len(red_df)
  return crater_count

#bin by bin Craters, H km^-2Ga^-1 numbers
bin_neg2 = 4.02 * 10**(-3) #craters between .5-.707km
bin_neg1 = 1.15 * 10**(-3) #0.707-1km
bin0 = 3.08 * 10**(-4) #1-1.41km
bin1 = 1.28 * 10**(-4) #1.41-2km
bin2 = 6.85 * 10**(-5) #2-2.83km
bin3 = 3.67 * 10**(-5) #2.83-4km
bin4 = 1.98 * 10**(-5) #4-5.66km
bin5 = 1.06 * 10**(-5) #5.66-8km
bin6 = 5.68 * 10**(-6) #8-11.3km
bin7 = 3.04 * 10**(-6) #11.3-16km
bin8 = 1.62 * 10**(-6) #16-22.6km
bin9 = 8.71 * 10**(-7) #22.6-32km
bin10 = 4.67 * 10**(-7) #32-45.3km
bin11 = 2.40 * 10**(-7) #45.3-64km
bin12 = 1.12 * 10**(-7) #64-90.5km
bin13 = 5.21 * 10**(-8) #90.5-128km

bin_constants = [bin_neg2, bin_neg1, bin0, bin1, bin2, bin3, bin4, bin5, bin6,\
           bin7, bin8, bin9, bin10, bin11, bin12, bin13]

b1 = count_craters(dfall_craters[dfall_craters.Region.str.contains('1')], min_diam=0.5, max_diam=1)

bin_dict = OrderedDict()
bin_dict[-2] = [0.5 * 1000,0.707 * 1000]
bin_dict[-1] = [0.707 * 1000, 1. * 1000]
bin_dict[0] = [1. * 1000, 1.41 * 1000]
bin_dict[1] = [1.41 * 1000, 2. * 1000]
bin_dict[2] = [2. * 1000,2.83 * 1000]
bin_dict[3] = [2.83 * 1000, 4. * 1000]
bin_dict[4] = [4. * 1000, 5.66 * 1000]
bin_dict[5] = [5.66 * 1000, 8. * 1000]
bin_dict[6] = [8. * 1000, 11.3 * 1000]
bin_dict[7] = [11.3 * 1000, 16. * 1000]
bin_dict[8] = [16. * 1000, 22.6 * 1000]
bin_dict[9] = [22.6 * 1000, 32 * 1000]
bin_dict[10] = [32 * 1000, 45.3 * 1000]
bin_dict[11] = [45.3 * 1000, 64 * 1000]
bin_dict[12] = [64 * 1000, 90.5 * 1000]
bin_dict[13] = [90.5 * 1000, 128 * 1000]

bin_list = [bin_dict[-2], bin_dict[-1], bin_dict[0], bin_dict[1], bin_dict[2], \
           bin_dict[3], bin_dict[4], bin_dict[5], bin_dict[6], bin_dict[7],\
           bin_dict[8], bin_dict[9], bin_dict[10], bin_dict[11], bin_dict[12], bin_dict[13]]

#defining values
second = 1/60/60/24/365.2422/(10**9) #in Ga
area = find_area(data_list) #total area
start_time = second
```

```
end_time = 4.5
points = 1000

def find_region_bin_craters(reg_n, all=False):
  '''
  Finds number of standard craters in each bin for a region.
  Input:
    reg_n: region number
    all: if True, then considers all craters, including marked craters
  Output:
    count_list: list of 16 numbers representing craters in each bin
  '''
  min_diam_list = [0.5,0.707,1,1.41,2,2.83,4,5.66,8,11.3,16,22.6,32,45.3,64,90.5]
  count_list = []
  str_n = str(reg_n)
  for i, diam in enumerate(min_diam_list):
    if i != len(min_diam_list) - 1:
      if not all:
        count_list.append(count_craters(dfall_craters[dfall_craters.Region.str.contains(str_n)], min_diam=diam, max_diam=min_diam_list[i+1]))
      else:
        count_list.append(count_craters(dfall_craters[dfall_craters.tag.str.contains('standard')], min_diam=diam, max_diam=min_diam_list[i+1]))
    else:
      if not all:
        count_list.append(count_craters(dfall_craters[dfall_craters.Region.str.contains(str_n)], min_diam=diam))
      else:
        count_list.append(count_craters(dfall_craters[dfall_craters.tag.str.contains('standard')], min_diam=diam))
  return count_list



def find_mid_depth(diam_min, diam_max):
  '''
  Takes minimum and maximum diameters in meters and returns log halfway depth.
  '''
  logmid_diam = 10**((np.log10(diam_min)+np.log10(diam_max))/2) / 1000 #in km
  if diam_min < 2822.21362731415: #D=2822 km is intersection
    logmid_depth = logmid_diam * 0.2
  else:
    logmid_depth = 0.323*logmid_diam**0.538
  return logmid_depth*1000.

def find_mid_diam(diam_min, diam_max):
  '''
  Takes minimum and maximum diameters in meters and returns log10 halfway diameter.
  Input:
    diam_min: minimum diameter
    diam_max: maximum diameter
  Output: Log halfway diameter.
  '''
  logmid_diam = 10**((np.log10(diam_min)+np.log10(diam_max))/2)
  return logmid_diam
find_mid_diam(10, 1000)

def find_erosion_pdf(T_start, T_end, B_start, B_end, mid_depth, num_points, n, area_counted, cum_craters,  tlin=False, blin=False):
  '''
  Find Poisson probability array of observing n craters.
```

```
  Input:
    T_start: starting age
    T_end: ending age
    B_start: starting beta
    B_end: ending beta
    mid_depth: log10 mid-depth of the bin
    num_points: number of points to use in the age and beta arrays
    n: number of craters
    area_counted: area (km^2) of the site
    cum_craters: H value (craters/km^2) from Table 1 of Michael 2013
    tlin: if True then function uses a linear time array
    blin: if True then function uses a linear beta array
  Output:
    T: age array
    B: beta array
    P: probability array
  '''
  if tlin:
    T = np.linspace(T_start, T_end, num_points)
  else:
    T = np.geomspace(T_start, T_end, num_points)
  if blin:
    B = np.linspace(B_start, B_end, num_points) #trying linspace vs. geomspace
  else:
    B = np.geomspace(B_start, B_end, num_points)
  Z = np.zeros(len(T)*len(B))
  Z = Z.reshape((len(T), len(B)))
  for i, t in enumerate(T):
    for j, b in enumerate(B):
      exp_craters_erosion = cum_craters * mid_depth / b
      exp_craters_no_erosion = cum_craters * t
      if exp_craters_erosion < exp_craters_no_erosion:
        dbt = mid_depth / b
        N1db = 3.79e-14 * (np.exp(6.93*dbt) - 1) + 5.84e-4 * dbt
        N1_wrongdb = 5.84e-4 * dbt
        db_factor = N1db / N1_wrongdb
        mu = exp_craters_erosion * area_counted * db_factor
      else:
        N1 = 3.79e-14 * (np.exp(6.93*t) - 1) + 5.84e-4 * t
        N1_wrong = 5.84e-4 * t
        correction_factor = N1 / N1_wrong
        mu = exp_craters_no_erosion * area_counted * correction_factor
      Z[i][j] = mu
  P = poisson.pmf(n, Z)
  return T, B, P

def find_cdf(mult_prob):
  '''
  Create cdf.
  Inputs:
    T_start: Start time in Ga units
    T_end: End time in Ga units
    num_points: number of points within time array (and plot)
    n: number of craters
  Output:
    Plot of cdf, time array and probability array
```

```
    '''
    cdf = mult_prob.cumsum()
    #normalize
    scale = 1.0/cdf[-1]
    prob = scale * cdf  #this is normalized cdf
    return prob



def multiply_bins(reg_n,t_start, t_end, b_start, b_end, num_points, area, tlins=False, blins=False, all=False):
    '''
    Loops through all 16 crater bins and finds the total probability.
    Inputs:
      reg_n: region number
      t_start: start time
      t_end: end time
      b_start: start beta
      b_end: end beta
      num_points: number of points
      area: area of site (km^2)
      tlins: if True, function creates linear time array otherwise log time
      blins: if True, function creates linear beta array, otherwise log beta
      all: if True, craters used include marked (not just standard)
    Output:
      X, Y, and probability arrays
    '''
    all_pdfs = []
    pdf_product = None
    crater_bins = find_region_bin_craters(reg_n, all)
    for i, crater_count in enumerate(crater_bins):
      mid_depth_val = find_mid_depth(bin_list[i][0], bin_list[i][-1])
      X,Y,P = find_erosion_pdf(t_start, t_end, b_start, b_end, mid_depth_val, num_points,\
                               crater_count, area_counted=area, cum_craters=bin_constants[i], tlin=tlins, blin=blins) #not actually cumulative anymore
      all_pdfs.append(P)
    for i, pdf in enumerate(all_pdfs):
      if i==0:
        pdf_product = pdf
      else:
        pdf_product = pdf_product * pdf
    return X, Y, pdf_product



def plot_contour(reg_n, T_start, T_end, B_start, B_end, num_points, area, log=False, tli=False,bli=False, all=False):
    '''
    Plots two-parameter contour plot.
    Inputs:
      reg_n: region number
      T_start: start time
      T_end: end time
      B_start: start beta
      B_end: end beta
      num_points: number of points
      area: area of site (km^2)
      tlins: if True, function creates linear time array otherwise log time
      blins: if True, function creates linear beta array, otherwise log beta
      all: if True, craters used include marked (not just standard)
```

```
    '''
    X, Y, Z = multiply_bins(reg_n, T_start, T_end, B_start, B_end, num_points, area, tlins=tli, blins=bli, all=all)
    fig,ax = plt.subplots()
    if log:
      ax.set_xscale('log')
    levels = np.linspace(np.min(Z), np.max(Z), 100)
    cp = ax.contourf(X, Y, Z.T, levels)
    cbar = plt.colorbar(cp)
    one_sig, two_sig, three_sig = find_contours(Z)
    cp2 = plt.contour(cp, levels=[one_sig, two_sig, three_sig], colors=['red', 'red','red'],\
                      linestyles=['solid','dashed',':'], origin='lower')
    cbar.add_lines(cp2)
    cbar.lines[-1].set_linestyles(cp2.linestyles)
    cbar.set_label('Probability')
    ax.axhline(y=1000, linestyle='--', color='white') #ice table
    if B_end <= 5000:
      t5k = [1,5]
      b5k= [5000,1000]
      fx = interp1d(t5k, b5k, kind='linear')
      plt.plot(t5k, fx(t5k), color='dodgerblue',linestyle=':')
    else:
      t5km = [0.1,0.2, 0.45, 0.5, 0.6, 0.7, 0.8,0.9, 1,1.1, 1.5, 2,4,5]
      b5km = [50000,25000, 11111.11111111111, 10000, 8333.3333333333, 7142.857143, 6250,5555.555555, 5000,4545.45455,3333.333, 2500,1250, 1000]
      f = interp1d(t5km, b5km, kind='cubic')
      plt.plot(t5km, f(t5km), color='dodgerblue', linestyle = ':')
    ax.set_xlabel('Age (Ga)')
    ax.set_ylabel('   (nm/a)')
    fig_name = str(reg_n) +'_2dcontour' + '.png'
    ax.set_ylim(0,B_end)
    ax.set_xlim(0,T_end)
    plt.show()
    fig.savefig(fig_name, dpi=300, bbox_inches='tight')

#area 1a Central Medusae Fossae 1
plot_contour('1a', start_time, 4.5, 1, 1100, points, area1a, log=False, tli=True,bli=True)
#area 1b Central Medusae Fossae 1
plot_contour('1b', start_time, 4.5, 0, 1100, points, area1b, log=False, tli=True, bli=True)
#area 1c Central Medusae Fossae 1
plot_contour('1c', start_time, 4.5, 0, 1100, points, area1c, log=False, tli=True, bli=True)

#area 2 Aeolis Planum 3D
plot_contour(2, start_time, 4.5, 1, 3000, points, area2, log=False, tli=True, bli=True)

#area 3 Eastern Candor
plot_contour('3', start_time, 4.5, 1, 10000, points, area3, log=False, tli=True, bli=True)

#area 4a Central Medusae Fossae 2
plot_contour('4a', second, 4.5, second, 1100, points, area4a, log=False, tli=True, bli=True)
#area 4b Central Medusae Fossae 2
plot_contour('4b', start_time, 4.5, 1, 1100, points, area4b, log=False, tli=True, bli=True)
#area 4c Central Medusae Fossae 2
plot_contour('4c', start_time, 4.5, 1, 400, points, area4c, log=False, tli=True, bli=True)

#area 5a Far East Medusae Fossae
plot_contour('5a', start_time, 4.5, 1, 14000, points, area5a, log=False, tli=True, bli=True)
#area 5b Far East Medusae Fossae
```

```
plot_contour('5b', start_time, 4.5, 1, 1200, points, area5b, log=False, tli=True, bli=True)
#area 5c Far East Medusae Fossae
plot_contour('5c', start_time, 4.5, 1, 3000, points, area5c, log=False, tli=True, bli=True)

#area 6a East Medusae Fossae
plot_contour('6a', start_time, 4.5, 1, 1100, points, area6a, log=False, tli=True, bli=True)
#area 6b East Medusae Fossae
plot_contour('6b', start_time, 4.5, 1, 5000, points, area6b, log=False, tli=True, bli=True)

#area 7 Upper Mount Sharp
plot_contour(7, start_time, 4.5, 1, 1500, points, area7, log=False, tli=True, bli=True)



def find_error(X,Y,Z, sigma=0.9545):
  '''
  Finds the min and max betas and times within a given sigma error, default is two sigma.
  '''
  z = Z.flatten()
  # print('x', z, 'maxz', max(z))
  sig2 = (1 - sigma) * max(z)
  # print(sig2, 'sigma val')
  z2 = sorted(i for i in z if i >= sig2)
  print('z2', z2)
  max_p = max(z2)
  min_p = min(z2)
  z_2sigma_region = np.argwhere((Z>= min_p) & (Z <= max_p))
  t_indices = z_2sigma_region[:,0]
  b_indices = z_2sigma_region[:,-1]
  # times = X[[t_indices]]
  times = np.take(X, t_indices)
  betas = np.take(Y, b_indices)
  min_beta = min(betas)
  max_beta = max(betas)
  min_time = min(times)
  max_time = max(times)
  print('min time',min_time)
  return min_beta, max_beta, min_time, max_time

#Finds the best fit age, beta, and thickness
def find_thickness_lost(time, beta):
  '''
  Returns thickness lost in meters.
  '''
  thickness = beta*time
  return thickness

area_names =  ['1a', '1b', '1c', '2', '3','4a','4b','4c', '5a', '5b', '5c', '6a', '6b',\
              '7']
th_list =[]
for area_name in area_names: #finds best fit age and beta and multiplies for thickness list
  area = globals()['area' + area_name]
  X, Y, Z = multiply_bins(area_name, second, 5, 1, 5000, 1000, area)
  t, b = find_max(X,Y,Z)
  print(t,b)
  th = find_thickness_lost(t,b)
```

```
    th_list.append(th)

d = {'Region Name': area_names, 'Thickness (m)': th_list}
#thickness lost
df = pd.DataFrame(data=d)

#inserting output from above here:
b1a = 204.39381529995762 / 1e9
b1b = 558.9630839127448 / 1e9
b1c = 646.142878152407 / 1e9
b2 = 1907.9544041932393 / 1e9
b3 = 1153.746253806376 / 1e9
b4a = 394.0701567007533 / 1e9
b4b = 491.8617336391133 / 1e9
b4c = 87.88265229401804 / 1e9
b5a = 3971.895758898476 / 1e9
b5b = 746.9198431935246 / 1e9
b5c = 1693.2870008117998 / 1e9
b6a = 662.8825397233585 / 1e9
b6b = 2549.5225810348293 / 1e9
b7 = 167.99883840212075 / 1e9

bs = [b1a, b1b, b1c, b2, b3, b4a, b4b, b4c, b5a, b5b, b5c, b6a, b6b, b7]
b = 516.2481221520928 / 1e9
area_names =  ['1a', '1b', '1c', '2', '3','4a','4b','4c', '5a', '5b', '5c', '6a', '6b',\
              '7']
# Region Name  Thickness Lost (m)
t1a = 299.063957
t1b = 1338.653434
t1c = 1902.797905
t2 = 1087.427396
t3 = 474.807609
t4a = 737.673571
t4b = 1796.341421
t4c = 295.610843
t5a = 1904.854194
t5b = 494.612084
t5c = 675.499968
t6a = 475.179685
t6b = 985.918496
t7 = 337.539687
t1a = 299.063957
t1b = 1037.459451
t1c = 1107.862869
t2 =  884.343927
t3 =  474.807609
t4a = 731.411108
t4b = 1304.273171
t4c = 295.610843
t5a = 1099.644757
t5b  = 494.612084
t5c = 618.717073
t6a = 475.179685
t6b = 1091.645198
t7 = 337.539687
t1s = [t1a, t1b, t1c, t2, t3, t4a, t4b, t4c, t5a, t5b, t5c, t6a, t6b, t7]
```

```
tl = 516.2481221520928 * 1.374447682317356

#1 km for Upper Mt Sharp, 0.3 km for Aeolis Planum, and 1 km for Eastern Candor
pt1a = 599
pt1b = 2197
pt1c = 1973
pt2 = 0.3e3
pt3 = 1e3
pt4a = 1901
pt4b = 477.3333333
pt4c = 1232.333333
pt5a = 801.2636303393872
pt5b = 388.0972157604289
pt5c = 475.034930299745
pt6a = 1230
pt6b = 3909
pt7 = 1e3
pts = [pt1a, pt1b, pt1c, pt2, pt3, pt4a, pt4b, pt4c, pt5a, pt5b, pt5c, pt6a, pt6b, pt7]
pt = sum(pts)

area1a = 27713.29763278
area1b = 87796.47999555
area1c = 107609.67515457
area2 = 77786.2716485
area3 = 6690.98049521
area4a = 63822.22919981
area4b = 52604.4708217
area4c = 97751.49648003
area5a = 54503.27273563
area5b = 131604.2333553
area5c = 196372.6222765
area6a = 117524.47729916
area6b = 234087.18400037
area7 = 1000.82082676
areas = [area1a, area1b, area1c, area2, area3, area4a, area4b, area4c, area5a, area5b, \
         area5c, area6a, area6b, area7]

sed_rate= 0.0001797727273 #m/yr sedimentation rate
sed_rate_p = 0.0005494545455 #m/yr sed rate
sed_rate_n = 0.0001601515152 #m/yr sed rate

def find_thickness(T, pt, tl, sed_r, b, area):
  '''
  Finds the thickness over time.
  Inputs:
    T: time array
    pt: present thickness (m)
    tl: thickness lost (m)
    sed_r: global sedimentation rate
    b: beta
    area: area of site
  Output:
    age, thickness, and volume arrays
  '''
  maxt = pt + tl #max thickness = present thickness + thickness lost
  ys = []
```

```
  vs = []
  ages = []
  dummy_v = 0
  # maxta = (maxt - pt) / b
  for i,age in enumerate(T):
    y = pt + b * age  #convert beta to meters
    if y < maxt:
      v = y / 1000 *area  #volume in km^3
      ys.append(y)
      vs.append(v)
      ages.append(age)
    else:
      if dummy_v == 0:
        age_offset = T[i]
        dummy_v += 1
      new_age = age-age_offset
      y = maxt - sed_r * new_age
      # y = maxt - sed_r * age
      v = y/1000 * area  #volume in km^3
      if y >= 0:
        ys.append(y)
        vs.append(v)
        ages.append(age)
      elif dummy_v == 1:
        last_age = maxt/sed_r + age_offset
        ages.append(last_age)
        ys.append(0.0)
        vs.append(0.0) #only works for positive volumes
        dummy_v += 1
      else:
        break
  return ages, ys, vs

def calc_thick(name, beta_ages, age_list, thickness_list, vol_list, t_array, b_array, z_array, area, pt, sig=0.9545):
  '''
  Helper function for find_sedplot. Calculates the site's thickness over time.
  Input:
    name: name of region
    beta_ages: age array
    age_list: list of ages
    thickness_list: list of thicknesses
    vol_list: list of volumes
    t_array: age array that was used to find probability array
    b_array: beta array that was used to find beta array
    z_array: probability array
    area: site's area (km^2)
    pt: present thickness (m)
    sig: sigma value to use
  Output:
    mint: minimum thickness
    maxt: maximum thickness
    plot_ages: general list of ages
    ages: age array for ages less than or equal to the maximum age
    mina: minimum age
  '''
  plot_ages = np.array(age_list)
```

```
  minb, maxb, mina, maxa = find_error(t_array, b_array, z_array, sigma=sig) #2 beta values, replaced in_maxt, in_mint
  mina = mina * 1e9
  maxa = maxa * 1e9
  beta_ages = beta_ages[beta_ages <= maxa] / (1e9) #changed units y to Gyr
  mint = beta_ages * minb + pt
  maxt = beta_ages * maxb + pt
  ages = np.array(beta_ages) * 1e9
  return mint, maxt, plot_ages, ages, mina


def find_sedplot(name, beta_ages, age_list, thickness_list, vol_list, t_array, b_array, z_array, area, pt, volume=False):
  '''
  Helper function for join_all. Creates the volume or thickness plot for a particular region.
  Input:
    name: name of region
    beta_ages: age array
    age_list: list of ages
    thickness_list: list of thicknesses
    vol_list: list of volumes
    t_array: age array that was used to find probability array
    b_array: beta array that was used to find beta array
    z_array: probability array
    area: site's area (km^2)
    pt: present thickness (m)
    volume: if volume is True, finds volume plot not thickness plot
  '''
  in_mint, in_maxt, plot_ages, in_ages, in_mina = calc_thick(name, beta_ages, age_list, thickness_list, vol_list, t_array, b_array, z_array, area, pt)
  in_mint1, in_maxt1, plot_ages1, in_ages1, in_mina1 = calc_thick(name, beta_ages, age_list, thickness_list, vol_list, t_array, b_array, z_array, area,
  fig,ax = plt.subplots()
  if volume:
    ax.plot(plot_ages, vol_list, color='k')
    in_maxv = in_maxt/1000 * area #km^3
    in_minv = in_mint/1000 * area #km^3
    in_maxv1 = in_maxt1/1000 * area
    in_minv1 = in_mint1/1000 * area
    ax.fill_between(in_ages, in_minv, in_maxv, where=in_ages<in_mina, color='c', alpha = 0.3, linewidth=0)
    ax.fill_between(in_ages, 0, in_maxv, where=in_ages>=in_mina, color='c', alpha=0.3,linewidth=0.6)
    #for one sigma:
    ax.fill_between(in_ages1, in_minv1, in_maxv1, where=in_ages1<in_mina1, color='c', alpha = 0.7, linewidth=0)
    ax.fill_between(in_ages1, 0, in_maxv1, where=in_ages1>=in_mina1, color='c',alpha=0.7,linewidth=0.6)
    plt.xlabel('Age (yr)')
    plt.ylabel('Volume (km$^3$)')
  else:
    ax.plot(plot_ages, thickness_list, color='c')
    ax.fill_between(in_ages, in_mint, in_maxt, where=in_ages<in_mina, color='c', alpha = 0.3, linewidth=0)
    if pt > 0:
      ax.fill_between(in_ages, 0, in_maxt, where=in_ages>=in_mina, color='c', alpha=0.3, linewidth=0.6)
    else:
      ax.fill_between(in_ages, pt, in_maxt, where=in_ages>=in_mina, color='c', alpha=0.3, linewidth=0)
    plt.xlabel('Age (yr)')
    plt.ylabel('Thickness (m)')
  area_name = name + '.png'

def join_all(title, t_start, t_end, pt, tl, sed_r, b, area, t_array, b_array, z_array, vol_plot=False, n_points=1000):
  '''
  Joins find_thickness and find_sedplot functions as one function to plot thickness or volume.
```

```
  Input:
    title: name of region
    t_start: starting age
    t_end: ending age
    pt: present thickness (m)
    tl: thickness lost
    sed_r: global sedimentation rate
    b: best fit beta
    area: site's area (km^2)
    t_array: age array that was used to find probability array
    b_array: beta array that was used to find beta array
    z_array: probability array
    vol_plot: if True, finds volume plot not thickness plot
    n_points: number of points to put into age array
  '''
  age_array = np.linspace(t_start, t_end, n_points)
  age, thick, vol = find_thickness(age_array, pt, tl, sed_rate, b,area)
  find_sedplot(title, age_array, age, thick, vol, t_array, b_array, z_array, area, pt, volume=vol_plot)


def plot_vol(titles, t_start, t_end, pts, tls, sed_r, bs, areas, t_arrays, b_arrays, z_arrays, n_points=1000, sep=False,log=False):
  '''
  Plots cumulative volume for all areas.
  Inputs:
    titles: list of names of all regions
    t_start: start time
    t_end: end time
    pts: present thicknesses (m)
    tls: thicknesses lost (m)
    sed_r: global average sedimentation rate
    bs: best fit betas
    areas: areas (km^2) of regions
    t_arrays: age arrays
    b_arrays: beta arrays
    z_arrays: probability arrays
    n_points: number of points
    sep: if False, function lumps all volumes together; if True, sets volumes up for separate labels
    log: if True, sets x axis to be log
  '''
  age_array = np.linspace(t_start, t_end, n_points)
  df_list = []
  du_list = []
  dl_list = []
  for i, title in enumerate(titles):
    age, thick, vol = find_thickness(age_array, pts[i], tls[i], sed_rate, bs[i],areas[i])
    mint, maxt, plot_ages, ages, mina = calc_thick(title, age_array, age, thick, vol, t_arrays[i], b_arrays[i], z_arrays[i], areas[i], pts[i])
    # plot_ages = np.array(age)
    vol_name = 'volume ' + str(title)
    d = pd.DataFrame({'age': plot_ages, vol_name: vol})
    # d = {'age': plot_ages, vol_name: vol}
    df_list.append(d)
    if not sep:
      maxv = maxt / 1000 * areas[i] #need to base on beta
      minv = mint /1000 * areas[i]
      vol_name_up = 'max error' + vol_name
      du = {'e_age': ages, vol_name_up: maxv}
      du_list.append(du)
```

```
        vol_name_low = 'min error' + vol_name
        dl = pd.DataFrame({'e_age':ages, vol_name_low:minv})
        dl[vol_name_low] = dl[vol_name_low].where(dl.e_age < mina, 0.0)
        dl_list.append(dl)
    for i, d in enumerate(df_list):
      if i ==0:
        df = d
      else:
        df = pd.merge(df, d,how='outer')
    if sep:
      ax = df.plot.area(x='age',linewidth=0)
      plt.savefig('cum_vol_indiv',dpi=300)
    else:
      for i, du in enumerate(du_list):
        du = pd.DataFrame.from_dict(du)
        if i==0:
          dfu = du
        else:
          dfu = pd.merge(dfu, du, how='outer')
      for i, dl in enumerate(dl_list):
        if i==0:
          dfl = dl
        else:
          dfl = pd.merge(dfl, dl, how='outer')
      dfu['total_err_up_vol'] = dfu.iloc[:,1:].sum(axis=1)
      dfl['total_err_low_vol'] = dfl.iloc[:,1:].sum(axis=1)
      df['total_volume'] = df.iloc[:,1:].sum(axis=1)
      ax = dfu.plot.area(x='e_age', y='total_err_up_vol', color='c', alpha=0.3, linewidth=0)
      if log:
        ax.set_xscale('log')
      df.plot.area(x='age', y='total_volume', ax=ax, linewidth=0, color='c')
      dfl.plot.area(x='e_age', y='total_err_low_vol', ax=ax, color='w', linewidth=0.5)
      ax.get_legend().remove()
      ax.set_xlabel('Age (yr)')
      ax.set_ylabel('Volume (km$^3$)')
      plt.savefig('cum_vol_error.png',dpi=300)
    return df, ax

x1a, y1a, z1a = multiply_bins('1a', 0.662, 3.66,147, 293, points, area1a, tlins=True, blins=True)
join_all('1at', second, 4.5e9, pt1a, t1a, sed_rate, b1a, area1a, x1a, y1a, z1a)
join_all('1av',second, 4.5e9, pt1a, t1a, sed_rate, b1a, area1a, x1a, y1a, z1a, vol_plot=True)

x1b, y1b, z1b = multiply_bins('1b', 0.419, 4.09, 422, 762, points, area1b, tlins=True, blins=True)
join_all('1bt',second, 4.5e9, pt1b, t1b, sed_rate, b1b, area1b, x1b, y1b, z1b)
join_all('1bv', second, 4.5e9, pt1b, t1b, sed_rate, b1b, area1b, x1b, y1b, z1b, vol_plot=True)

x1c, y1c, z1c = multiply_bins('1c', 0.635, 4.18, 491, 869, points, area1c, tlins=True, blins=True)
join_all('1ct', second, 4.5e9, pt1c, t1c, sed_rate, b1c, area1c, x1c, y1c, z1c)
join_all('1cv', second, 4.5e9, pt1c, t1c, sed_rate, b1c, area1c, x1c, y1c, z1c, vol_plot=True)

x2, y2, z2 = multiply_bins(2, 0.060, 4.5, 0, 3580, points, area2, tlins=True, blins=True)
join_all('2t', second, 4.5e9, pt2, t2, sed_rate, b2, area2, x2, y2, z2)
join_all('2v', second, 4.5e9, pt2, t2, sed_rate, b2, area2, x2, y2, z2, vol_plot=True)

x3, y3, z3 = multiply_bins(3, 0.017, 4.5, 0,8970, points, area3, tlins=True, blins=True)
join_all('3t', second, 4.5e9, pt3, t3, sed_rate, b3, area3, x3, y3, z3)
```

```
join_all('3v', second, 4.5e9, pt3, t3, sed_rate, b3, area3, x3, y3, z3, vol_plot=True)

x4a, y4a, z4a = multiply_bins('4a', 0.548, 3.90, 298, 537, points, area4a, tlins=True, blins=True)
join_all('4at', second, 5e9, pt4a, t4a, sed_rate, b4a, area4a, x4a, y4a, z4a)
join_all('4av', second, 4.5e9, pt4a, t4a, sed_rate, b4a, area4a, x4a, y4a, z4a, vol_plot=True)

x4b, y4b, z4b = multiply_bins('4b', 0.687, 4.13, 423, 720, points, area4b, tlins=True, blins=True)
join_all('4bt', second, 4.5e9, pt4b, t4b, sed_rate, b4b, area4b, x4b, y4b, z4b)
join_all('4bv', 1, 4.5e9, pt4b, t4b, sed_rate, b4b, area4b, x4b, y4b, z4b, vol_plot=True)

x4c, y4c, z4c = multiply_bins('4c', 2.98, 3.51, 77.7, 99.2, points, area4c, tlins=True, blins=True)
join_all('4ct', second, 4.5e9, pt4c, t4c, sed_rate, b4c, area4c, x4c, y4c, z4c)
join_all('4cv', second, 4.5e9, pt4c, t4c, sed_rate, b4c, area4c, x4c, y4c, z4c, vol_plot=True)

x5a, y5a, z5a = multiply_bins('5a', 0.063, 4.5, 0, 13000, points, area5a, tlins=True, blins=True)
join_all('5at', second, 4.5e9, pt5a, t5a, sed_rate, b5a, area5a, x5a, y5a, z5a)
join_all('5av', second, 4.5e9, pt5a, t5a, sed_rate, b5a, area5a, x5a, y5a, z5a, vol_plot=True)



x5b, y5b, z5b = multiply_bins('5b', 0.305, 4.24, 570, 1020, points, area5b, tlins=True, blins=True)
join_all('5bt', second, 4.5e9, pt5b, t5b, sed_rate, b5b, area5b, x5b, y5b, z5b)
join_all('5bv', second, 4.5e9, pt5b, t5b, sed_rate, b5b, area5b, x5b, y5b, z5b, vol_plot=True)

x5c, y5c, z5c = multiply_bins('5c', 0.111, 4.5, 1220, 2440, points, area5c, tlins=True, blins=True)
join_all('5cv', second, 4.5e9, pt5c, t5c, sed_rate, b5c, area5c, x5c, y5c, z5c, vol_plot=True)
join_all('5ct', 1, 4.5e9, pt5c, t5c, sed_rate, b5c, area5c, x5c, y5c, z5c)

x6a, y6a, z6a = multiply_bins('6a', 0.32, 4.12, 500, 885, points, area6a, tlins=True, blins=True)
join_all('6at', second, 4.5e9, pt6a, t6a, sed_rate, b6a, area6a, x6a, y6a, z6a)
join_all('6av', second, 4.5e9, pt6a, t6a, sed_rate, b6a, area6a, x6a, y6a, z6a, vol_plot=True)

x6b, y6b, z6b = multiply_bins('6b', 0.202, 4.5, 1790, 3890, points, area6b, tlins=True, blins=True)
join_all('6bv', second, 4.5e9, pt6b, t6b, sed_rate, b6b, area6b, x6b, y6b, z6b, vol_plot=True)
join_all('6bt', second, 4.5e9, pt6b, t6b, sed_rate, b6b, area6b, x6b, y6b, z6b)

x7, y7, z7 = multiply_bins(7, 0.146, 4.5, 0, 1308, points, area7, tlins=True, blins=True)
join_all('7t', second, 4.5e9, pt7, t7, sed_rate, b7, area7, x7, y7, z7)
join_all('7v', second, 4.5e9, pt7, t7, sed_rate, b7, area7, x7, y7, z7, vol_plot=True)

x, y,z = multiply_bins('area', 0.828, 2.34,478, 560, points, area, tlins=True, blins=True)
join_all('allv',second, 4.5e9, pt, tl, sed_rate, b, area, x, y, z, vol_plot=True, n_points=1000)

xs = [x1a, x1b, x1c, x2, x3, x4a, x4b, x4c, x5a, x5b, x5c, x6a, x6b, x7]
ys = [y1a, y1b, y1c, y2, y3, y4a, y4b, y4c, y5a, y5b, y5c, y6a, y6b, y7]
zs = [z1a, z1b, z1c, z2, z3, z4a, z4b, z4c, z5a, z5b, z5c, z6a, z6b, z7]

df, ax = plot_vol(area_names, 0, 4.5e9, pts, tls, sed_rate, bs, areas, xs, ys, zs, sep=False)

#individual volumes shown in cumulative plot
dtrial = df.sort_values(by=['age'])
dtrial['volume 4b'][(dtrial['age'] > 1.7e9) & (dtrial['age'] < 1.9e9)].interpolate(method='linear', limit_direction='forward',axis=0)
dtrial['volume 4c'][(dtrial['age'] > 1.7e9) & (dtrial['age'] < 1.9e9)].interpolate(method='linear', limit_direction='forward',axis=0)
pic = dtrial.plot.area(x='age', linewidth=0.001)
pic.set_xlabel('Age (Ga)')
pic.set_ylabel('Volume (km$^3$)')
fig, ax2 = plt.subplots()
```

```
colormap = plt.cm.tab20
colors = [colormap(i) for i in np.linspace(0, 1,16)]
ax2.set_prop_cycle('color', colors)
ax2 = df.plot.area(x='age',linewidth=0, stacked=True, color=colors)
ax2.get_legend().remove()
ax2.set_xlabel('Age (yr)')
ax2.set_ylabel('Volume (km$^3$)')
plt.legend(loc='upper left', bbox_to_anchor=(0.2, 1.1), ncol=3)
plt.savefig('sep_tot_vol.png', dpi=300,bbox_inches='tight')

def find_max(X,Y,Z):
  '''
  Finds best fit age and beta.
  '''
  z = max(Z.flatten())
  max_loc = np.where(Z == z)
  time_index = max_loc[0][0]
  time = X[time_index]
  beta_index = max_loc[1][0]
  beta = Y[beta_index]
  return time, beta

def find_crater_density(H, depth, time, beta=False):
  '''
  Finds crater density.
  Input:
    H: incremental value from Michael et al. 2013 in craters/km^2/Ga
    depth: mid-depth (m)
    time: age (Ga)
    beta: erosion rate (nm/a)
  Output:
    crater_density: density of craters (craters/km^2)
  '''
  dbt = depth / beta #depth/beta to replace t above used to find N1
  N1db = 3.79e-14 * (np.exp(6.93*dbt) - 1) + 5.84e-4 * dbt
  N1_wrongdb = 5.84e-4 * dbt
  db_factor = N1db / N1_wrongdb
  N1 = 3.79e-14 * (np.exp(6.93*time) - 1) + 5.84e-4 * time
  N1_wrong = 5.84e-4 * time
  correction_factor = N1 / N1_wrong
  if beta is False:
    crater_density = H * correction_factor * time
    return crater_density
  craters_erosion =  H * db_factor * depth / beta
  craters_no_erosion = H * correction_factor * time
  if craters_erosion < craters_no_erosion:
    crater_density = craters_erosion
  else:
    crater_density = craters_no_erosion
  return crater_density

def find_best_fit(reg_n, T_start, T_end, B_start, B_end, num_points, area, tli=False,bli=False, all=False):
  '''
  Finds the model's best fit prediction for the 16 crater bins.
  Input:
      reg_n: region number
```

```
    T_start: start time
    T_end: end time
    B_start: start beta
    B_end: end beta
    num_points: number of points
    area: area of site (km^2)
    tli: if True, function creates linear time array otherwise log time
    bli: if True, function creates linear beta array, otherwise log beta
    all: if True, includes marked craters with standard craters.
Output:
   mid_diams: list of mid-log diameters
   best_crater_density: best fit crater densities
   data_crater_densities: data crater densities
   error_list: list of tuples of lower and upper error
'''
X, Y, Z = multiply_bins(reg_n, T_start, T_end, B_start, B_end, num_points, area, tlins=tli, blins=bli,all=all)
t, b = find_max(X,Y,Z)
print('age,beta',t,b) #prints best fit age and beta
mid_diams = []
best_crater_density = []
for i in range(16):
  mid_diam = find_mid_diam(bin_list[i][0], bin_list[i][-1])
  mid_diams.append(mid_diam/1000.0)
  mid_depth = find_mid_depth(bin_list[i][0], bin_list[i][-1])
  H_craters = bin_constants[i]
  #for testing age correction factor
  crater_density = find_crater_density(H_craters, mid_depth, t, b)
  best_crater_density.append(crater_density)
crater_bins = find_region_bin_craters(reg_n,all=all)
data_crater_densities = []
error_list = []
for i, num in enumerate(crater_bins):
  data_density = num/area
  data_crater_densities.append(data_density)
  if num > 100:
    min_n = num - num
    max_n = num + num
  else:
    min_n = 0
    max_n = 100
  n = np.linspace(0.1, max_n, 1000)
  mu = num
  cdf = poisson.cdf(n, mu)
  upper = np.interp(0.8413, cdf, n)
  center = np.interp(0.5, cdf, n)
  lower = np.interp(0.1587, cdf, n)
  upper = (upper-center) / area
  lower = (center - lower) / area
  if lower < 1e-8: #dealing with 0 craters case, should make into function
    mid_diam = find_mid_diam(bin_list[i][0], bin_list[i][-1])
    mid_depth = find_mid_depth(bin_list[i][0], bin_list[i][-1])
    H_craters = bin_constants[i]
    t = np.linspace(T_start, T_end, 1000)
    x,y,p = find_erosion_pdf(T_start, T_end, B_start, B_end, mid_depth, num_points, 0, area, H_craters,  tlin=tli, blin=bli)
    p = p.sum(axis=1)
    c = find_cdf(p)
```

```
        upper_t = np.interp(0.8413, c, x) - np.interp(0.5, c,x)
        upper = find_crater_density(H_craters, mid_depth, upper_t)
        lower = upper
      error_pair = (lower,upper)
      error_list.append(error_pair)
    return mid_diams, best_crater_density, data_crater_densities, error_list

def plot_best_fit(reg_n,T_start, T_end, B_start, B_end, num_points, area, tli=False,bli=False,all=False):
    '''
    Plots the model's best fit prediction along the data's crater distribution on a log scale.
    for all 16 crater bins.
    Input:
        reg_n: region number
        T_start: start time
        T_end: end time
        B_start: start beta
        B_end: end beta
        num_points: number of points
        area: area of site (km^2)
        tli: if True, function creates linear time array otherwise log time
        bli: if True, function creates linear beta array, otherwise log beta
        all: if True, includes marked craters with standard craters.
    '''
    mid_diams, best_crater_density, data_crater_densities, error_list = find_best_fit(reg_n,T_start, T_end, B_start, B_end, num_points, area,tli=False,bl
    fig,ax = plt.subplots()
    ax.set_xscale('log')
    ax.set_yscale('log')
    ax.set_xlabel('Crater Diameter (km)')
    ax.set_ylabel('Crater Density (craters km$^{-2}$)')
    ax.plot(mid_diams, best_crater_density, color='mediumturquoise')
    yerr = np.array(error_list).T
    ax.errorbar(mid_diams, data_crater_densities, yerr, fmt='.', color='k', ecolor='k')
    name = str(reg_n) + 'best_fit.png'
    plt.savefig(name,dpi=300,bbox_inches='tight')

plot_best_fit('1a', second, 4.5, 1, 1500, 1000, area1a)
plot_best_fit('1b', second, 4.5, 1, 3000, 1000, area1b)
plot_best_fit('1c', second, 4.5, 1, 5000, 1000, area1c)
plot_best_fit('2', second, 4.5, 1, 5000, 1000, area2)
plot_best_fit('3a', second, 4.5, 1, 6000, 1000, area3a)
plot_best_fit('3b', second, 4.5, 1, 5000, 1000, area3b)
plot_best_fit('4a', second, 4.5, 1, 5000, 1000, area4a)
plot_best_fit('4b', second, 4.5, 1, 5000, 1000, area4b)
plot_best_fit('4c', second, 4.5, 1, 500, 1000, area4c)
plot_best_fit('5a', second, 4.5, 1, 10000, 1000, area5a)
plot_best_fit('5b', second, 4.5, 1, 5000, 1000, area5b)
plot_best_fit('5c', second, 4.5, 1, 5000, 1000, area5c)
plot_best_fit('6a', second, 4.5, 1, 5000, 1000, area6a)
plot_best_fit('6b', second, 4.5, 1, 5000, 1000, area6b)
plot_best_fit('7', second, 4.5, 1, 10000, 1000, area7)
plot_best_fit('area', second,4.5, 1, 2000, 1000, area, tli=False, bli=False, all=True)

def find_1d_pdf(reg_n, T_start, T_end, B_start, B_end, num_points, area, p=False, beta=False, tli=False, bli=False,all=False):
    '''
    Collapses two-parameter model probability predictions along one axis (either age or beta)
    to find a one-parameter probablity distribution.
```

```
    Inputs:
        reg_n: region number
        T_start: start time
        T_end: end time
        B_start: start beta
        B_end: end beta
        num_points: number of points
        area: area of site (km^2)
        p: if True, finds PDF. If False, finds CDF
        beta: default is False so that the output is time on x-axis. True is beta on x-axis
        tli: if True, function creates linear time array otherwise log time
        bli: if True, function creates linear beta array, otherwise log
        all: if True, includes marked craters with standard craters
    Output:
      x_val: age array
      prob: probability array
    '''
    X, Y, Z = multiply_bins(reg_n, T_start, T_end, B_start, B_end, num_points, area, tlins=tli, blins=bli,all=all) #can also output cdf....
    if beta:
      z = Z.sum(axis=0)
      x_val = Y
    else:
      z = Z.sum(axis=1)
      x_val = X
    if p:
      y_val = z
      scale = 1/np.sum(z)
      prob = scale * y_val
      a = np.where(prob.cumsum() == np.average(prob.cumsum()))
    else:
      cdf = z.cumsum()
      y_val = cdf
      scale = 1.0/y_val[-1]
      prob = scale * y_val
    return x_val, prob


def plot_1d_pdf(reg_n, T_start, T_end, B_start, B_end, num_points, area, p=False, beta=False, tli=False, bli=False):
    '''
    Plots one parameter PDF if p=True or CDF if p=False.
    Inputs:
      reg_n: region number
      T_start: start time
      T_end: end time
      B_start: start beta
      B_end: end beta
      num_points: number of points
      area: area of site (km^2)
      p: if True, finds PDF. If False, finds CDF
      beta: Default is False so that the output is time on x-axis. True is beta on x-axis
      tlin: if True, function creates linear time array otherwise log time
      blin: if True, function creates linear beta array, otherwise log beta
    '''
    fig, ax = plt.subplots()
    fig_name = str(reg_n)
    if beta:
      plt.xlabel('Beta (nm/a)')
```

```
    fig_name = fig_name + '_beta'
  else:
    plt.xlabel('Age (Ga)')
    fig_name = fig_name + '_age'
  if p:
    plt.ylabel('Probability')
    fig_name = fig_name + 'pdf'
  else:
    plt.ylabel('Cumulative Probability')
    plt.axhline(y=0.5, color='r', linestyle=':')
    plt.axhline(y=0.841, color = 'r', linestyle=':')
    plt.axhline(y=0.159, color = 'r', linestyle=':')
    fig_name = fig_name + 'cdf'
  x_array, prob_array = find_1d_pdf(reg_n, T_start, T_end, B_start, B_end, num_points, area, p, beta, tli, bli)
  ax.plot(x_array, prob_array)
  ax.grid(True)
  ax.xaxis.set_minor_locator(AutoMinorLocator())
  ax.yaxis.set_minor_locator(AutoMinorLocator())
  ax.grid(which='major', linewidth='1')
  ax.grid(which='minor', linestyle=':', linewidth='0.5', color='black')
  ax.ticklabel_format(style='sci', axis='y', scilimits=(0,0))
  fig_name = fig_name + '.png'
  fig.savefig(fig_name, dpi=300)
  plt.show()

#time pdfs - run this
xall, pall = find_1d_pdf('area', start_time, 5, 1, 8000, 1000, area, p=True, beta=False, tli=False, bli=False, all=True)
x1a0, p1a0 = find_1d_pdf('1a', start_time, 5, 1, 8000, 1000, area1a, p=True)
x1b0, p1b0 = find_1d_pdf('1b', start_time, 5, 1, 8000, 1000, area1b, p=True)
x1c0, p1c0 = find_1d_pdf('1c', start_time, 5, 1, 8000, 1000, area1c, p=True)
x20, p20 = find_1d_pdf('2', start_time, 5, 1, 8000, 1000, area2, p=True)
x30, p30 = find_1d_pdf('3', start_time, 5, 1, 8000, 1000, area3, p=True)
x4a0, p4a0 = find_1d_pdf('4a', start_time, 5, 1, 8000, 1000, area4a, p=True)
x4b0, p4b0 = find_1d_pdf('4b', start_time, 5, 1, 8000, 1000, area4b, p=True)
x4c0, p4c0 = find_1d_pdf('4c', start_time, 5, 1, 8000, 1000, area4c, p=True)
x5a0, p5a0 = find_1d_pdf('5a', start_time, 5, 1, 8000, 1000, area5a, p=True)
x5b0, p5b0 = find_1d_pdf('5b', start_time, 5, 1, 8000, 1000, area5b, p=True)
x5c0, p5c0 = find_1d_pdf('5c', start_time, 5, 1, 8000, 1000, area5c, p=True)
x6a0, p6a0 = find_1d_pdf('6a', start_time, 5, 1, 8000, 1000, area6a, p=True)
x6b0, p6b0 = find_1d_pdf('6b', start_time, 5, 1, 8000, 1000, area6b, p=True)
x70, p70 = find_1d_pdf('7', start_time, 5, 1, 8000, 1000, area7, p=True)
fig, ax = plt.subplots()
plt.xlabel('Age (Ga)')
plt.ylabel('PDF')
colormap = plt.cm.tab20
colors = [colormap(i) for i in np.linspace(0, 1,16)]
ax.set_prop_cycle('color', colors)
ax.plot(x1a0, p1a0, label='1a')
ax.plot(x1b0, p1b0, label='1b')
ax.plot(x1c0, p1c0, label='1c')
ax.plot(x20, p20, label='2')
ax.plot(x30, p30, label='3')
ax.plot(x4a0, p4a0, label='4a')
ax.plot(x4b0, p4b0, label='4b')
ax.plot(x4c0, p4c0, label='4c')
ax.plot(x5a0, p5a0, label='5a')
```

```
ax.plot(x5b0, p5b0, label='5b')
ax.plot(x5c0, p5c0, label='5c')
ax.plot(x6a0, p6a0, label='6a')
ax.plot(x6b0, p6b0, label='6b')
ax.plot(x70, p70, label='7')
ax.plot(xall, pall, label='All 14 regions')
ax.xaxis.set_minor_locator(AutoMinorLocator())
ax.yaxis.set_minor_locator(AutoMinorLocator())
ax.ticklabel_format(style='sci', axis='y', scilimits=(0,0))
ax.legend(loc='upper right',bbox_to_anchor=(1.15,1.05))
fig.savefig('all_pdfs.png',dpi=300, bbox_inches='tight')

#run this - no 4c
fig, ax = plt.subplots()
plt.xlabel('Age (Ga)')
plt.ylabel('PDF')
colormap = plt.cm.tab20
colors = [colormap(i) for i in np.linspace(0, 1,16)]
ax.set_prop_cycle('color', colors)
ax.plot(x1a0, p1a0, label='1a')
ax.plot(x1b0, p1b0, label='1b')
ax.plot(x1c0, p1c0, label='1c')
ax.plot(x20, p20, label='2')
ax.plot(x30, p30, label='3')
ax.plot(x4a0, p4a0, label='4a')
ax.plot(x4b0, p4b0, label='4b')
ax.plot(x5a0, p5a0, label='5a')
ax.plot(x5b0, p5b0, label='5b')
ax.plot(x5c0, p5c0, label='5c')
ax.plot(x6a0, p6a0, label='6a')
ax.plot(x6b0, p6b0, label='6b')
ax.plot(x70, p70, label='7')
ax.plot(xall, pall, label='All Areas')
ax.set_xlim(0,4.5)
ax.legend(loc='upper right',bbox_to_anchor=(1.15,1.05))
fig.savefig('agepdfs_no4c.png', dpi=300,bbox_inches='tight')


#all beta pdfs - run this
x1a, p1a = find_1d_pdf('1a', start_time, 4.5, 1, 8000, 1000, area1a, p=True, beta=True, tli=False, bli=False)
x1b, p1b = find_1d_pdf('1b', start_time, 4.5, 1, 8000, 1000, area1b, p=True, beta=True, tli=False, bli=False)
x1c, p1c = find_1d_pdf('1c', start_time, 4.5, 1, 8000, 1000, area1c, p=True, beta=True, tli=False, bli=False)
x2, p2 = find_1d_pdf('2', start_time, 4.5, 1, 8000, 1000, area2, p=True, beta=True, tli=False, bli=False)
x3, p3 = find_1d_pdf('3', start_time, 4.5, 1, 8000, 1000, area3, p=True, beta=True, tli=False, bli=False)
x4a, p4a = find_1d_pdf('4a', start_time, 4.5, 1, 8000, 1000, area4a, p=True, beta=True, tli=False, bli=False)
x4b, p4b = find_1d_pdf('4b', start_time, 4.5, 1, 8000, 1000, area4b, p=True, beta=True, tli=False, bli=False)
x4c, p4c = find_1d_pdf('4c', start_time, 4.5, 1, 8000, 1000, area4c, p=True, beta=True, tli=False, bli=False)
x5a, p5a = find_1d_pdf('5a', start_time, 4.5, 1, 8000, 1000, area5a, p=True, beta=True, tli=False, bli=False)
x5b, p5b = find_1d_pdf('5b', start_time, 4.5, 1, 8000, 1000, area5b, p=True, beta=True, tli=False, bli=False)
x5c, p5c = find_1d_pdf('5c', start_time, 4.5, 1, 8000, 1000, area5c, p=True, beta=True, tli=False, bli=False)
x6a, p6a = find_1d_pdf('6a', start_time, 4.5, 1, 8000, 1000, area6a, p=True, beta=True, tli=False, bli=False)
x6b, p6b = find_1d_pdf('6b', start_time, 4.5, 1, 8000, 1000, area6b, p=True, beta=True, tli=False, bli=False)
x7, p7 = find_1d_pdf('7', start_time, 4.5, 1, 8000, 1000, area7a, p=True, beta=True, tli=False, bli=False)
xall, pall = find_1d_pdf('area', start_time, 5, 1, 8000, 1000, area, p=True, beta=True, tli=False, bli=False, all=True)
fig, ax = plt.subplots()
ax.set_xscale('log')
```

```
colormap = plt.cm.tab20
colors = [colormap(i) for i in np.linspace(0, 1,16)]
ax.set_prop_cycle('color', colors)
plt.xlabel('\u03B2 (nm/a)')
plt.ylabel('PDF')
ax.plot(x1a, p1a, label='1a')
ax.plot(x1b, p1b, label='1b')
ax.plot(x1c, p1c, label='1c')
ax.plot(x2, p2, label='2')
ax.plot(x3, p3, label='3')
ax.plot(x4a, p4a, label='4a')
ax.plot(x4b, p4b, label='4b')
ax.plot(x4c, p4c, label='4c')
ax.plot(x5a, p5a, label='5a')
ax.plot(x5b, p5b, label='5b')
ax.plot(x5c, p5c, label='5c')
ax.plot(x6a, p6a, label='6a')
ax.plot(x6b, p6b, label='6b')
ax.plot(x7, p7, label='7')
ax.plot(xall, pall, label='All Areas')
ax.xaxis.set_minor_locator(AutoMinorLocator())
ax.yaxis.set_minor_locator(AutoMinorLocator())
ax.ticklabel_format(style='sci', axis='y', scilimits=(0,0))
ax.legend(loc='upper left')
fig.savefig('beta_pdfs.png',dpi=300)


#age cdfs - run this
x1a, c1a = find_1d_pdf('1a', start_time, 5, 1, 8000, 1000, area1a, p=False)
x1b, c1b = find_1d_pdf('1b', start_time, 5, 1, 8000, 1000, area1b, p=False)
x1c, c1c = find_1d_pdf('1c', start_time, 5, 1, 8000, 1000, area1c, p=False)
x2, c2 = find_1d_pdf('2', start_time, 5, 1, 8000, 1000, area2, p=False)
x3, c3 = find_1d_pdf('3', start_time, 5, 1, 8000, 1000, area3, p=False)
x4a, c4a = find_1d_pdf('4a', start_time, 5, 1, 8000, 1000, area4a, p=False)
x4b, c4b = find_1d_pdf('4b', start_time, 5, 1, 8000, 1000, area4b, p=False)
x4c, c4c = find_1d_pdf('4c', start_time, 5, 1, 8000, 1000, area4c, p=False)
x5a, c5a = find_1d_pdf('5a', start_time, 5, 1, 8000, 1000, area5a, p=False)
x5b, c5b = find_1d_pdf('5b', start_time, 5, 1, 8000, 1000, area5b, p=False)
x5c, c5c = find_1d_pdf('5c', start_time, 5, 1, 8000, 1000, area5c, p=False)
x6a, c6a = find_1d_pdf('6a', start_time, 5, 1, 8000, 1000, area6a, p=False)
x6b, c6b = find_1d_pdf('6b', start_time, 5, 1, 8000, 1000, area6b, p=False)
x7, c7 = find_1d_pdf('7', start_time, 5, 1, 8000, 1000, area7, p=False)
fig, ax = plt.subplots()
colormap = plt.cm.tab20
colors = [colormap(i) for i in np.linspace(0, 1,16)]
ax.set_prop_cycle('color', colors)
plt.xlabel('Age (Ga)')
plt.ylabel('Cumulative Probability')
ax.plot(x1a, c1a, label='1a')
ax.plot(x1b, c1b, label='1b')
ax.plot(x1c, c1c, label='1c')
ax.plot(x2, c2, label='2')
ax.plot(x3, c3, label='3')
ax.plot(x4a, c4a, label='4a')
ax.plot(x4b, c4b, label='4b')
ax.plot(x4c, c4c, label='4c')
```

```
ax.plot(x5a, c5a, label='5a')
ax.plot(x5b, c5b, label='5b')
ax.plot(x5c, c5c, label='5c')
ax.plot(x6a, c6a, label='6a')
ax.plot(x6b, c6b, label='6b')
ax.plot(x7, c7, label='7')
ax.grid(True)
ax.xaxis.set_minor_locator(AutoMinorLocator())
ax.yaxis.set_minor_locator(AutoMinorLocator())
ax.grid(which='major', linewidth='1', linestyle=':', color='black')
ax.grid(which='minor', linestyle=':', linewidth='0.5', color='black')
ax.ticklabel_format(style='sci', axis='y', scilimits=(0,0))
plt.axhline(y=0.5, color='r', linestyle='--')
plt.axhline(y=0.841, color = 'r', linestyle='dotted')
plt.axhline(y=0.159, color = 'r', linestyle='dotted')
ax.legend()
fig.savefig('age_cdfs.png', dpi=300)

#beta cdfs - run this
x1a, c1a = find_1d_pdf('1a', start_time, 4.5, 1, 8000, 1000, area1a, p=False, beta=True, tli=False, bli=False)
x1b, c1b = find_1d_pdf('1b', start_time, 4.5, 1, 8000, 1000, area1b, p=False, beta=True, tli=False, bli=False)
x1c, c1c = find_1d_pdf('1c', start_time, 4.5, 1, 8000, 1000, area1c, p=False, beta=True, tli=False, bli=False)
x2, c2 = find_1d_pdf('2', start_time, 4.5, 1, 8000, 1000, area2, p=False, beta=True, tli=False, bli=False)
x3, c3 = find_1d_pdf('3', start_time, 4.5, 1, 8000, 1000, area3, p=False, beta=True, tli=False, bli=False)
x4a, c4a = find_1d_pdf('4a', start_time, 4.5, 1, 8000, 1000, area4a, p=False, beta=True, tli=False, bli=False)
x4b, c4b = find_1d_pdf('4b', start_time, 4.5, 1, 8000, 1000, area4b, p=False, beta=True, tli=False, bli=False)
x4c, c4c = find_1d_pdf('4c', start_time, 4.5, 1, 8000, 1000, area4c, p=False, beta=True, tli=False, bli=False)
x5a, c5a = find_1d_pdf('5a', start_time, 4.5, 1, 8000, 1000, area5a, p=False, beta=True, tli=False, bli=False)
x5b, c5b = find_1d_pdf('5b', start_time, 4.5, 1, 8000, 1000, area5b, p=False, beta=True, tli=False, bli=False)
x5c, c5c = find_1d_pdf('5c', start_time, 4.5, 1, 8000, 1000, area5c, p=False, beta=True, tli=False, bli=False)
x6a, c6a = find_1d_pdf('6a', start_time, 4.5, 1, 8000, 1000, area6a, p=False, beta=True, tli=False, bli=False)
x6b, c6b = find_1d_pdf('6b', start_time, 4.5, 1, 8000, 1000, area6b, p=False, beta=True, tli=False, bli=False)
x7, c7 = find_1d_pdf('7', start_time, 4.5, 1, 8000, 1000, area7, p=False, beta=True, tli=False, bli=False)
xcball, cball = find_1d_pdf('area', start_time, 4.5, 1, 8000, 1000, area, p=False, beta=True, tli=False, bli=False, all=True)
fig, ax = plt.subplots()
ax.set_xscale('log')
colormap = plt.cm.tab20
colors = [colormap(i) for i in np.linspace(0, 1,16)]
ax.set_prop_cycle('color', colors)
plt.xlabel('\u03B2 (nm/a)')
plt.ylabel('Cumulative Probability')
ax.plot(x1a, c1a, label='1a')
ax.plot(x1b, c1b, label='1b')
ax.plot(x1c, c1c, label='1c')
ax.plot(x2, c2, label='2')
ax.plot(x3, c3, label='3')
ax.plot(x4a, c4a, label='4a')
ax.plot(x4b, c4b, label='4b')
ax.plot(x4c, c4c, label='4c')
ax.plot(x5a, c5a, label='5a')
ax.plot(x5b, c5b, label='5b')
ax.plot(x5c, c5c, label='5c')
ax.plot(x6a, c6a, label='6a')
ax.plot(x6b, c6b, label='6b')
ax.plot(x7, c7, label='7')
ax.plot(xcball,cball, label='All Areas')
```

```
ax.xaxis.set_minor_locator(AutoMinorLocator())
ax.yaxis.set_minor_locator(AutoMinorLocator())
ax.axhline(y=0.5, color='r', linestyle='--' )
ax.axhline(y=0.841, color = 'r', linestyle='dotted')
ax.axhline(y=0.159, color = 'r', linestyle='dotted' )
ax.ticklabel_format(style='sci', axis='y', scilimits=(0,0))
ax.legend(loc='upper right',bbox_to_anchor=(1.15,1.05))
fig.savefig('beta_cdfs.png', dpi=300)
```

References

Ash, R., Dowler, W., and Varsi, G. (1978). Feasibility of rocket propellant production on Mars. *Acta Astronautica*, 5(9):705–724.

Bradley, B. and Sakimoto, S. (2001). Relationships between the Medusae Fossae Formation (MFF), fluvial channels, and the dichotomy boundary southeast of Nicholson Crater, Mars. In *Lunar and Planetary Science Conference*, page 1335.

Bradley, B. A., Sakimoto, S. E., Frey, H., and Zimbelman, J. R. (2002). Medusae Fossae Formation: New perspectives from Mars Global Surveyor. *Journal of Geophysical Research: Planets*, 107(E8):2–1.

Byrne, S. (2009). The polar deposits of Mars. *Annual Review of Earth and Planetary Sciences*, 37.

Campbell, B. A., Watters, T. R., and Morgan, G. A. (2021). Dielectric properties of the Medusae Fossae Formation and implications for ice content. *Journal of Geophysical Research: Planets*, 126(3):e2020JE006601.

Carter, L. M., Campbell, B. A., Watters, T. R., Phillips, R. J., Putzig, N. E., Safaeinili, A., Plaut, J. J., Okubo, C. H., Egan, A. F., Seu, R., et al. (2009). Shallow radar (SHARAD) sounding observations of the Medusae Fossae Formation, Mars. *Icarus*, 199(2):295–302.

Christensen, P. R. (1986). The spatial distribution of rocks on Mars. *Icarus*, 68(2):217–238.

Daubar, I., McEwen, A., Byrne, S., Kreslavsky, M., Saper, L., and Kennedy, M. (2014). New dated impacts on Mars and an updated current cratering rate. In *Eighth International Conference on Mars*, volume 1791, page 1007.

Daubar, I., McEwen, A. S., Byrne, S., Kennedy, M., and Ivanov, B. (2013). The current martian cratering rate. *Icarus*, 225(1):506–516.

Dunning, I. T. (2019). Mapping the previous extent of the Medusae Fossae Formation, Mars.

Edgett, K. S., Banham, S. G., Bennett, K. A., Edgar, L. A., Edwards, C. S., Fairén, A. G., Fedo, C. M., Fey, D. M., Garvin, J. B., Grotzinger, J. P., et al. (2020). Extraformational sediment recycling on Mars. *Geosphere*, 16(6):1508–1537.

El-Baz, F., Breed, C., Grolier, M., and McCauley, J. (1979). Eolian features in the western desert of Egypt and some applications to Mars. *Journal of Geophysical Research: Solid Earth*, 84(B14):8205–8221.

Fassett, C. I., Levy, J. S., Dickson, J. L., and Head, J. W. (2014). An extended period of episodic northern mid-latitude glaciation on Mars during the Middle to Late Amazonian: Implications for long-term obliquity history. *Geology*, 42(9):763–766.

Feldman, W., Prettyman, T., Maurice, S., Plaut, J., Bish, D., Vaniman, D., Mellon, M., Metzger, A., Squyres, S., Karunatillake, S., et al. (2004). Global distribution of near-surface hydrogen on Mars. *Journal of Geophysical Research: Planets*, 109(E9).

Forsythe, R. D. and Zimbelman, J. R. (1988). Is the PGordii Dorsum escarpment on Mars an exhumed transcurrent fault? *Nature*, 336(6195):143–146.

Frey, H., Sakimoto, S. E., and Roark, J. (1998). The MOLA topographic signature at the crustal dichotomy boundary zone on Mars. *Geophysical research letters*, 25(24):4409–4412.

Gabasova, L. R. and Kite, E. S. (2018). Compaction and sedimentary basin analysis on Mars. *Planetary and Space Science*, 152:86–106.

Greeley, R. and Guest, J. (1987). Geologic map of the eastern equatorial region of Mars.

Greeley, R., Kuzmin, R. O., and Haberle, R. M. (2001). Aeolian processes and their effects on understanding the chronology of Mars. *Space Science Reviews*, 96(1):393–404.

Grimm, R. E. and Solomon, S. C. (1986). Tectonic tests of proposed polar wander paths for Mars and the Moon. *Icarus*, 65(1):110–121.

Grindrod, P. M. and Warner, N. (2014). Erosion rate and previous extent of interior layered deposits on Mars revealed by obstructed landslides. *Geology*, 42(9):795–798.

Halevy, I. and Head, J. W. (2014). Episodic warming of early Mars by punctuated volcanism. *Nature Geoscience*, 7(12):865–868.

Halevy, I. and Schrag, D. (2009). Sulfur dioxide inhibits calcium carbonate precipitation: Implications for early Mars and Earth. *Geophysical Research Letters*, 36(23).

Halevy, I., Zuber, M. T., and Schrag, D. P. (2007). A sulfur dioxide climate feedback on early Mars. *Science*, 318(5858):1903–1907.

Hartmann, W. K. (2005). Martian cratering 8: Isochron refinement and the chronology of Mars. *Icarus*, 174(2):294–320.

Head, J. and Kreslavsky, M. (2004). Medusae Fossae Formation: Ice-rich airborne dust deposited during periods of high obliquity? In *Lunar and Planetary Science Conference*, page 1635.

Head, J. and Kreslavsky, M. A. (2001). Medusae Fossae Formation as volatile-rich sediments deposited during high obliquity: An hypothesis and tests. In *Conference on the Geophysical Detection of Subsurface Water on Mars*, page 7053.

Head, J. W. and Wilson, L. (1998). Tharsis Montes as composite volcanoes?: 1. the role of explosive volcanism in edifice construction and implications for the volatile contents of edifice-forming magmas. In *Lunar and Planetary Science Conference*, number 1127, page 1127.

Horvath, D. G., Moitra, P., Hamilton, C. W., Craddock, R. A., and Andrews-Hanna, J. C. (2021). Evidence for geologically recent explosive volcanism in Elysium Planitia, Mars. *Icarus*, 114499.

Hudson, T. L., Aharonson, O., Schorghofer, N., Farmer, C. B., Hecht, M. H., and Bridges, N. T. (2007). Water vapor diffusion in Mars subsurface environments. *Journal of Geophysical Research: Planets*, 112(E5).

Hynek, B., Arvidson, R., and Phillips, R. (2002). Explosive volcanism from Tharsis: Global evidence in the Martian geologic record. In *Lunar and Planetary Science Conference*, page 1408.

Hynek, B. M., Phillips, R. J., and Arvidson, R. E. (2003). Explosive volcanism in the Tharsis region: Global evidence in the martian geologic record. *Journal of Geophysical Research: Planets*, 108(E9).

Jerolmack, D. J. and Sadler, P. (2007). Transience and persistence in the depositional record of continental margins. *Journal of Geophysical Research: Earth Surface*, 112(F3).

Kadish, S. J., Barlow, N. G., and Head, J. W. (2009). Latitude dependence of Martian pedestal craters: Evidence for a sublimation-driven formation mechanism. *Journal of Geophysical Research: Planets*, 114(E10).

Kerber, L., Dickson, J. L., Head, J. W., and Grosfils, E. B. (2017). Polygonal ridge networks on Mars: Diversity of morphologies and the special case of the eastern medusae fossae formation. *Icarus*, 281:200–219.

Kerber, L. and Head, J. W. (2010). The age of the Medusae Fossae Formation: Evidence of Hesperian emplacement from crater morphology, stratigraphy, and ancient lava contacts. *Icarus*, 206(2):669–684.

Kerber, L., Head, J. W., Madeleine, J.-B., Forget, F., and Wilson, L. (2011). The dispersal of pyroclasts from Apollinaris Patera, Mars: Implications for the origin of the Medusae Fossae Formation. *Icarus*, 216(1):212–220.

Kerber, L., Head, J. W., Madeleine, J.-B., Forget, F., and Wilson, L. (2012). The dispersal of pyroclasts from ancient explosive volcanoes on Mars: implications for the friable layered deposits. *Icarus*, 219(1):358–381.

Kieffer, H. H., Martin, T., Peterfreund, A. R., Jakosky, B. M., Miner, E. D., and Palluconi, F. D. (1977). Thermal and albedo mapping of Mars during the Viking primary mission. *Journal of Geophysical Research*, 82(28):4249–4291.

Kite, E. S., Howard, A. D., Lucas, A. S., Armstrong, J. C., Aharonson, O., and Lamb, M. P. (2015). Stratigraphy of Aeolis Dorsa, Mars: Stratigraphic context of the great river deposits. *Icarus*, 253:223–242.

Kite, E. S., Matsuyama, I., Manga, M., Perron, J. T., and Mitrovica, J. X. (2009). True polar wander driven by late-stage volcanism and the distribution of paleopolar deposits on Mars. *Earth and Planetary Science Letters*, 280(1-4):254–267.

Kite, E. S. and Mayer, D. P. (2017). Mars sedimentary rock erosion rates constrained using crater counts, with applications to organic-matter preservation and to the global dust cycle. *Icarus*, 286:212–222.

Kite, E. S., Sneed, J., Mayer, D. P., Lewis, K. W., Michaels, T. I., Hore, A., and Rafkin, S. C. (2016). Evolution of major sedimentary mounds on Mars: Buildup via anticompensational stacking modulated by climate change. *Journal of Geophysical Research: Planets*, 121(11):2282–2324.

Le Feuvre, M. and Wieczorek, M. A. (2008). Nonuniform cratering of the terrestrial planets. *Icarus*, 197(1):291–306.

Lewis, K. W. and Aharonson, O. (2014). Occurrence and origin of rhythmic sedimentary rocks on Mars. *Journal of Geophysical Research: Planets*, 119(6):1432–1457.

Liu, J., Yue, Z., Di, K., Gou, S., and Niu, S. (2021). A study about the temporal constraints on the Martian yardangs' development in Medusae Fossae Formation. *Remote Sensing*, 13(7):1316.

Malin, M., Carr, M., Danielson, G., Davies, M., Hartmann, W., Ingersoll, A., James, P., Masursky,

H., McEwen, A., Soderblom, L., et al. (1998). Early views of the martian surface from the Mars Orbiter Camera of Mars Global Surveyor. *Science*, 279(5357):1681–1685.

Malin, M. C., Bell, J. F., Cantor, B. A., Caplinger, M. A., Calvin, W. M., Clancy, R. T., Edgett, K. S., Edwards, L., Haberle, R. M., James, P. B., et al. (2007). Context camera investigation on board the Mars Reconnaissance Orbiter. *Journal of Geophysical Research: Planets*, 112(E5).

Malin, M. C. and Carr, M. H. (1999). Groundwater formation of Martian valleys. *Nature*, 397(6720):589–591.

Malin, M. C. and Edgett, K. S. (2000). Sedimentary rocks of early Mars. *Science*, 290(5498):1927–1937.

Mandt, K. E., de Silva, S., Zimbelman, J., and Crown, D. (2007). A synoptic approach to evaluating the origin of the Medusae Fossae Formation, Mars. In *Lunar and Planetary Science Conference*, number 1338, page 1823.

Mandt, K. E., de Silva, S. L., Zimbelman, J. R., and Crown, D. A. (2008). Origin of the Medusae Fossae Formation, Mars: Insights from a synoptic approach. *Journal of Geophysical Research: Planets*, 113(E12).

Mellon, M. T. and Jakosky, B. M. (1993). Geographic variations in the thermal and diffusive stability of ground ice on Mars. *Journal of Geophysical Research: Planets*, 98(E2):3345–3364.

Michael, G. (2013). Planetary surface dating from crater size–frequency distribution measurements: Multiple resurfacing episodes and differential isochron fitting. *Icarus*, 226(1):885–890.

Mouginis-Mark, P. (1993). The influence of oceans on Martian volcanism. In *Lunar and Planetary Science Conference*, volume 24.

Mouginis-Mark, P. J. and Zimbelman, J. R. (2020). Rafted pumice: A new model for the formation of the Medusae Fossae Formation, Mars. *Icarus*, 343:113684.

Mouginot, J., Pommerol, A., Kofman, W., Beck, P., Schmitt, B., Herique, A., Grima, C., Safaeinili, A., and Plaut, J. (2010). The 3–5 mhz global reflectivity map of Mars by MARSIS/Mars Express: Implications for the current inventory of subsurface H2O. *Icarus*, 210(2):612–625.

Nussbaumer, J. (2005). Extent and further characteristics of former glaciated terrain in Elysium Planitia, Mars. In *36th Annual Lunar and Planetary Science Conference*, page 1949.

Ojha, L., Karunatillake, S., and Iacovino, K. (2019). Atmospheric injection of sulfur from the Medusae Fossae forming events. *Planetary and Space Science*, 179:104734.

Ojha, L. and Lewis, K. (2018). The density of the Medusae Fossae Formation: Implications for its composition, origin, and importance in martian history. *Journal of Geophysical Research: Planets*, 123(6):1368–1379.

Ojha, L., Lewis, K., Karunatillake, S., and Schmidt, M. (2018). The Medusae Fossae Formation as the single largest source of dust on Mars. *Nature communications*, 9(1):1–7.

Orosei, R., Rossi, A. P., Cantini, F., Caprarelli, G., Carter, L. M., Papiano, I., Cartacci, M., Cicchetti, A., and Noschese, R. (2017). Radar sounding of Lucus Planum, Mars, by MARSIS. *Journal of Geophysical Research: Planets*, 122(7):1405–1418.

Palluconi, F. D. and Kieffer, H. H. (1981). Thermal inertia mapping of Mars from 60 S to 60 N. *Icarus*, 45(2):415–426.

Palucis, M. C., Jasper, J., Garczynski, B., and Dietrich, W. E. (2020). Quantitative assessment of uncertainties in modeled crater retention ages on Mars. *Icarus*, 341:113623.

Parker, T. (1991). A comparison of the Martian Medusae Fossae Formation with terrestrial carbonate platforms. In *Lunar and Planetary Science Conference*, volume 22.

Pathare, A. V., Feldman, W. C., Prettyman, T. H., and Maurice, S. (2018). Driven by excess? climatic implications of new global mapping of near-surface water-equivalent hydrogen on Mars. *Icarus*, 301:97–116.

Pike, R. J. (1980). Control of crater morphology by gravity and target type-Mars, Earth, Moon. In *Lunar and Planetary Science Conference Proceedings*, volume 11, pages 2159–2189.

Quantin-Nataf, C., Craddock, R., Dubuffet, F., Lozac'h, L., and Martinot, M. (2019). Decline of crater obliteration rates during early martian history. *Icarus*, 317:427–433.

Rice, J. W. (1997). *Aqueous sedimentary basins on Mars*. Arizona State University.

Sakimoto, S. E., Frey, H. V., Garvin, J. B., and Roark, J. H. (1999). Topography, roughness, layering, and slope properties of the Medusae Fossae formation from Mars Orbiter Laser Altimeter (MOLA) and Mars Orbiter Camera (MOC) data. *Journal of Geophysical Research: Planets*, 104(E10):24141–24154.

Schorghofer, N. (2007). Dynamics of ice ages on Mars. *Nature*, 449(7159):192–194.

Schultz, P. H. and Lutz, A. B. (1988). Polar wandering of Mars. *Icarus*, 73(1):91–141.

Schultz, R. A. (2002). Stability of rock slopes in Valles Marineris, Mars. *Geophysical Research Letters*, 29(19):38–1.

Schultz, R. A., Moore, J. M., Grosfils, E. B., Tanaka, K. L., Mège, D., and Chapman, M. (2007). The canyonlands model for planetary grabens: Revised physical basis and implications. *The Geology of Mars: Evidence from Earth-Based Analogs*, pages 371–399.

Scott, D. H. and Tanaka, K. L. (1982). Ignimbrites of Amazonis Planitia region of Mars. *Journal of Geophysical Research: Solid Earth*, 87(B2):1179–1190.

Scott, D. H. and Tanaka, K. L. (1986). Geologic map of the western equatorial region of Mars.

Shahrzad, S., Kinch, K. M., Goudge, T. A., Fassett, C. I., Needham, D. H., Quantin-Nataf, C., and Knudsen, C. P. (2019). Crater statistics on the dark-toned, mafic floor unit in Jezero Crater, Mars. *Geophysical Research Letters*, 46(5):2408–2416.

Smith, D. E., Zuber, M. T., Frey, H. V., Garvin, J. B., Head, J. W., Muhleman, D. O., Pettengill, G. H., Phillips, R. J., Solomon, S. C., Zwally, H. J., et al. (2001). Mars Orbiter Laser Altimeter: Experiment summary after the first year of global mapping of Mars. *Journal of Geophysical Research: Planets*, 106(E10):23689–23722.

Smith, M. R., Gillespie, A. R., and Montgomery, D. R. (2008). Effect of obliteration on crater-count chronologies for Martian surfaces. *Geophysical research letters*, 35(10).

Smith, P. H., Tamppari, L., Arvidson, R., Bass, D., Blaney, D., Boynton, W. V., Carswell, A., Catling, D., Clark, B., Duck, T., et al. (2009). H2o at the Phoenix landing site. *Science*, 325(5936):58–61.

Starr, S. O. and Muscatello, A. C. (2020). Mars in situ resource utilization: a review. *Planetary and Space Science*, 182:104824.

Takagi, M. and Zimbelman, J. (2001). Geomorphic mapping and analysis of the eastern Medusae Fossae region of Mars. In *Lunar and Planetary Science Conference*, page 1579.

Tanaka, K. L. (2000). Dust and ice deposition in the Martian geologic record. *Icarus*, 144(2):254–266.

Tanaka, K. L., Skinner Jr, J. A., Dohm, J. M., Irwin III, R. P., Kolb, E. J., Fortezzo, C. M., Platz, T., Michael, G. G., and Hare, T. M. (2014). Geologic map of Mars: U.S. Geological Survey Scientific Investigations Map 3292, scale 1:20,000,000, pamphlet 43.

Thomson, B., Bridges, N., Milliken, R., Baldridge, A., Hook, S., Crowley, J., Marion, G., de Souza Filho, C., Brown, A., and Weitz, C. (2011). Constraints on the origin and evolution of the layered mound in Gale Crater, Mars using Mars Reconnaissance Orbiter data. *Icarus*, 214(2):413–432.

Thomson, B., Bridges, N., Milliken, R., Bell, J., Calvin, W., and Weitz, C. (2008). New constraints

on the origin and evolution of the layered deposits in Gale crater, Mars. In *Lunar and Planetary Science Conference*, number 1391, page 1456.

Tian, F., Claire, M. W., Haqq-Misra, J. D., Smith, M., Crisp, D. C., Catling, D., Zahnle, K., and Kasting, J. F. (2010). Photochemical and climate consequences of sulfur outgassing on early Mars. *Earth and Planetary Science Letters*, 295(3-4):412–418.

Tornabene, L. L., Watters, W. A., Osinski, G. R., Boyce, J. M., Harrison, T. N., Ling, V., and McEwen, A. S. (2018). A depth versus diameter scaling relationship for the best-preserved melt-bearing complex craters on mars. *Icarus*, 299:68–83.

Wall, J. V. and Jenkins, C. R. (2012). *Practical statistics for astronomers*. Cambridge University Press.

Wang, J., Xiao, L., Reiss, D., Hiesinger, H., Huang, J., Xu, Y., Zhao, J., Xiao, Z., and Komatsu, G. (2018). Geological features and evolution of yardangs in the Qaidam Basin, Tibetan Plateau (NW China): a terrestrial analogue for Mars. *Journal of Geophysical Research: Planets*, 123(9):2336–2364.

Ward, A. W. (1979). Yardangs on Mars: Evidence of recent wind erosion. *Journal of Geophysical Research: Solid Earth*, 84(B14):8147–8166.

Wasilewski, B. and Gregg, T. (2021). The Medusae Fossae Formation, Mars: Finding the former extent of an enigmatic deposit. In *Lunar and Planetary Science Conference*, number 2548, page 2374.

Watters, T. R., Campbell, B., Carter, L., Leuschen, C. J., Plaut, J. J., Picardi, G., Orosei, R., Safaeinili, A., Clifford, S. M., Farrell, W. M., et al. (2007). Radar sounding of the Medusae Fossae Formation Mars: Equatorial ice or dry, low-density deposits? *Science*, 318(5853):1125–1128.

Watters, W. A., Geiger, L. M., Fendrock, M., and Gibson, R. (2015). Morphometry of small recent impact craters on Mars: Size and terrain dependence, short-term modification. *Journal of Geophysical Research: Planets*, 120(2):226–254.

Werner, S. C. (2005). *Major aspects of the chronostratigraphy and geologic evolutionary history of Mars*. Cuvillier Verlag.

Williams, R. M., Irwin III, R. P., Burr, D. M., Harrison, T., and McClelland, P. (2013). Variability in martian sinuous ridge form: Case study of Aeolis Serpens in the Aeolis Dorsa, Mars, and insight from the Mirackina paleoriver, South Australia. *Icarus*, 225(1):308–324.

Wilson, J. T., Eke, V. R., Massey, R. J., Elphic, R. C., Feldman, W. C., Maurice, S., and Teodoro, L. F. (2018). Equatorial locations of water on Mars: Improved resolution maps based on Mars Odyssey Neutron Spectrometer data. *Icarus*, 299:148–160.

Zimbelman, J., Sakimoto, S., and Frey, H. (2000). Evidence for a fluvial contribution to the complex story of the Medusae Fossae Formation on Mars. In *Geol. Soc. Am. Abstr. Programs*, volume 32, page A303.

Zimbelman, J. R., Crown, D. A., Grant, J. A., and Hooper, D. M. (1997). The Medusae Fossae Formation, Amazonis Planitia, Mars: Evaluation of proposed hypotheses of origin. *Lunar Planet. Sci*, 28:1623–1624.

Zimbelman, J. R. and Griffin, L. J. (2010). HiRISE images of yardangs and sinuous ridges in the lower member of the Medusae Fossae Formation, Mars. *Icarus*, 205(1):198–210.

Zimbelman, J. R. and Scheidt, S. (2012a). Crater retention ages indicate a Hesperian age for western and central portions of the Medusae Fossae Formation, Mars. In *Lunar and Planetary Science Conference*, number 1659, page 2052.

Zimbelman, J. R. and Scheidt, S. P. (2012b). Hesperian age for western Medusae Fossae Formation, Mars. *Science*, 336(6089):1683–1683.